Satellite Quenching and the Lifecycle of Dwarf Galaxies

by

Colin T. Slater

A dissertation submitted in partial fulfillment
of the requirements for the degree of
Doctor of Philosophy
(Astronomy and Astrophysics)
in The University of Michigan
2015

Doctoral Committee:

Professor Eric F. Bell, Chair
Professor August Evrard
Professor Mario L. Mateo
Professor Hans-Walter Rix, Max Planck Institute for Astronomy
Associate Research Professor Monica Valluri

LIGHTS ALL ASKEW
IN THE HEAVENS

Men of Science More or Less
Agog Over Results of Eclipse
Observations.

EINSTEIN THEORY TRIUMPHS

Stars Not Where They Seemed
or Were Calculated to be,
but Nobody Need Worry.

—*The New York Times*, 10 November 1919.

ACKNOWLEDGMENTS

It has been a pleasure to spend the past several years working with Eric Bell on the work presented here, in addition to sharing, speculating, and learning about countless other subjects ranging across early-type galaxies, galaxy shape distributions, low surface brightness infrared imaging, atmospheric cloud physics, soil erosion, and beyond. The fun of science is to be able to seek out and explore whatever topics are most interesting personally, and I am grateful that we could share so many of these experiences.

Much of that exploration has felt like a seamless extension of my time as an undergrad working with Paul Harding at Case Western Reserve University. The questions were just as wide-ranging, and my answers at the time were significantly poorer, but I am still still learning from those experiences as I rediscover topics only to remember that Paul had already explained it to me, and it had just taken several more years for that information to sink in. He and Heather Morrison ensured that their students were thinking about galaxies hierarchically and cosmologically from the very start, and that has motivated this work substantially.

I also received a tremendous amount of support from a network of collaborators loosely centered around the MPIA and the CfA. Nicolas Martin, Eddie Schlafly, Hans-Walter Rix, Mario Juric, and Doug Finkbeiner were all vitally important to many of the papers presented here. The work depending on Pan-STARRS also owes credit to the team who built and operated the survey: W. S. Burgett, K. C. Chambers, T. Dombeck, T. Grav, J. N. Heasley, K. W. Hodapp, R. Jedicke, N. Kaiser, Rolf

Kudritzki, Gerald Luppino, Robert H. Lupton, Eugene A. Magnier, David G. Monet, J. S. Morgan, P. M. Onaka, P. A. Price, P. H. Rhoads, Walter A. Siegmund, C. W. Stubbs, John L. Tonry, Richard J. Wainscoat, M. F. Waterson, C. G. Wynn-Williams, amongst many other science collaborators.

Part of the challenge of graduate school is staying sane. For help in this I owe much to many fellow grad students, in an approximately chronological order, Mike Anderson, Sasha Muratov, Ilse Cleeves, Anne Jaskot, Ashley King, Jeb Bailey, Rachael Roettenbacher, Kamber Schwarz, and Traci Johnston. And perhaps the least visible but most significant support in all of this comes from my parents and sister.

TABLE OF CONTENTS

CHAPTER

LIST OF FIGURES

Figure

LIST OF TABLES

Table

ABSTRACT

In the past ten years the known population of Local Group dwarf galaxies has expanded substantially, both to greater distances from the Milky Way and to lower dwarf masses. This growing sample allows us to study the dwarf system as a population, and ask which processes and events are most responsible for setting the properties of dwarfs. The dichotomy between star forming dwarf irregulars and quenched dwarf spheroidals is the principal differentiation we see in this population, but we do not have a definitive understanding of what causes this distinction. With the aim of advancing our understanding of this problem, I present the discovery and characterization of additional dwarf galaxies, further building up this sample. From this, I combine the known Local Group dwarfs with models of the Galaxy's formation to understand if interactions with a massive host could be responsible for transforming dwarf irregulars into dwarf spheroidals. I also use these models to investigate the changing efficiency of this transformation between the lowest mass and higher mass satellites. Finally, I show evidence of a past interactions between dwarf galaxies and the Milky Way disk, presenting a wide field map of the resulting debris. Together these efforts attempt to place the Local Group system of dwarfs in a cosmological context to yield an improved picture of their origin and evolution.

CHAPTER I

Introduction

1.1 The Cosmological Framework

The fundamental basis of modern galaxy formation and evolution is the cold dark matter paradigm of structure formation. From an initial set of small density perturbations in the early universe, overdense regions are able to collapse into halos and grow under the dominant dynamics of the collisionless dark matter. This behavior is understood in terms of a few basic cosmological parameters: the relative fractions of baryonic and non-baryonic matter, the “cold” nature of the dark matter, the power spectrum of the initial perturbations, and the contribution of dark energy to the expansion history of the universe. These parameters are constrained by measurements of the cosmic microwave background with satellites such as *COBE* (Smoot et al., 1992), *WMAP* (Hinshaw et al., 2013), and *Planck* (Planck Collaboration et al., 2015), supernovae measurements (Sullivan et al., 2011), and baryon acoustic oscillations (Blake et al., 2012). From a cosmological model with these parameters specified, one can simulate the evolution of the large scale dark matter picture which provides the stage for the formation of the galaxies we see (e.g., Springel et al., 2005; Vogelsberger et al., 2014, amongst many others).

In these simulations the universe we see is shockingly dynamic. The density power spectrum yields a large number of small scale structures for every one dark

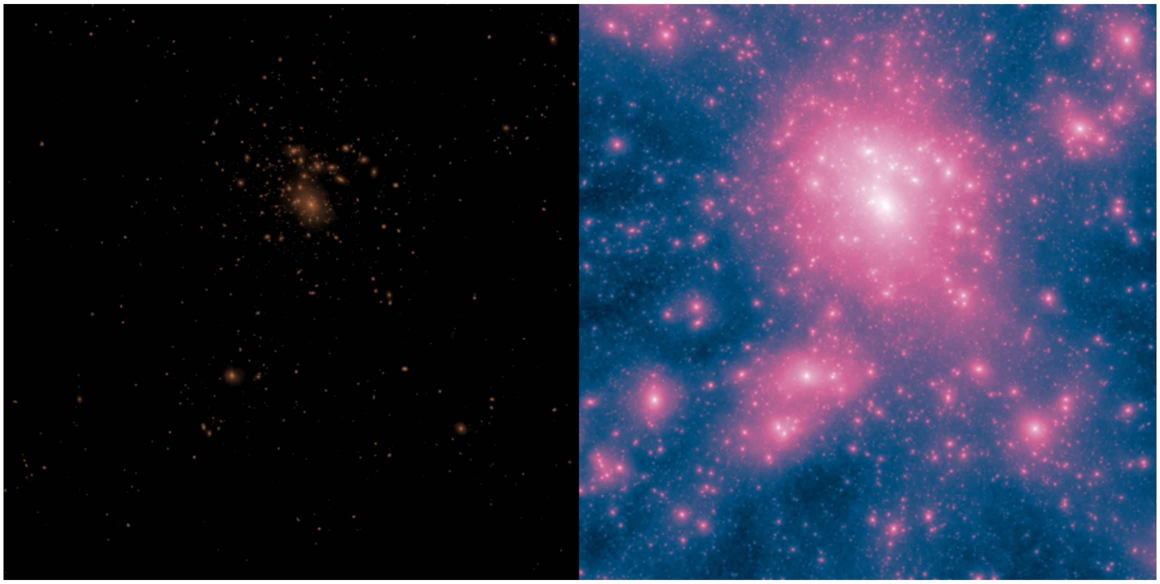

Figure 1.1: Mock observation images (*left*) and dark matter density (*right*) for a region of the Illustris hydrodynamical simulation (Vogelsberger et al., 2014). The luminous component of galaxies that we observe is a tracer of only the dense central regions of much more extended dark matter structures, in this case a large galaxy cluster.

matter halo capable of hosting the Milky Way. These structures are continuously on the move; they merge with each other, they merge with larger structures nearby, sometimes remaining as coherent density peaks inside the larger halo, and sometimes simply supplying the larger structure with mass with which to grow. Because on a cosmological scale the amount of dark matter greatly dominates the amount of gas and stars, it is the dynamics we see in these dark matter simulations that determine the bulk behavior of the baryonic component. To first order the baryons are "along for the ride" as this process of mergers and interactions proceeds.

Although we believe this bulk behavior of the dark matter is relatively well understood, this alone cannot tell us how galaxies form. The remaining component of the story, and the one in which nearly all of the uncertainty lies, is the behavior of gas and the means by which it is turned into stars. In the broadest terms, gas must cool radiatively for it to condense into the potential wells provided by the dark matter

(White & Rees, 1978). An illustration of this condensation process is shown in Figure 1.1, where in the simulated image the luminous components of galaxies occupy only the very peaks of the total density distribution. This cooling process naturally results in galactic disks, since the material still retains its angular momentum it cannot shrink further. This cold gas disk is the site of star formation, where densities can become great enough that molecular hydrogen and CO_2 can form (Hollenbach et al., 1971) and avoid photodissociation thanks to the high opacities provided by dust and H_2 self-shielding, thus further enabling the collapse of gas into molecular clouds and eventually stars. This process is modulated by the influence of turbulence and magnetic fields, and potentially the large scale dynamics of the disk, which adds tremendous complexity to the process (McKee & Ostriker, 2007).

Star formation naturally depends on this chain of cooling processes, but there are numerous processes which may alter or inhibit this progression. It has long been understood that, without some form of heating to slow star formation, galaxies would convert all their gas into stars far too rapidly (Cole, 1991; White & Frenk, 1991). Star formation must proceed inefficiently if realistic galaxies are to be formed. This energy injection may come from the strong winds and radiation from newly formed stars, collectively known as feedback, but their effects are not always well understood and are a particularly difficult challenge for simulations (Dekel & Silk, 1986; Navarro & White, 1993; Springel & Hernquist, 2003; Stinson et al., 2006).

This heating is present and important whenever stars are formed. In galaxies with Milky Way-like masses and above, gas falling into a dark matter potential well is thought to do so supersonically, leading to the formation of an accretion shock which turns much of the energy of infall into heat (Birnboim & Dekel, 2003). This leads to a diffuse but potentially massive halo of hot gas surrounding the galaxy, which is too hot to cool quickly but can only slowly feed the galaxy near the center where densities are high. This hot gas may be further supported energetically by star formation feedback processes, or possibly by energetic jets from the supermassive black hole at the center of the galaxy (Croton et al., 2006; Somerville et al., 2008; Danielson et al., 2012). Together these heating sources may contribute to regulating the rate of star formation in a galaxy, or potentially may shut off star formation entirely (Cattaneo et al., 2006).

This broad outline of the interconnection between gas in various states and the star formation in a galaxy is schematically plausible, but difficult to turn into precise predictions and equally difficult to unambiguously confirm many of these details observationally. The challenge in predictive models is that high resolution simulations with accurate physical processes are required to trace the behavior of gas, but the current state of the art depends on numerous sub-grid prescriptions for most of the processes that inject energy into the gas. Numerous numerical difficulties can present serious challenges in this due to the strong dependence that observed properties like star formation rates have on these feedback properties. Additionally, for the dwarf galaxies that will be the focus of this work, simulations need tremendous dynamic range to properly resolve both small satellites and their massive hosts, particularly when gas is involved in both. This is computationally infeasible at present. Observationally, this picture depends heavily on the behaviour of low density hot gas, but this can only be detected around the Milky Way with weak X-ray absorption and is even more difficult to see in external galaxies (Anderson & Bregman, 2010; Miller & Bregman, 2013). The role of intermediate temperature phases (sometimes called "warm" or "warm-hot") at large radii, either as the result of outflows or infall, is only recently becoming observationally accessible with HST/COS (Werk et al., 2014; Peeples et al., 2014). The characterization offered by these studies, of both hot and "warm" phases, remains general and uncertain in many details.

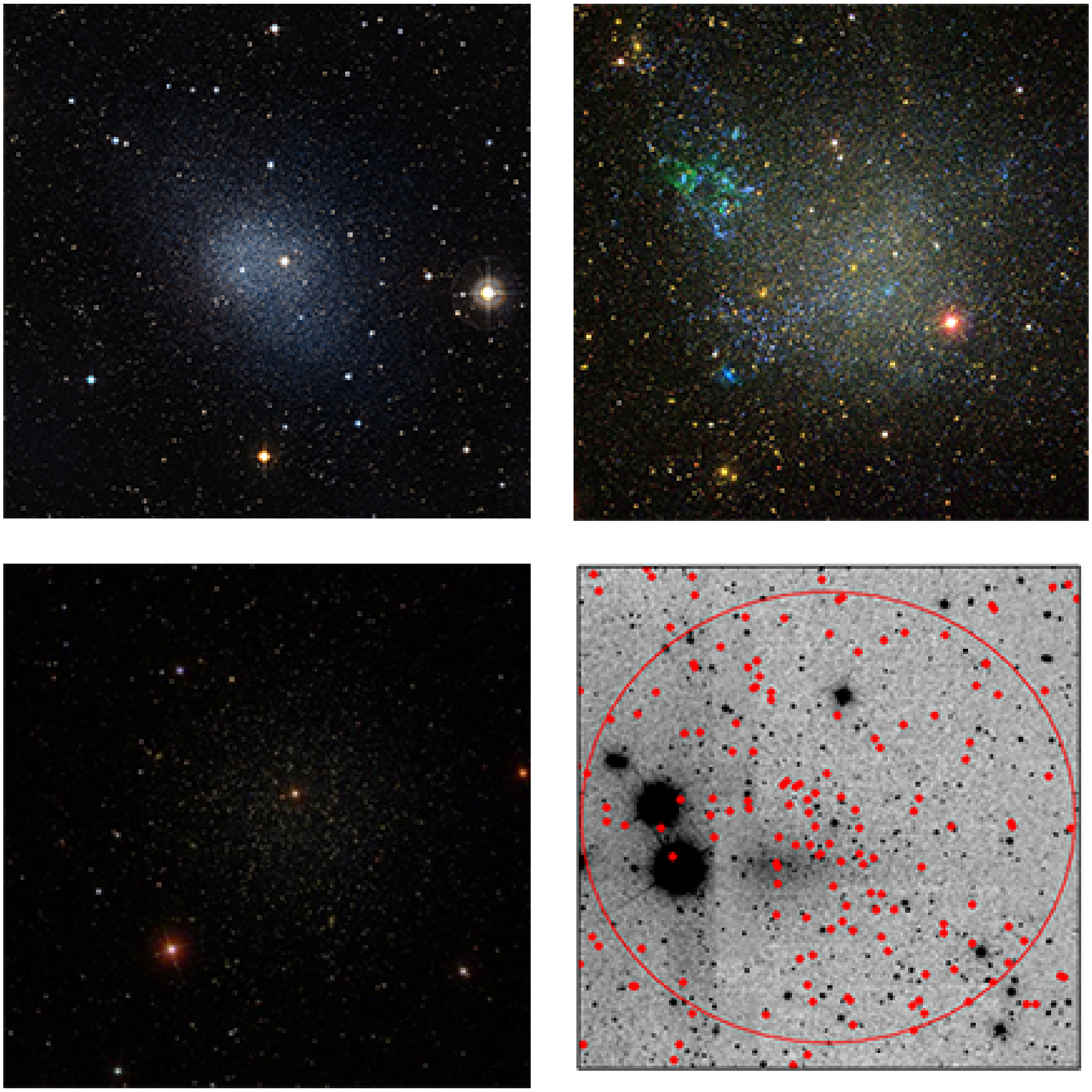

Figure 1.2: Images from SDSS of several dwarf galaxies. Clockwise from top left, Fornax dSph ($M_V = -13.4$), IC 1613 (dIrr, $M_V = -15.2$), Coma dSph (red giant branch stars overplotted and a circle at the half light radius, $M_V = -4.1$), and Leo II dSph ($M_V = -9.8$).

1.2 Dwarf Galaxies

A further complication is that these processes are all theoretically at work over the entire range of galaxy masses. But galaxies are clearly not so simplistic that the same gas dynamics affect them all in the same ways regardless of mass. There are almost certainly different components of this story that become more or less important at high masses or at low masses, which complicates our efforts to quantify these effects. For example, low mass galaxies are less likely to develop large reservoirs of hot gas, but they often contain more cold gas per stellar mass than large galaxies, and may be more likely to be affected by the hot gas of their neighbors. Before a complete picture of galaxy formation can be assembled it may be necessary to first understand smaller pieces of the galaxy parameter space.

The focus of this work is on the dwarf galaxies, corresponding to roughly Magellanic cloud-mass galaxies and below. Observationally, the most fundamental distinction we observe in dwarf galaxies is between star forming, rotationally supported, and often "irregularly" shaped dwarf irregular galaxies (dIrrs) and the more elliptical-shaped, non-star forming dwarf spheroidal galaxies (dSphs) (Gallagher & Wyse, 1994; Mateo, 1998; McConnachie, 2012). Almost all Local Group dwarfs fall into one of these categories with only rare examples of galaxies that exhibit a mixture of these properties. A sample of Local Group dwarfs at varying luminosities is shown in Figure 1.2. It is now commonly believed that dwarf irregulars transform into dwarf spheroidals via some process that shuts down the star formation present in the galaxy, removes all cold gas from the system, and transforms the morphology of existing stars from disk-like to more a more spheroidal distribution (Grebel et al., 2003). This transformation event I will broadly refer to as "quenching" throughout this work. That this transition occurs is now well accepted, but what physical process is responsible for quenching is still much in dispute. Improving our knowledge of that triggers quenching and via what physical mechanisms quenching proceeds is a major goal of this work.

Potential mechanisms for quenching galaxies in general can be broadly categorized as either internally-driven or externally-driven events, depending on whether the something about the galaxy itself causes it to shut down star formation or if it requires the action of other actors in the the galaxy's nearby environment for quenching to occur.

Internally, a galaxy could lose the ability to form stars if its reservoir of cold gas is heated to the point of being inaccessible to star formation, or if it is depleted by star formation and not replenished. Such a heating process could occur via active galactic nuclei (AGN) jets which can inject large amounts of energy into their surrounding material, or via energetic winds from the formation of massive stars and/or the associated supernovae. AGN are more commonly associated with large galaxies than with dwarfs (though larger dwarfs may also host them too, Reines et al., 2013), but the energy input from star formation or supernovae is certainly available to dwarfs. The ability of star formation to clear a dwarf of cold gas may even be substantially greater than in larger galaxies, due to the shallow potential well that dwarfs inhabit. Energetically, even small numbers of supernovae may be able to clear dwarfs of gas under suitable conditions (Dekel & Silk, 1986; Sawala et al., 2010).

External processes are also important to consider as triggers for quenching. For observational reasons, most of the dwarfs that were known prior to the SDSS were in the near vicinity of the Milky Way. Dwarfs at this distance are strongly affected by the tidal field of the Milky Way, which is likely to distort the galaxies and randomize orbits of their constituent stars, driving them towards a spheroidal morphology rather than disks (Mayer et al., 2001, 2006; Kazantzidis et al., 2011a). This tidal process is unavoidable, only depending on the structure of the dwarf and its orbit through the host, from which the effects can be reliably calculated (Łokas et al., 2010, 2011; Kazantzidis et al., 2013). Tides do not necessarily remove cold gas from galaxy though, so it is not clear that they can be solely responsible for quenching.

Gas in the dwarfs may, however, be affected by ram pressure from the host galaxy's hot halo (Einasto et al., 1974; Grebel et al., 2003; Grcevich & Putman, 2009). This is the drag-like force that the dwarf's gas feels as it moves rapidly along its orbit through a stationary medium surrounding the host galaxy. The classic treatment of this force in Gunn & Gott (1972) assumes that it is a momentum transfer problem. In this model, when the ram pressure force per unit area ρv^2 exceeds the restoring force provided by the gravity of the stellar disk, then stripping will occur. This can be treated as a function of radius, given the changing stellar surface densities, to compute the fraction of gas lost. This process is deeply dependent on gas dynamics and the density of the host galaxy's gaseous halo, along with the distribution of cold gas in the dwarf itself, all of which make it much more difficult to assess ram pressure's role in the quenching process. Recent work has also shown that the momentum transfer analysis may not fully capture the physics at work; in the structured interstellar medium of the dwarf the hot gas may punch holes through cold gas, or ablate it into a warm phase (Weinberg, 2014). Star formation may also play a role in heating and puffing up the ISM during stripping, possibly enhancing the effectiveness of the process. All of this adds complications to a detailed study of the actual stripping event itself.

There is one other external process that must be mentioned, which is the effect of cosmic reionization on gas in dwarf galaxies. In the early universe at $z \sim 10$ the intergalactic medium surrounding galaxies goes from neutral to ionized, potentially heating that gas such that it is not able to be confined within the low mass dark matter halos that host dwarf galaxies (Efstathiou, 1992; Bullock et al., 2000; Gnedin, 2000). This process would limit galaxies to essentially the stellar mass that they had at the time reionization occurred, leaving them in a quenched state. This process is notably different in its observational effect as it quenches all dwarfs below a certain mass, regardless of their nearby environment, whereas all other environmental processes will operate differently on dwarfs with nearby large galaxies compared to isolated dwarfs. In general I will not focus on quenching by reionization in this work as it is hypothesized to affect the very lowest mass dwarfs, below the typical lower limit for my samples of galaxies (since these dwarfs are not detectable beyond the inner regions of the Milky Way). Consequently, any extension of the results in this work to lower mass systems must be appropriately cautious of the possibility of reionization-related quenching (or the inclusion of such dwarfs in larger galaxies by merging).

Both externally- and internally-triggered quenching processes can be shown to plausibly effect the required transformation, and it has been difficult to show which mode of quenching is actually at work. Part of this is due to the observational bias that dwarfs near the Milky Way are much more accessible to study, making it difficult to disentangle environmental effects from internal effects. Another difficulty is that the various quenching mechanisms do not leave unambiguous signatures of their effects in individual dwarfs; there is no way to distinguish a dwarf that has had its gas removed by ram pressure from one that has lost its gas via supernova winds, at least not with our present understanding of these processes. In clusters there are many galaxies that exhibit morphological features characteristic of ongoing ram pressure stripping (Chung et al., 2007; Cortese et al., 2007; Yagi et al., 2010; **?**). Such effects are much less commonly seen in dwarf galaxies. Extra-tidal stars have been found on occasion, as has gas that may be in the process of stripping, but cases are seldom conclusive enough to be proof of environmental quenching rather than an diffuse and extended but bound population (Palma et al., 2003; Majewski et al., 2005). Evidence of galactic outflows have been seen in a relatively small fraction of dwarf galaxies (Martin, 1999), but it is difficult to show that these winds will cause quenching.

The lack of decisive information in individual quenched dwarfs leads us to use the *population* of dwarfs as a method for distinguishing between different quenching processes. Though for any one dwarf it may be difficult to tell if, e.g., ram pressure caused its gas to be removed, it may be possible to show that the distribution of quenched and star forming dwarf galaxies is consistent or inconsistent with any given quenching process. In particular it should be possible to distinguish between environmental quenching and internally-driven quenching processes, and potentially to place constraints on the detailed active processes in these categories.

1.3 The role of this work

With this goal of a population-based study in mind, I would like to outline how the components of this thesis map onto the steps of this process. First and foremost, population-based studies require building up a sizable catalog of known and well-characterized dwarf galaxies. This process has required significant effort over many decades. Dwarf galaxies are rare, they are small, and they are faint. The process of discovering new Local Group dwarfs has progressed through several eras of technical capabilities, and with each new dataset becoming available another handful of systems were discovered. The brightest of these, other than the naked-eye Magellanic Clouds, were discovered by visual inspection of photographic plates, many of which were taken as part of the Palomar Observatory Sky Survey which covered the entire celestial sphere. New, fainter satellites were discovered when these photographic plates were digitized, allowing them to be searched programmatically and fainter systems recognized. These observations were still limited to a modest aperture telescope and the relatively insensitive (by modern standards, compared to CCDs) photographic plates, and both of these issues were alleviated with the advent of the Sloan Digital Sky Survey (SDSS). The SDSS covered over a quarter of the sky to much greater depth than any prior large survey, yielding a dramatic slew of new dwarf galaxies.

Some of the dwarfs found in the SDSS have fundamentally changed our understanding of galaxies by their mere existence. These are galaxies that have less stellar mass than many star clusters (gravitationally bound groups of stars formed simultaneously and with no dark matter), blurring that distinction in many ways (e.g., Willman et al., 2005; Belokurov et al., 2007). In addition to seeing fainter, the SDSS has enabled us to see farther, detecting dwarf galaxies at large distances than would be otherwise possible. This has extended the reach of our census from simply the Milky Way's dwarf system to also include Andromeda's satellites. Much of this work will thus treat these galaxies in common as Local Group dwarfs, defined roughly as all galaxies of Magellanic cloud brightness or fainter and within 3 Mpc of the Milky Way (Andromeda lies at 785 kpc, McConnachie et al., 2005).

Chapters II and III are a contribution to the field's efforts to discover and characterize the dwarfs of the Local Group, in this case focusing on the galaxies Andromeda XXVIII and Andromeda XXIX (confusingly abbreviated as And XXVIII or And XXIX). These galaxies occupy an interesting niche in their discovery, as they were found in SDSS imaging of the Southern Galactic hemisphere conducted relatively late in the survey. This data had been searched for nearby Milky Way dwarfs by various groups, but the imaging also contained a considerable amount of area that surrounded Andromeda. Searching for dwarfs at the distance of Andromeda is not qualitatively any different, but it does require that one's search is properly optimized for the difference. Part of the reason why other groups did not attempt this is because another much deeper survey (PAndAS, McConnachie et al., 2009) had already discovered a large number of satellites, particularly those that are too faint for SDSS, but this did not extend out in area as far as the SDSS data did. The result of all of this is that the distant outskirts of Andromeda were an ideal place to find dwarfs, and our search found two of them. The first is reported in Chapter II, and the second in Bell et al. (2011).

With only the initial discovery data our understanding of these galaxies was extremely poor. It was evident that a stellar system was present (we were confident that it was not a cluster of galaxies at moderate redshift, one of the principal contaminants), but the distance, size, and luminosity were only rough estimates. Most importantly for the work in this thesis, there was no evidence of whether the galaxies were star-forming or quenched. This determination requires a search for young stars, which if the star formation rate is relatively low as it is in many dwarfs, may be considerably fainter than the handful of giant stars that we had been able to detect in the SDSS. Deeper observations would be needed to check for these stars. We thus obtained long imaging observations of both galaxies on Gemini North/GMOS, which are presented in Chapter III. We combined this data with other observations that had been conducted independently by other groups, which obtained spectroscopy of stars in the galaxies and had searched for cold gas in And XXVIII. The result of these studies was to confirm that the galaxies are indeed quenched dwarf spheroidals, despite their large distances from Andromeda.

From a broadly qualitative standpoint, these galaxies were exceptions to the idea that dSphs were only found near their hosts. They were not the only exceptions, Tucana and Cetus are two galaxies that are often cited as similarly distant dSphs, but one would hope that the number of exceptions would not continue to proliferate.

A more quantitative theory behind this qualitative observation is not easily available, for the exact mechanism by dwarf galaxies are quenched is not known conclusively. As I argue in Chapter IV, a combination of tidal and ram pressure forces are likely to be at work, but these interactions with the host galaxy are complex and their results depend on numerous unknowns. The hot gas halo around the Milky Way is measured but with significant uncertainties (and its history is certainly unknown), as is true for the distribution of cold gas in dwarf irregulars. Most importantly, while analytic formulations are available for estimating when ram pressure is effective, these are simplified models based on momentum transfer that do not treat the gas dynamics in any detail.

The approach that is advanced in Chapters IV and V is thus: if we make a set of simplified assumptions about when satellites do or do not quench, can that reproduce the observed distribution of dwarf galaxies? The key to both chapters is that while our quenching assumptions are necessarily simplified, we can provide the cosmological context necessary to relate these assumptions to their present-day observable results. This is done by using simulations of the behavior of dark matter halos in cosmological simulations, which provide the history of interactions between halos that could cause quenching. Our assumptions thus impute the behavior of gas onto this dark matter-only cosmological framework. In Chapter IV the distribution we are attempting to match is the radial profile of quenched satellites, which is remarkably decisive in distinguishing between various simple models for quenching.

Chapter V focuses on the mass dependence of quenched satellites, where lower-mass satellites are almost ubiquitously quenched, compared to satellites at masses closer to the Magellanic clouds where quenching appears much less effective (the number of star forming galaxies that exist as satellites of a larger host is much larger). The observation of this effect is novel, as it requires comparing galaxies seen only in the Local Group with galaxies that are only seen in sufficient numbers at large distances beyond the Local Group. Both samples come with distinct selection effects and biases, and our efforts to homogenize these two samples is relatively unique. The significant change in the effectiveness of quenching is not anticipated by any preexisting models, and thus it is difficult for us to confirm or rule-out any particular theory of this change. Our efforts focus on providing a physical interpretation of this change, as a difference in the "susceptibility" of the galaxies to ram pressure, or as a variation in the timescale over which satellites quench in their host halos. Neither of these methods are truly *predictive*, but they are useful physical interpretations for understanding the observed quenching fractions.

Chapter VI deviates somewhat from the goals of the previous chapters. In this chapter the focus is not on how the host galaxy affects its satellites, but instead how satellites might affect the evolution of their host galaxy. This is most commonly seen in the buildup of stellar halos and the presence of stellar streams in the halo. It is also possible that these satellites exhibit an effect on the disk of their hosts: by bombarding it with relatively massive satellite halos (by dwarf standards) there could be significant dynamical heating of the stellar disk.

This has been hypothesized to be the cause of the "Monoceros Ring" (MRi) in the outer Galactic disk. Chapter VI presents the first large-area filled map of the MRi on both the northern and southern sides of the Galactic disk. This structure has been until then only seen in the SDSS (with much less area than is available in Pan-STARRS1) and in various individually pointed observations, which were never able to fully capture the extended morphology of the structure. There was thus a proliferation of models between various tidal streams and various disk interaction scenarios, but very little conclusive differentiation was available. Our Pan-STARRS1 map gives a much better handle on this, and Chapter VI shows a direct comparison between these maps and numerical models, projected and sampled as similarly as possible to enable strong comparisons. Between models of streams and models of disk interactions we find that no present model perfectly reproduces all the features we observe, but that is as expected as these models predate our observations and thus are not tuned to match the new features we see. However, we there appear to be more challenges ahead for stream models than for the disk interaction models, and it seems reasonable that a fuller exploration of the possibilities of disk interactions may yield even better agreement than the simple models currently in use.

CHAPTER II

Andromeda XXVIII: A Dwarf Galaxy More Than 350 kpc from Andromeda[1]

2.1 Abstract

We report the discovery of a new dwarf galaxy, Andromeda XXVIII, using data from the recently-released SDSS DR8. The galaxy is a likely satellite of Andromeda, and, at a separation of 365^{+17}_{-14} kpc, would be one of the most distant of Andromeda's satellites. Its heliocentric distance is 650^{+150}_{-80} kpc, and analysis of its structure and luminosity show that it has an absolute magnitude of $M_V = -8.5^{+0.4}_{-1.0}$ and half-light radius of $r_h = 210^{+60}_{-50}$ pc, similar to many other faint Local Group dwarfs. With presently-available imaging we are unable to determine if there is ongoing or recent star formation, which prevents us from classifying it as a dwarf spheroidal or dwarf irregular.

2.2 Introduction

In recent years the environment of Andromeda has been a prime location for the discovery of dwarf galaxies and tidal structures, much of which has been enabled

---

[1] This chapter was originally published in the Astrophysical Journal Letters by Colin T. Slater, Eric F. Bell, and Nicolas F. Martin 2011, 742, 14.

by large surveys on the Isaac Newton Telescope (Ferguson et al., 2002; Irwin et al., 2008) and the Canada-France-Hawaii telescope (Ibata et al., 2007; McConnachie et al., 2009; Martin et al., 2006, 2009). These surveys have obtained deep observations over a significant fraction of the area within 180 kpc of Andromeda, and yielded a considerable number of new discoveries. In addition to these dedicated surveys, two satellites of Andromeda have been found in the Sloan Digital Sky Survey (SDSS) imaging (And IX and X, Zucker et al., 2004, 2007), using an early SDSS scan targeting Andromeda specifically. More recently, the SDSS project has released Data Release 8 (DR8, Aihara et al., 2011), which adds ~ 2500 deg^2 of imaging coverage in the south Galactic cap and covers almost half of the area within 35° of Andromeda. While the SDSS is substantially shallower than the dedicated M31 surveys, it is deep enough to enable the discovery of relatively bright (by today's standards) dwarf galaxies.

It is in this new SDSS coverage that we report the discovery of a dwarf galaxy, which we are preliminarily calling Andromeda XXVIII. The dwarf is separated from Andromeda by 27.7° on the sky, which gives it a minimum distance to M31 of 365 kpc. This distance is significantly larger than the virial radius of Andromeda ($r_{\rm vir} = 300$ kpc, Klypin et al., 2002). And XXVIII is therefore one of a handful of known examples of dwarf galaxies that are less likely to be significantly influenced by the environment of their host galaxy, which makes them important test cases for theories of dwarf galaxy formation and evolution.

2.3 Detection

At the distance of Andromeda (785 ± 25 kpc, McConnachie et al., 2005), searches for dwarf galaxies in the SDSS are limited to using red giant branch (RGB) stars as tracers of the underlying population of main-sequence and subgiant stars. Alternative tracers commonly used for detecting dwarf galaxies around the Milky Way, such as horizontal branch or main sequence turn-off stars, are much too faint to be detected.

To detect dwarf galaxies in SDSS we compute star counts in $2' \times 2'$ bins, selecting only stars with $0.3 < \mathrm{r} - \mathrm{i} < 0.8$, colors roughly similar to metal-poor giant branch stars. Overdensities are readily apparent upon visual inspection of the resulting map as "hot pixels", typically with counts of 10-15 objects as compared to the background of 1-3 objects per bin. Most of these overdensities are galaxy clusters at intermediate redshift, which contain many spatially-unresolved member galaxies that are erroneously classified as stars and have similar colors as giant branch stars. Visual inspection of the SDSS image along with the color-magnitude diagram is sufficient to reject these false-positives.

The SDSS image of And XXVIII is shown in Figure 2.1, along with an image of And IX for comparison, and the properties of And XXVIII are summarized in Table 2.1. The color-magnitude diagram of the dwarf is shown in Figure 2.2, along with a CMD of the field region surrounding the dwarf, a plot of measured star positions, and a histogram as a function of i-band magnitude. These plots are also shown for And IX, another dwarf galaxy that was discovered in SDSS. An isochrone from Dotter et al. (2008) of an old, metal-poor system (12 Gyr old, [Fe/H] = -2.0) is also shown on the CMD to illustrate the position of the red giant branch. An overdensity at $0.3 < (\mathrm{r} - \mathrm{i})_0 < 0.8$ is clearly visible. The RGB is very wide in color, owing to considerable photometric uncertainty at very faint magnitudes in SDSS, which is illustrated by the error bar on the left side of the CMD (estimated from repeat imaging of SDSS stripe 82; Bramich et al., 2008).

2.4 Properties of And XXVIII

We computed the distance to And XXVIII by measuring the magnitude of the tip of the red giant branch (TRGB), which has a roughly constant absolute magnitude in metal-poor stellar systems (Bellazzini et al., 2001). This method has been used extensively for dwarf galaxies (e.g., McConnachie et al., 2005; Martin et al., 2009), since

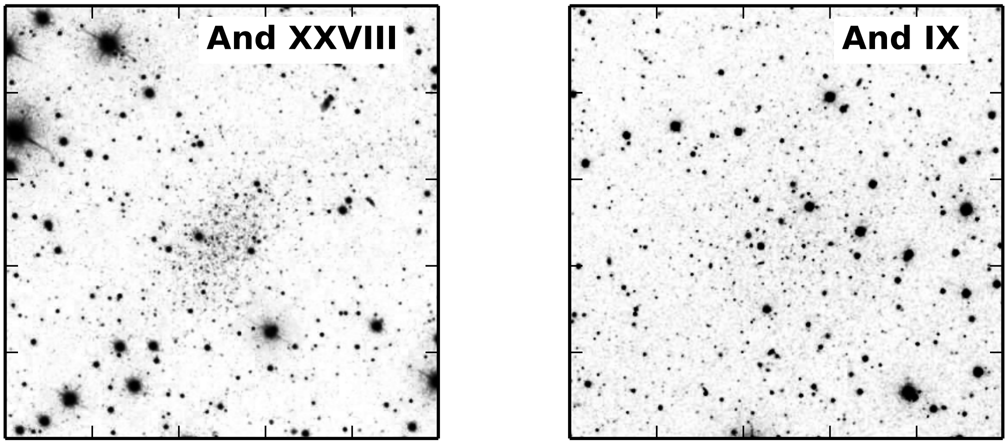

Figure 2.1: SDSS image of And XXVIII (*left*), and, for comparison, an SDSS image of And IX (*right*), which was also discovered in SDSS (Zucker et al., 2004). Both images were obtained from the SDSS SkyServer, and are $6.6' \times 6.6'$. North is up, and east is to the left.

Table 2.1: Properties of And XXVIII

Parameter	
α (J2000)	$22^{\mathrm{h}}\ 32^{\mathrm{m}}\ 41\overset{\mathrm{s}}{.}2$
δ (J2000)	$31^\circ\ 12'\ 58.2''$
E(B-V)	0.087
Ellipticity	0.34 ± 0.13
Position Angle (N to E)	$39^\circ \pm 16$
r_h	$1\overset{\prime}{.}11 \pm 0\overset{\prime}{.}21$
r_h	210^{+60}_{-50} pc
D	650^{+150}_{-80} kpc
$(m-M)_0$	$24.1^{+0.5}_{-0.2}$
r_{M31}	365^{+17}_{-14} kpc
M_V	$-8.5^{+0.4}_{-1.0}$

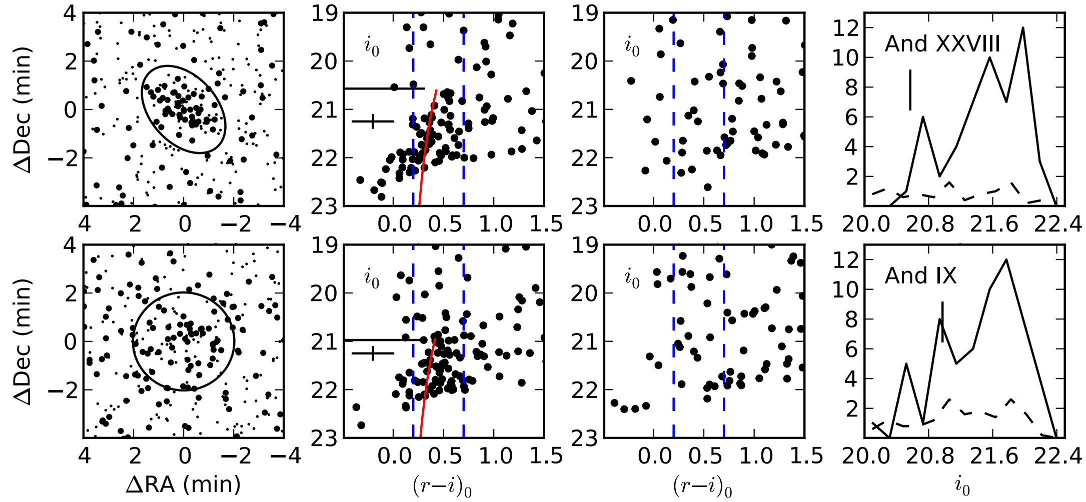

Figure 2.2: Detection plots for And XXVIII (*top row*), with the same plots for And IX shown for comparison ($M_V \sim -8.3$, *bottom row*). *Far left*: the position of stars detected in SDSS is plotted, with stars that fall within our color-cut as large points, and other stars as small points. An ellipse at 1.5 times the half light radius is also shown. *Middle left*: color-magnitude diagram of stars inside twice the half-light radius. The color-cut used to detect RGB stars is shown by the dashed vertical lines. An isochrone from Dotter et al. (2008) is overplotted ([Fe/H]=-2.0 for And XXVIII, [Fe/H]=-2.2 for And IX), along with a horizontal line indicating the tip of the red giant branch, and a representative photometric error bar on the left. *Middle right*: color-magnitude diagram of a background annulus. *Far right*: luminosity function of the color-selected red giant stars (solid line), and the background annulus (dashed). The vertical line denotes the measured TRGB position.

the TRGB is often the only distinguishable feature in the color-magnitude diagram of distant systems.

Quantitatively measuring the position of the TRGB is more complicated than it would appear from looking at the color-magnitude diagram. This is especially true in dwarf galaxies, where the giant branch is sparsely populated and the small number counts lead to significant "shot noise" (Martin et al., 2008). We used the maximum-likelihood estimator described in Makarov et al. (2006), which modeled the TRGB luminosity function as

$$\psi = \begin{cases} 10^{a(m-m_{\mathrm{TRGB}})+b} & m - m_{\mathrm{TRGB}} \geq 0, \\ 10^{c(m-m_{\mathrm{TRGB}})} & m - m_{\mathrm{TRGB}} < 0. \end{cases} \tag{2.1}$$

This broken power-law form takes three parameters: a and c are the slopes of the luminosity function fainter and brigher than the TRGB, while b is the strength of the transition at the TRGB. We adopted the values from Makarov et al. (2006) of $a = 0.3$ and $c = 0.2$, and $b = 0.6$. For the TRGB fit we selected stars in our RGB color cuts with magnitudes $19.5 < i < 21.7$ to avoid incompleteness at faint magnitudes. Though the data at the faintest magnitudes are not critical for finding the position of breaks in the luminosity function that might correspond to the TRGB, the faint end of the luminosity function does affect our ability to determine the statistical significance of a measured TRGB position. As a result we try to use the deepest data possible without reaching significant photometric incompleteness. The SDSS photometry was converted to Johnson I-band using the prescriptions of Jordi et al. (2006), and an intrinsic I-band magnitude of the TRGB was assumed of -4.04 ± 0.12 (Bellazzini et al., 2001). The likelihood function of the model as a function of TRGB position is shown in Figure 2.3. We find that the likelihood is maximized at $m_{I,\mathrm{TRGB}} = 20.1$, but a second peak also appears at $m_{I,\mathrm{TRGB}} = 20.6$ (in the Gunn-i filter, 20.6 and 21.1, respectively). This is the result of a clump of stars slightly fainter than $m_I = 20.1$,

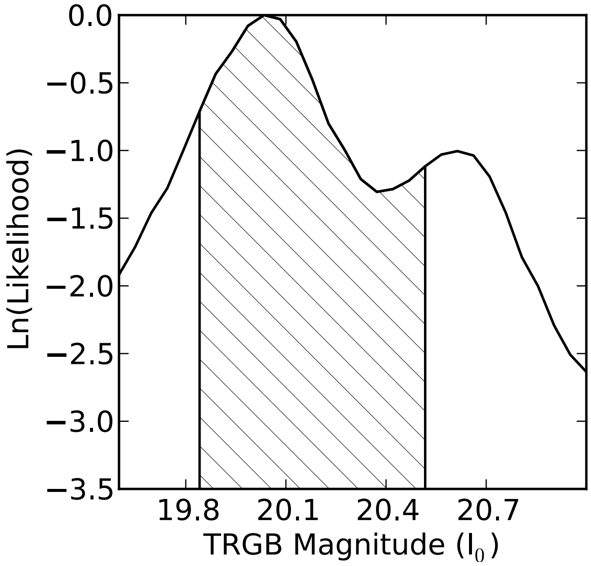

Figure 2.3: Likelihood function of the TRGB position of And XXVIII, arbitrarily normalized. The hatched region is the 67% confidence interval. The secondary maximum is clearly visible and less significant than the primary peak, but cannot be ruled out.

which causes the TRGB magnitude to change significantly depending on whether or not they are included as part of the RGB. Though the fainter peak cannot be ruled out, the TRGB magnitude we quote of $m_{I,\mathrm{TRGB}} = 20.1^{+0.5}_{-0.1}$ is the center of the more likely peak. The uncertainty on this TRGB value is the 67% confidence interval, which was computed by creating a cumulative probability distribution function and measuring the 16.5% through 83.5% region. The resulting uncertainties are asymmetric, and this asymmetry will propagate into all derived quantities, but this is a natural result of the bimodal likelihood function. The measured TRGB position yields a distance modulus of $24.1^{+0.5}_{-0.2}$, which places the dwarf at a heliocentric distance of 650^{+150}_{-80} kpc. Because this is very similar to the point of closest approach to Andromeda along this line of sight (the "tangent point"), the distance between And XXVIII and M31 is largely insensitive to errors in the heliocentric distance, and is measured to be $r_{\mathrm{M31}} = 365^{+17}_{-14}$ kpc.

To measure the luminosity of And XXVIII, we computed luminosity functions from SDSS data for three similar dwarf galaxies with known distances and luminosities (And III, $M_V = -9.87 \pm 0.3$, McConnachie & Irwin 2006; And V, $M_V = -9.22 \pm 0.3$, McConnachie & Irwin 2006; And X, $M_V = -8.13 \pm 0.5$, Zucker et al. 2007). We scaled these galaxies to a fiducial luminosity and distance by correcting the dereddened apparent magnitude of each galaxy's stars for their respective distances, and by scaling the number of stars in each luminosity bin by the total luminosity of the galaxy. We then took the mean of these profiles to produce a composite luminosity function that was less affected by the "shot noise" inherent in such low number count systems. Since our comparison objects span a range of distances, we applied a faint-magnitude cut to ensure that the luminosity function of even the most distant comparison dwarf was still photometrically complete. For stars with colors typical of RGB stars we find that the data are complete to approximately $i = 21.7$ (non-dereddened). Since the most distant comparison dwarf has a distance modulus that is greater than than of And XXVIII by 0.4, our corresponding completeness cut on And XXVIII for the luminosity function comparison was $i = 21.3$ ($i_0 = 21.5$). This binned, composite luminosity function was then scaled to match that of And XXVIII (again using a maximum likelihood method to properly account for Poissonian uncertainties, and with uncertainties on the comparison dwarfs' luminosities included), and the scaling factor thus determined the luminosity of the galaxy relative to the fiducial luminosity. This method produces results largely equivalent to the method of Martin et al. (2008) for relatively bright dwarfs. The luminosity determined by this method is $M_V = -8.5^{+0.4}_{-1.0}$ (the large uncertainty is primarily due to the uncertainity in the distance measurement) is generally similar to that of other local group dwarfs. To ensure that issues of photometric completeness or other systematics did not bias our composite luminosity function, we also constructed a luminosity function from deep observations of the Draco dwarf (obtained on the Canada-France-Hawaii Telescope, Ségall et al., 2007), and used the same scaling method to measure the luminosity of And XXVIII, which resulted in an identical value. As a final check, we compared And XXVIII to the model luminosity functions of Dotter et al. (2008), and again obtained a luminosity that is in good agreement with the other methods ($M_V = -8.32$).

The considerable scatter in color of the RGB stars due to photometric error makes it difficult to determine the metallicity of the galaxy. This uncertainty is illustrated by the CMD of And IX (Figure 2.2, bottom middle-left), which was measured by Collins et al. (2010) with deep imaging to have [Fe/H] $= -2.2 \pm 0.2$. Though the fit to the Dotter isochrone is very good in the Collins et al. (2010) data, the SDSS data show significant scatter in color and appear to be systematically offset in color from the isochrone. It is unclear whether this is the result of inaccuracies in the isochrone or calibration error at very faint magnitudes in the SDSS, but because of these uncertainties, it is not be possible to constrain the metallicity of the galaxy with the observations available. We can nevertheless say that the CMD of And XXVIII is not obviously dissimilar to other metal-poor dwarf galaxies.

We computed the radial profile of And XXVIII, along with the position, half-light radius, eccentricity, and position angle using the maximum likelihood technique described by Martin et al. (2008). This method assumes an exponential profile for the dwarf galaxy and a constant background level. Figure 2.4 shows on the left maximum likelihood contours of the half-light radius, ellipticity (ϵ), position angle (θ), and number of detected stars in the overdensity within the SDSS data ($N_\star$), while the right side shows the radial profile fit. The structural parameters have one-dimensional 1- , 2- , and 3-σ confidence areas overlaid. And XXVIII is well-populated enough, even in the relatively shallow SDSS data, to permit easy determination of these parameters without large uncertainties. The fact that $N_\star = 0$ is excluded at $\gg 3\sigma$ provides a quantitative indication that this overdensity is unlikely to be a statistical artifact. The fact that the half-light radius is well-determined also gives confidence that the

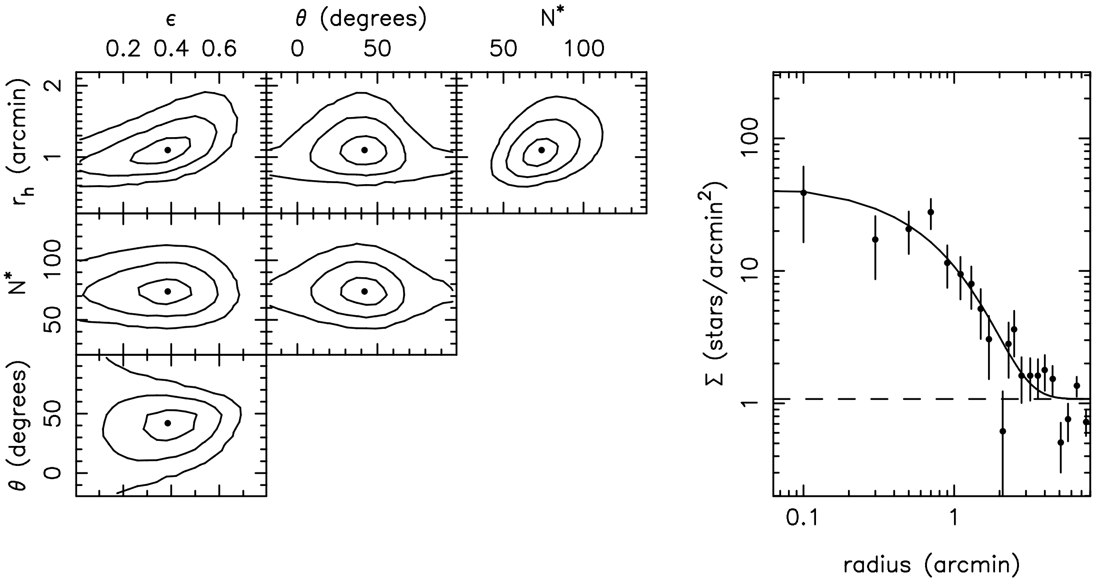

Figure 2.4: Structural parameters and radial profile of And XXVIII. *Left:* Confidence areas for the measurement of half-light radius, ellipticity, position angle, and number of detected stars. The contours correspond, when projected on the axes, to 1-, 2-, and 3-σ uncertainties (to allow reading of the marginalized $1-\sigma$ value straight from the plot for each parameter). The filled circles correspond to the peak of the maximum likelihood function. *Right:* Radial profile of And XXVIII, where stars have been binned according to the best-fit structural parameters with Poisson uncertainties on each bin. The solid black line is the best-fit exponential profile, while the dashed horizontal line is the measured background level.

overdensity is real, since the fitting procedure usually finds unreasonably large values for r_h when run on non-galaxies. The half-light radius of $r_h = 210^{+60}_{-50}$ pc is typical of other Local Group dwarf galaxies and is roughly the size of Draco. The position angle has a considerable uncertainty associated with it, along with some covariance with ellipticity. These factors may make the ellipse in the top-left panel of Figure 2.2 appear slightly misaligned when juding the fit by eye.

2.5 Discussion

Throughout this work we have referred to the newly discovered dwarf galaxy as Andromeda XXVIII, but this may not be the most accurate identifier to use. The dwarf is actually located in the constellation Pegasus, and could also be identified as Pegasus II, as is the convention with Milky Way and Local Group satellites. However, its properties make it a likely satellite of M31, and hence we follow the convention of naming satellites of M31 with the prefix Andromeda regardless of their actual position. Since we have neither its radial velocity nor its proper motion, we certainly cannot say whether the dwarf galaxy is bound to M31, but its distance to M31 is within the range of other galaxies in the M31 system, and it is much further from the Milky Way than we would expect for dwarfs bound to the Milky Way. If, on further study, the galaxy is determined to be unbound from M31, then it should properly be referred to as Pegasus II. Further discussion of the complexities of dwarf galaxy names can be found in the Appendix of Martin et al. (2009).

The most intriguing feature of And XXVIII is its large distance from Andromeda, which suggests that it might not have been strongly affected by interactions with other galaxies. This could make it a prime test case for studies of dwarf galaxy formation. The morphology and star formation history of And XXVIII are of particular interest, as dwarf galaxies in the Local group that lay beyond 300-400 kpc from their host tend to be dwarf irregular galaxies, while those in close proximity with their host tend to be dwarf spheroidals. This morphology-density relationship (Grebel et al., 2003) is not without exceptions; for instance, the dwarf spheroidals Tucana, Cetus, and the possible dwarf spheroidal And XVIII are all more than 400 kpc from the nearest non-dwarf galaxy. These distant dwarf spheroidals are a unique test for theories which suggest that dwarf spheroidals form from dwarf irregulars via tidal interactions or ram pressure stripping (Mayer et al., 2006; Weisz et al., 2011), since these galaxies could be in the beginning stages of such a process and could exhibit evidence of such an ongoing transformation. If And XXVIII were confirmed to be a dwarf spheroidal without any recent star formation, it would add another test case for these theories.

Alternatively, if star formation is detected in And XXVIII, it would be one of the lowest mass star-forming galaxies known, and roughly analagous to LGS 3 (Thuan & Martin, 1979) or Leo T (Irwin et al., 2007). The ability of such low mass galaxies to retain gas and form stars is poorly understood, and identifying another member of this class of galaxies would be a benefit to efforts to further elucidate their nature.

Unfortunately, with shallow SDSS imaging we cannot conclusively determine whether or not And XXVIII has ongoing or recent star formation. From the CMD of Leo T, the blue-loop stars that indicate recent star formation are roughly 1.5 - 2 magnitudes fainter than the tip of the red giant branch. Since the SDSS data of And XXVIII only extend approximately one magnitude below the TRGB, blue-loop stars are not detectable. We have also looked for HI in the galaxy using the Leiden/Argentine/Bonn Survey (Kalberla et al., 2005). This survey clearly detects the HI gas present in LGS 3 and Leo T ($M_{\rm HI} = 1.6 \times 10^5$, $\sim 4.3 \times 10^5 M_\odot$, respectively, Grcevich & Putman, 2009), but shows no emission from And XXVIII. This could, however, be the result of the velocity of the dwarf falling outside the bandwidth used for the survey ($-400 < v_{\rm LSR} < 400$ km s^{-1}), so a conclusive determination of the HI gas content will require a measurement of the radial velocity of the galaxy.

Though the exact significance of And XXVIII will not be known until follow-up observations are conducted, it is clear that dwarf galaxies in the outer regions of the Local Group are in a unique environment that enables their detailed study before their properties are significantly altered by interactions with their host galaxy upon infall. Increasing the sample of nearby but isolated dwarfs thus provides the data necessary to advance theories of dwarf galaxy formation and evolution.

CHAPTER III

A Deep Study of the Dwarf Satellites Andromeda XXVIII & Andromeda XXIX[1]

3.1 Abstract

We present the results of a deep study of the isolated dwarf galaxies Andromeda XXVIII and Andromeda XXIX with Gemini/GMOS and Keck/DEIMOS. Both galaxies are shown to host old, metal-poor stellar populations with no detectable recent star formation, conclusively identifying both of them as dwarf spheroidal galaxies (dSphs). And XXVIII exhibits a complex horizontal branch morphology, which is suggestive of metallicity enrichment and thus an extended period of star formation in the past. Decomposing the horizontal branch into blue (metal poor, assumed to be older) and red (relatively more metal rich, assumed to be younger) populations shows that the metal rich are also more spatially concentrated in the center of the galaxy. We use spectroscopic measurements of the Calcium triplet, combined with the improved precision of the Gemini photometry, to measure the metallicity of the galaxies, confirming the metallicity spread and showing that they both lie on the luminosity-metallicity relation for dwarf satellites. Taken together, the galaxies exhibit largely typical properties for dSphs despite their significant distances from M31.

---

[1] This chapter was originally published in the Astrophysical Journal by Colin T. Slater, Eric F. Bell, Nicolas F. Martin, Erik J. Tollerud, and Nhung Ho, 2015, 806, 230.

These dwarfs thus place particularly significant constraints on models of dSph formation involving environmental processess such as tidal or ram pressure stripping. Such models must be able to completely transform the two galaxies into dSphs in no more than two pericentric passages around M31, while maintaining a significant stellar populations gradient. Reproducing these features is a prime requirement for models of dSph formation to demonstrate not just the plausibility of environmental transformation but the capability of accurately recreating real dSphs.

3.2 Introduction

The unique physical properties and environments of dwarf galaxies make them excellent test cases for improving our understanding of the processes that affect the structure, stellar populations, and evolution of galaxies. Because of their shallow potential wells, dwarf galaxies are particularly sensitive to a wide range of processes that may only weakly affect larger galaxies. These processes range from cosmological scales, such as heating by the UV background radiation (Gnedin, 2000), to interactions at galaxy scales such as tidal stripping and tidal stirring (Mayer et al., 2001; Klimentowski et al., 2009; Kravtsov et al., 2004), resonant stripping (D'Onghia et al., 2009), and ram pressure stripping (Mayer et al., 2006), to the effects of feedback from from the dwarfs themselves (Dekel & Silk, 1986; Mac Low & Ferrara, 1999; Gnedin & Zhao, 2002; Sawala et al., 2010).

Many studies have focused on understanding the differences between the gas-rich, star forming dwarf irregular galaxies (dIrrs) and the gas-poor, non-star-forming dwarf spheroidals. While a number of processes could suitably recreate the broad properties of this differentiation, finding observational evidence in support of any specific theory has been difficult. One of the main clues in this effort is the spatial distribution of dwarfs; while dIrrs can be found throughout the Local Group, dSphs principally are only found within 200-300 kpc of a larger host galaxy such as the

Milky Way or Andromeda (Einasto et al., 1974; van den Bergh, 1994; Grebel et al., 2003). This is trend is also reflected in the gas content of Local Group dwarfs (Blitz & Robishaw, 2000; Grcevich & Putman, 2009). This spatial dependence seems to indicate that environmental effects such as tides and ram pressure stripping are likely to be responsible for creating dSphs. However, there are outliers from this trend, such as Cetus, Tucana, and Andromeda XV, which are dSphs that lie more than 700 kpc from either the Milky Way or Andromeda. The existence of such distant dSphs may suggest that alternative channels for dSph formation exist (Kazantzidis et al., 2011b), or it could be an incidental effect seen in galaxies that have passed through a larger host on very radial orbits (Chapter IV, and see also Teyssier et al., 2012).

The set of isolated dwarf galaxies was recently enlarged by the discovery of Andromeda XXVIII and XXIX, which by their position on the sky were known to be approximately 360 and 200 kpc from Andromeda, respectively (Chapter II, and Bell et al., 2011). While And XXIX was identified as a dSph by the images confirming it as a galaxy, there was no comparable data on And XXVIII (beyond the initial SDSS discovery data) with which to identify it as a dSph or dIrr. We thus sought to obtain deeper imaging of both galaxies down to the horizontal branch level which would enable a conclusive identification of the galaxies as dSphs or dIrrs by constraining any possible recent star formation. In addition, the deep photometry permits more precise determination of the spatial structure and enables the interpretation of the spectroscopic Calcium triplet data from Tollerud et al. (2013) to obtain a metallicity measurement. As we will discuss, the information derived from these measurements along with dynamical considerations imposed by their position in the Local Group can together place significant constraints on plausible mechanisms for the origin of these two dSphs.

This work is organized as follows: we discuss the imaging data and the reduction process in Section 3.3, and illustrate the general features of the color-magnitude diagram in Section 3.4. Spectroscopic metallicities are presented in Section 3.5, and the structure and stellar populations of the dwarfs are discussed in Section 3.6. We discuss the implications of these results for theories of dSph formation in Section 3.7.

3.3 Imaging Observations & Data Reduction

Between 22 July 2012 and 13 August 2012 we obtained deep images of And XXVIII and XXIX with the GMOS instrument on Gemini-North (Gemini program GN-2012B-Q-40). The observations for each dwarf consisted of a total of 3150 seconds in SDSS-i band and 2925 seconds in r, centered on the dwarf. Because the dwarfs each nearly fill the field of view of the instrument, we also obtained a pair of flanking exposures for each dwarf to provide an "off-source" region for estimating the contamination from background sources. These exposures consisted of at least 1350 s in both r and i, though some fields received a small number of extra exposures. The images were all taken in 70th percentile image quality conditions or better, which yielded excellent results with the point source full width at half maximum ranging between $0.47''$and $0.8''$.

All of the images were bias subtracted, flat fielded, and coadded using the standard bias frames and twilight flats provided by Gemini. The reduced images can be seen in Figure 3.1. Residual flat fielding and/or background subtraction uncertainity exists at the 1% level (0.01 magnitudes, roughly peak to valley). PSF photometry was performed using DAOPHOT (Stetson, 1987), which enabled accurate measurements even in the somewhat crowded centers of the dwarfs. In many cases the seeing in one filter was much better than the other, such as for the core of And XXVIII where the seeing was $0.47''$ in i and $0.68''$ in r. In these cases we chose to first detect and measure the position of stars in the image with the best seeing, and then require the photometry of the other band to reuse the positions of stars detected in the better band. This significantly extends our detection limit, which would otherwise be set by the shallower band, but with limited color information at these faint magnitudes.

The images were calibrated to measurements from the Sloan Digital Sky Survey (SDSS), Data Release 9 (Ahn et al., 2012). For each stacked image we cross-matched all objects from the SDSS catalog that overlapped our fields, with colors between $-0.2 < (r-i)_0 < 0.6$, and classified as stars both by SDSS and DAOPHOT. Star-galaxy separation was performed using the "sharp" parameter from DAOPHOT. From this we measured the weighted mean offset between the SDSS magnitudes and the instrumental magnitudes to determine the zeropoint for each field. Between the saturation limit of the Gemini data, mitigated by taking several exposures, and faint limits of the SDSS data (corresponding to approximately $19 < i < 22.5$ and $19.5 < r < 22.5$) there were of order 100 stars used for the calibration of each frame. Based on the calculated stellar measurement uncertainties the formal uncertainty on the calibration is at the millimag level, but unaccounted systematic effects likely dominate the statistical uncertainty (e.g., precision reddening measurements). All magnitudes were dereddened with the extinction values from Schlafly & Finkbeiner (2011).

The photometric completeness of each stacked image was estimated by artificial star tests. For each field we took the PSF used by DAOPHOT for that field and inserted a large grid of artificial stars, with all of the stars at the same magnitude but with Poisson noise on the actual pixel values added to each image. This was performed for both r and i band images simultaneously, and the resulting pair of images was then run through the same automated DAOPHOT pipeline that was used on the original image. Artificial stars were inserted over a grid of i band magnitudes and r-i colors, producing measurements of the recovery rate that cover the entire CMD. The 50% completeness limit for both dwarfs is at least $r_0 = 25.5$, with slightly deeper data in the i-band for And XXVIII.

The observed CMDs suffer from both foreground and background contamination. Foreground dwarf stars in the Miky Way tend to contribute at the bright end of the

CMD. At the faint end, distant galaxies that are too small to be resolved become the dominant source of contamination. This effect can quickly become significant at fainter magnitudes due to the rapid rise in the observed galaxy luminosity function. This effect was minimized by the superb seeing at the Gemini observatory, which allowed smaller galaxies to be resolved and excluded from our sample.

3.4 Observed CMDs

The CMDs of And XXVIII and XXIX are shown in the left panels of Figures 3.2 and 3.3, respectively. A 12 Gyr old isochrone from Dotter et al. (2008) is overlaid at the distances and spectroscopic metallicities determined later in this work. Both dwarfs show a well-populated giant branch with a very prominent red clump/red horizontal branch (RC/RHB) near $r_0 \sim 24.5$ - 25.0. This feature is particularly clear as a large bump in the luminosity functions of each dwarf, shown by the thick black line in the right panels of Figure 3.2 and 3.3. In addition to the RC/RHB, And XXVIII also shows a blue horizontal branch (BHB) slightly fainter than $r_0 \sim 25.0$ and spanning $-0.3 < (r-i)_0 < 0.0$ in color. The luminosity function for stars with $(r-i)_0 < 0.0$ is shown by the thin line on the right panel of Figure 3.2. The presence of a complex horizontal branch suggests that And XXVIII has had an extended star formation history (SFH), since the BHB is typically seen in the oldest globular clusters, while the RHB tends to appear in globular clusters roughly 2-4 Gyr younger than the oldest populations (Stetson et al., 1989; Sarajedini et al., 1995), although a few globular clusters do show both BHB and RHB (An et al., 2008). The additional information from the spectroscopic metallicity spread, as will be discussed below, also confirms the extended star formation in both dwarfs. And XXIX does not show the same prominent BHB. There are 5-10 stars in a similar position as the BHB in And XXVIII, but this is almost negligible compared to the 100 or more stars in the BHB of And XXVIII and could be background contamination. This does not indicate that there is no ancient population in And XXIX, as, for example, the Draco dSph also contains very few BHB stars (Ségall et al., 2007).

There is a notable absence of any young main-sequence stars in the observed CMDs of both XXVIII and XXIX, which suggests that there has not been any recent star formation at appreciable rates in either galaxy. The handful of stars brighter than the HB and on the blue side of the RGB are consistent with foreground (or background) contamination. The CMD of And XXIX has an almost negligible number of stars bluewards of the RGB at any magnitude. The CMD of And XXVIII does show some blue detections below the BHB, but it is difficult to conclusively identify their origin. Since the precision of the colors degrades at faint magnitudes, these detections could be an (artificial) broadening of the RGB, possibly scattering more stars towards the blue due to the somewhat shallower depth of the r-band exposures. It is also possible that they are background sources or false detections from noise, both of which could be strongly weighted towards the faintest magnitudes. None of these origins are clearly favored and some combination could be at work, but there is not sufficient evidence to believe that these sources are main sequence stars.

The absence of observed young main sequence stars in And XXVIII is complemented by recent work that shows little to no cold gas in the galaxy. Observations with the Westerbork Synthesis Radio Telescope place a $5-\sigma$ upper limit on the total HI mass of 2.8×10^3 $M_\odot$ (T. Oosterloo, private communication). For comparison, the similarly low-mass dwarf Leo T has had recent star formation and contains $\sim 2.8\times10^5$ $M_\odot$ of HI (Ryan-Weber et al., 2008), while most dSphs have upper limits at this level or less (Grcevich & Putman, 2009). This stringent limit on the gas in And XXVIII adds further evidence that it is a dSph.

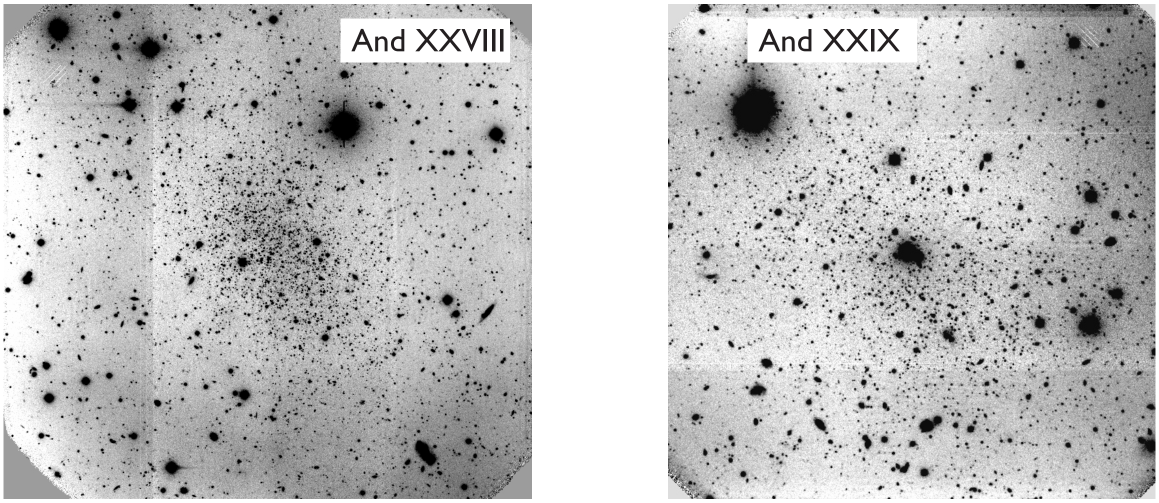

Figure 3.1: Stacked i-band image of And XXVIII on the left, and of And XXIX on the right. North is up, and East is to the left. Both images are approximately 5.6′on a side. The saturated feature near the center of And XXIX is a combination of a foreground star and two background galaxies.

Table 3.1: Properties of And XXVIII & XXIX

Parameter	And XXVIII	And XXIX
α (J2000)	$22^{\mathrm{h}}\ 32^{\mathrm{m}}\ 41\overset{\mathrm{s}}{.}5$	$23^{\mathrm{h}}\ 58^{\mathrm{m}}\ 55\overset{\mathrm{s}}{.}6$
δ (J2000)	$31^\circ\ 13'\ 3.7''$	$30^\circ\ 45'\ 20.2''$
E(B-V)	0.080	0.040
Ellipticity	0.43 ± 0.02	0.29 ± 0.04
Position Angle (N to E)	$34^\circ \pm 1^\circ$	$55^\circ \pm 4^\circ$
r_h	$1\overset{\prime}{.}20 \pm 0\overset{\prime}{.}03$	$1\overset{\prime}{.}39 \pm 0\overset{\prime}{.}08$
r_h	280 ± 20 pc	315 ± 15 pc
D	811 ± 48 kpc	829 ± 42 kpc
$(m-M)_0$	24.55 ± 0.13	24.59 ± 0.11
r_{M31}	385^{+18}_{-13} kpc	198^{+18}_{-10} kpc
M_V	-8.7 ± 0.4	-8.5 ± 0.3
$\langle[\mathrm{Fe/H}]\rangle$	-1.84 ± 0.15	-1.90 ± 0.12
$\sigma([\mathrm{Fe/H}])$	0.65 ± 0.15	0.57 ± 0.11
HI	$< 2.8 \times 10^3 M_\odot$	

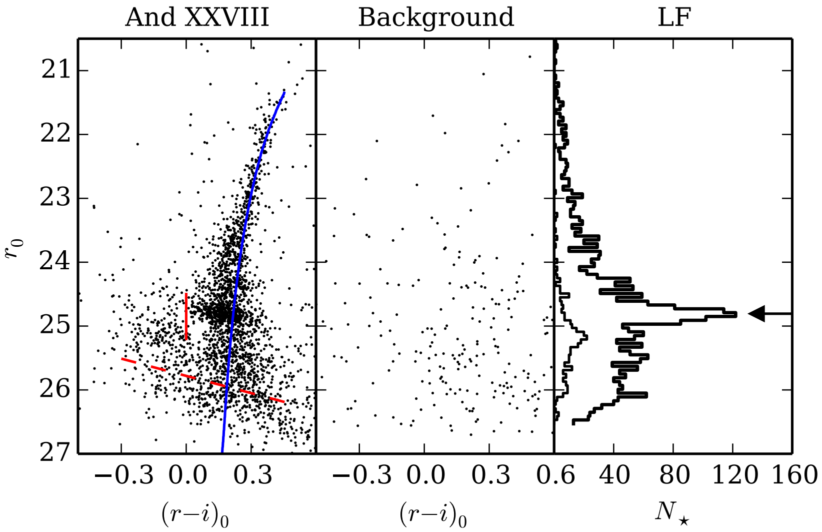

Figure 3.2: CMD of And XXVIII on the left (inside $2r_h$), with the CMD of an equal-sized background region in the center. The red dashed line indiciates the 50% completeness limit, while the vertical red line indiciates the approximate division between red and blue horizontal branches. The luminosity function of the dwarf is shown on the right, separated into a thick line showing stars with $(r-i)_0 > 0$ and a thin line showing stars with $(r-i)_0 < 0$. A 12 Gyr old, [Fe/H] = -1.84 isochrone is overplotted, and the measured apparent magnitude of the HB is indicated with an arrow.

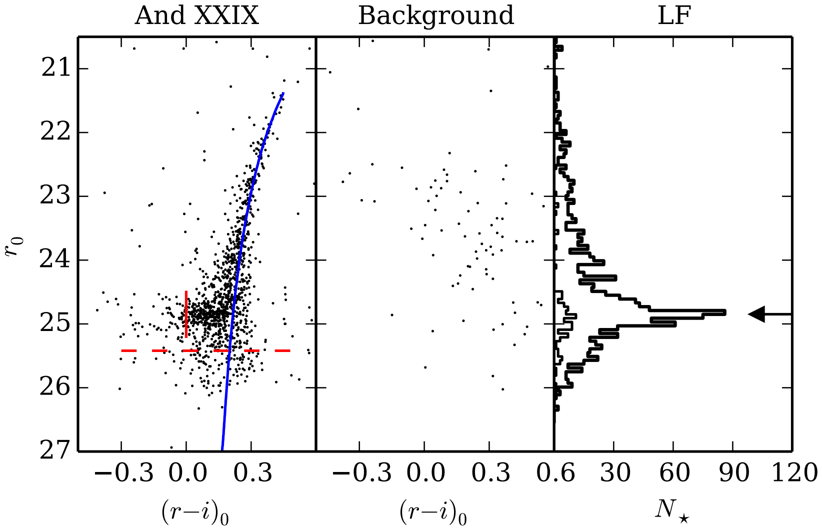

Figure 3.3: Deep CMD of And XXIX, showing the same panels as Figure 3.2. A 12 Gyr old, [Fe/H] = -1.92 isochrone is overplotted. As with And XXVIII there are no indications of recent star formation. Though there may be some hints of a BHB, if it does exist it is substantially less prominent than in And XXVIII.

3.4.1 Distance and Luminosity

The clear HB in both dwarfs enables an accurate measurement of the distance to the dwarfs, and hence their distance to M31. We fit a Gaussian plus a linear background model to the r-band luminosity function of each dwarf in the region of the HB, using only stars redder than $(r-i)_0 = 0$. The measured HB position is indicated in the right panels of Figure 3.2 and 3.3 by the horizontal arrow, and is $m_{g,0} = 24.81$ for And XXVIII and $m_{g,0} = 24.84$ for And XXIX. We use the RHB absolute magnitude calibration of Chen et al. (2009), which is based on globular clusters RHBs measured directly in the SDSS filter set. In the r-band this calibration, using a linear metallicity dependence and without the age term, is

$$M_r = 0.165[\mathrm{Fe/H}] + 0.569. \tag{3.1}$$

The resulting distances are 811 ± 48 kpc for And XXVIII and 829 ± 42kpc for And XXIX, using the spectroscopic metallicities as determined in Section 3.5. Both of these are slightly further than the measured distances from Chapter II and Bell et al. (2011), but just within (And XXVIII) or just outside (And XXIX) the formal one-sigma uncertainties. The updated heliocentric distances does not substantially change the measured distances between the dwarfs and M31, since both are near the tangent point relative to M31[2]. Based on these distances, both dwarfs lie well away from the plane of satellites from Conn et al. (2013) and Ibata et al. (2013). As seen from M31 the satellites are 80° (And XXVIII) and 60° (And XXIX) from the plane. The closest galaxy to And XXVIII is And XXXI at 164 kpc, while And XXIX's closest neighbor is And XIX at 88 kpc, making both relatively isolated from other dwarfs.

We measured the total luminosity of both dwarfs by comparing the portion of the LF brighter than the HB to the LF of the Draco dwarf. Using data from Ségall

---

[2] The distance between And XXIX and M31 reported in Bell et al. (2011) was incorrect due to a geometry error; it is fixed in this work.

et al. (2007) we constructed a background-subtracted LF for Draco inside r_h, then scaled the LF of the dwarfs such that they best matched the Draco LF. The resulting luminosities are $M_V = -8.7 \pm 0.4$ for And XXVIII and $M_V = -8.5 \pm 0.3$ for And XXIX, both of which are again in good agreement with values measured by previous works.

3.5 Spectroscopic Metallicity

To complement the imaging data, we also make use of metallicities derived from Keck/DEIMOS spectroscopy of the brightest RGB stars. The source data and spectroscopic reductions are described in Tollerud et al. (2013), and sample spectra can be seen in their Figure 1. We derive metallicities from the $\lambda \sim 8550$ Å Calcium triplet features, following the methodology described in Ho et al. (2015). Briefly, this procedure fits Gaussian profiles to the strongest two CaT lines, and uses these fits to derive CaT equivalent widths. In combination with absolute magnitudes from the aforementioned photometric data (Section 3.3), these data can be calibrated to act as effective proxies for [Fe/H] of these stars. For this purpose, we adopt the Carrera et al. (2013) metallicity calibration to convert our photometry and equivalent widths to [Fe/H].

A table of the spectroscopic metallicity measurements of individual stars in each dwarf is presented in Table 3.2. We determine the uncertainty in the mean [Fe/H] by performing 1000 Monte Carlo resamplings of the distribution. For each resampling, we add a random offset to the metalicity of each star drawn from a Gaussian with width of the per-star [Fe/H] uncertainty, and compute the mean of the distribution. For σ([Fe/H]), we report the second moment of the distribution and derive uncertainties from a resampling procedure like that for the mean [Fe/H].

The resulting metallicity distributions for And XXVIII and XXIX are shown as cumulative distribution functions in Figure 3.4. From this it is immediately clear

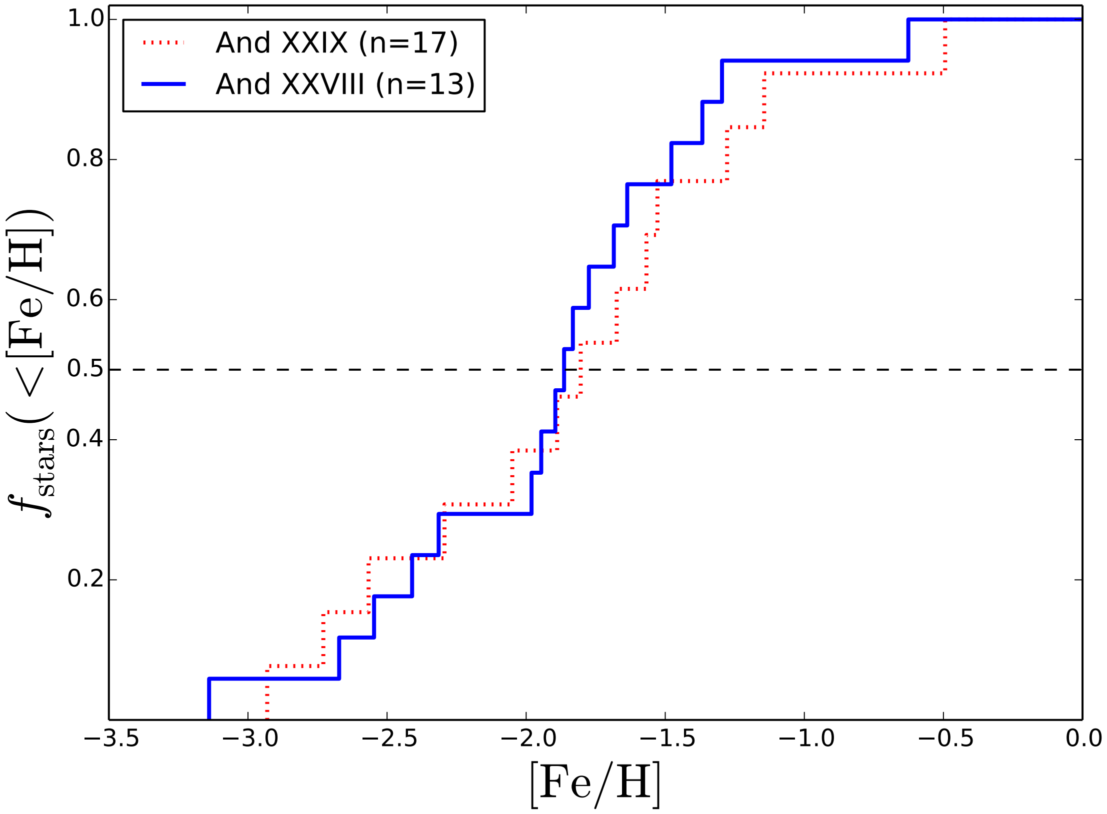

Figure 3.4: Cumulative distribution of [Fe/H] for And XXVIII (blue solid line) and XXIX (red dotted line).

that, while the number of stars are relatively small, the median of the distribution is at [Fe/H] ~ -2 (see Table 3.1). Motivated by this, in Figure 3.5, we show the luminosity-metallicity relation for the brighter M31 satellites (Ho et al., 2015) and the MW satellites (Kirby et al., 2011, 2013), using luminosities from Martin et al. (2015, submitted). The figure shows that that And XXVIII and XXIX are fully consistent with the metallicity-luminosity relation that holds for other Local Group satellites. Our measurement for And XXVIII is also consistent with the prior measurement by Collins et al. (2013) of [Fe/H] $= -2.1 \pm 0.3$, but at higher precision.

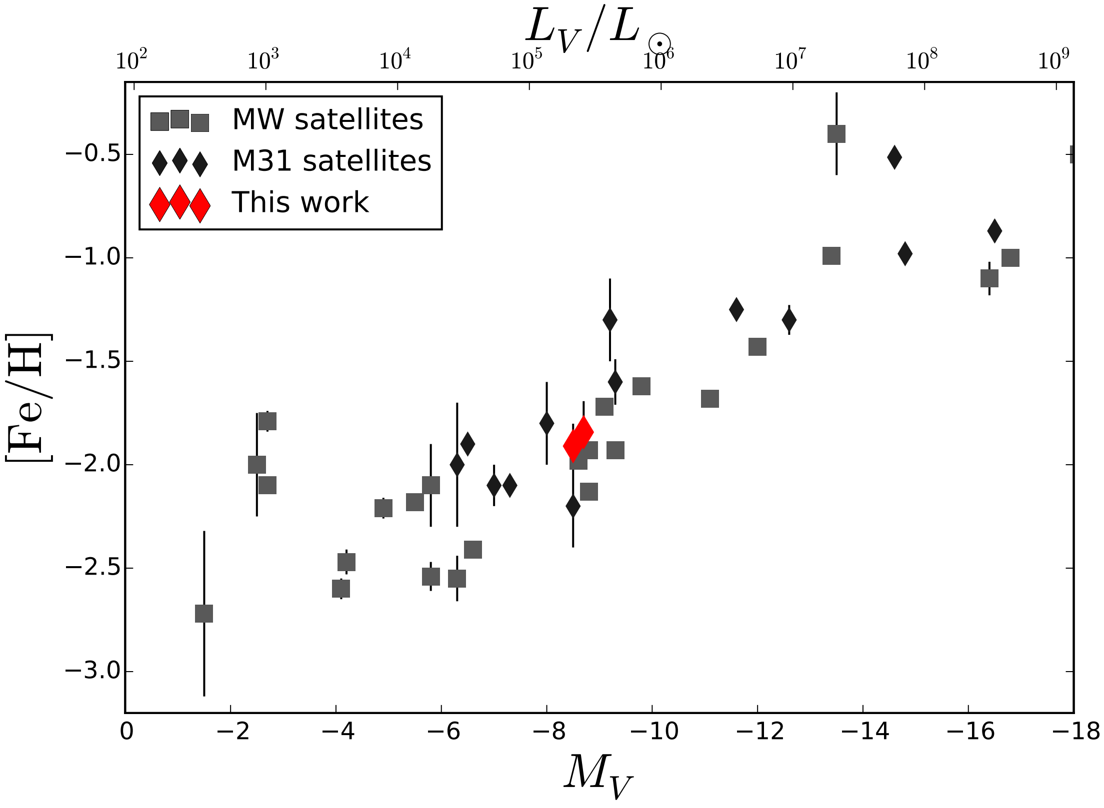

Figure 3.5: Luminosity-metallicity relation for Local Group satellites. Squares are MW satellites (Kirby et al., 2013), and diamonds are M31 satellites (Ho et al., 2015), with error bars from the Monte Carlo resampling of the [Fe/H] distribution for each galaxy. And XXVIII and XXIX are shown as the larger red diamonds. This demonstrates that And XXVIII and XXIX lie on the same metallicity-luminosity relation as other Local Group satellites.

Table 3.2: Metallicities of And XXVIII & XXIX Stars

Galaxy	RA (deg)	Dec (deg)	r_0	$(r-i)_0$	[Fe/H]	$\sigma_{\mathrm{[Fe/H]}}$
And XXVIII	338.16549	31.20840	21.397	0.53	-2.29	0.5
And XXVIII	338.18538	31.22404	21.404	0.44	-1.58	0.5
And XXVIII	338.15561	31.18421	21.381	0.45	-1.54	0.8
And XXVIII	338.14847	31.15615	21.001	0.24	-0.50	0.8
And XXVIII	338.17702	31.21802	21.548	0.42	-2.06	0.5
And XXVIII	338.17499	31.22058	21.969	0.35	-2.91	0.7
And XXVIII	338.18206	31.21668	21.509	0.41	-2.74	0.4
And XXVIII	338.16849	31.22444	22.344	0.42	-1.90	0.6
And XXVIII	338.18357	31.21526	21.332	0.38	-1.81	0.4
And XXVIII	338.17542	31.23720	21.57	0.70	-1.28	0.3
And XXVIII	338.15091	31.20916	21.578	0.46	-1.68	0.2
And XXVIII	338.18428	31.23235	21.861	0.37	-1.15	0.3
And XXVIII	338.22622	31.21862	21.78	0.37	-2.57	0.2
And XXIX	359.73912	30.74974	22.113	0.36	-1.83	0.5
And XXIX	359.72546	30.74484	21.467	0.45	-1.94	0.3
And XXIX	359.72690	30.76834	21.592	0.44	-1.29	0.4
And XXIX	359.74259	30.75986	22.084	0.42	-0.62	0.5
And XXIX	359.74561	30.75100	21.854	0.39	-2.40	0.4
And XXIX	359.71503	30.74976	21.369	0.40	-2.54	0.3
And XXIX	359.71755	30.74150	21.968	0.37	-3.14	0.5
And XXIX	359.71880	30.73644	22.003	0.40	-1.36	0.4
And XXIX	359.71957	30.76735	22.211	0.35	-1.86	0.6
And XXIX	359.75409	30.76225	21.172	0.45	-1.97	0.3
And XXIX	359.75959	30.76464	22.111	0.36	-1.77	0.6
And XXIX	359.73776	30.80015	21.266	0.20	-2.31	0.3
And XXIX	359.73609	30.79734	22.137	0.33	-1.68	0.5
And XXIX	359.68681	30.72895	21.959	0.36	-2.68	0.6
And XXIX	359.74074	30.76867	21.407	0.44	-1.89	0.4
And XXIX	359.74687	30.76948	21.751	0.29	-1.47	0.5
And XXIX	359.75467	30.75391	21.752	0.37	-1.63	0.5

3.6 Structure & Stellar Populations

We determined the structural properties of the dwarfs using an updated version of the maximum likelihood method presented in Martin et al. (2008). This method fits an exponential radial density profile to the galaxies without requiring the data to be binned, which enables more precise measurements of the structure in galaxies with only a small number of observed stars. The updated version samples the parameter space with a Markov Chain Monte Carlo process, and can more easily account for missing data (Martin et al. 2015, submitted.) This is necessary to account for the limited field of view of GMOS, which could cause a systematic size error (Muñoz et al., 2012), as well as the very center of And XXIX where an inconveniently-located bright foreground star contaminates the very center of the image and prevents reliable photometry in the surrounding region.

The resulting radial profiles and posterior probability distributions are shown in Figures 3.6 and 3.7. The half-light radii and ellipticities all have fairly typical values for other dwarfs of similar luminosities (Brasseur et al., 2011). The results are also consistent with the parameters estimated from the much shallower SDSS data (Chapter II, and Bell et al., 2011).

The separation between the red and blue horizontal branches in And XXVIII enables us to examine the spatial distribution of the metal-poor, older, and the more metal-rich, younger, stellar populations. Radial profiles of the two horizontal branches (separated at $(r-i)_0 = 0.0$) are shown in Figure 3.8. The difference in the radial profiles is easily seen in the right panel, and the posterior probability distributions for the half-light radius confirm the statistical significance of the difference. This behavior has been seen in other dwarf galaxies, such as Sculptor (Tolstoy et al., 2004), Fornax (Battaglia et al., 2006), Canes Venatici I (Ibata et al., 2006), And II (McConnachie et al., 2007), and Leo T (de Jong et al., 2008). In all of these cases the more metal-rich population is the more centrally concentrated one, consistent with

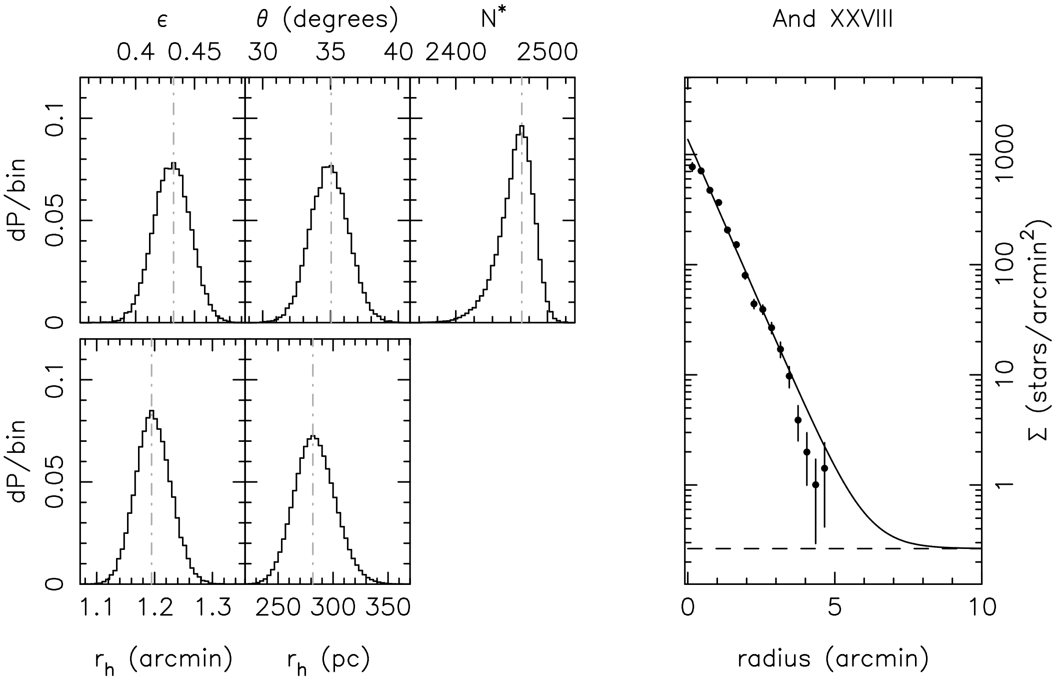

Figure 3.6: Structural parameters and radial profile for And XXVIII. Posterior probability distributions for the structural parameters fit for And XXVIII are shown on the left. From top-left to bottom-right, these show these correspond to the ellipticity (ϵ), the position angle from north to east (θ), the number of stars under the profile for the assumed depth limit (N^*), the angular major-axis half-light radius (r_h), and its corresponding physical length assuming the distance modulus measured above. The radial profile is shown on the right, with the best fit exponential profile shown by the solid line and the dashed line showing the background level.

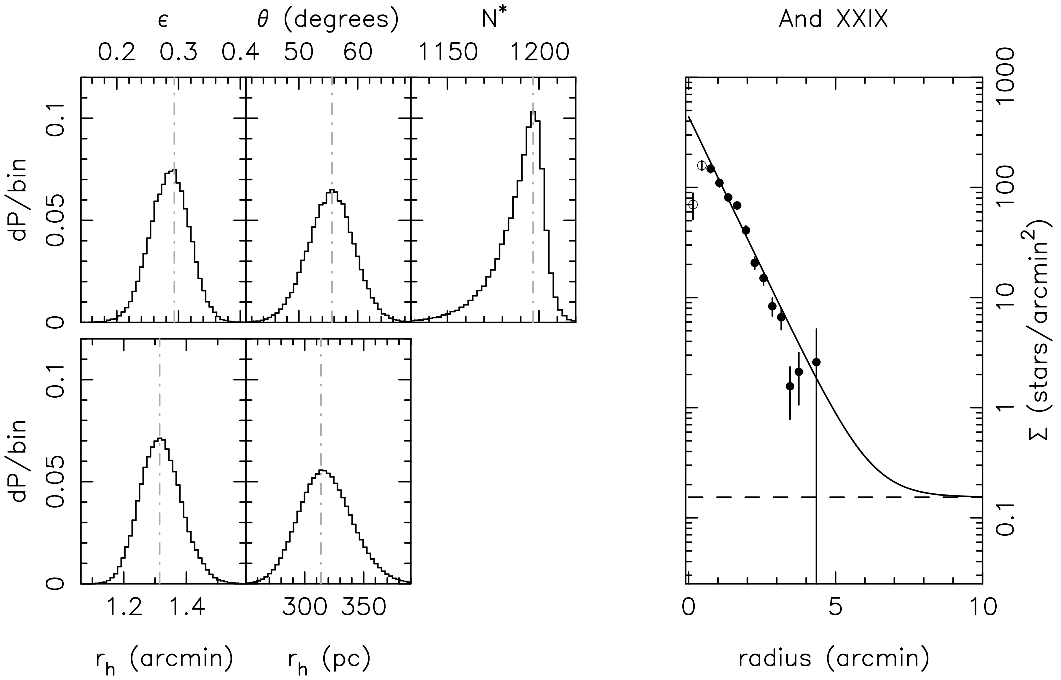

Figure 3.7: The posterior probability distributions and radial profile for And XXIX, as in Figure 3.6. The two innermost radial profile points (open circles) were not used in the fit due to the bright contamination in the center of the galaxy.

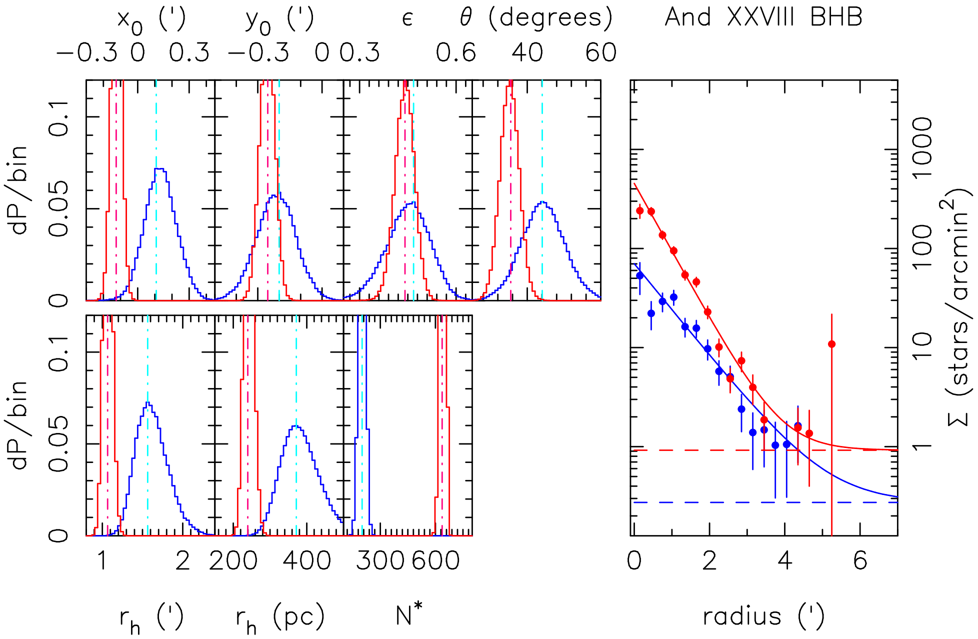

Figure 3.8: Posterior probability distributions for the structural fit of And XXVIII, performed separately for stars in the RHB (red lines) and the BHB (blue lines). The difference in the radial profile clearly visible in the panel on the right, and the significance is confirmed by the difference in half light radius (r_h). The ellipticities and position angles are similar in the two populations.

And XXVIII. Measuring the spatial structure of the two components independently shows that they appear to be simply scaled versions of each other; the half-light radii are 370 ± 60 pc and 240 ± 15 pc (blue and red, respectively), while the ellipticities of 0.48 ± 0.06 and 0.43 ± 0.03, along with position angles of $45^\circ \pm 5^\circ$ and $34^\circ \pm 3^\circ$, agree well with each other. Taken together this implies that the process that transformed the dwarf into a pressure-supported system did so without randomizing the orbital energies of individual stars enough to completely redistribute the older and younger populations, but both populations did end up with the same general morphology.

Simulations of isolated dwarfs by Kawata et al. (2006) are able to reproduce a radial metallicity gradient, but with some uncertainty over the number of stars at the lowest metallicity values and the total luminosity of the simulated dwarfs (and also see Revaz & Jablonka (2012) for simulated dwarfs without gradients). In these simulations the metallicity gradient is produced by the continuous accretion of gas to the center of the galaxy, which tends to cause more metal enrichment and a younger population (weighted by mass) at small radii when compared to the outer regions of the galaxy. This explanation suggests that the "two populations" we infer from the RHB and BHB of And XXVIII are perhaps more properly interpreted as two distinct tracers of what is really a continuous range of ages and metallicities present in the dwarf. In this scenario, the lack of observed multiple populations in And XXIX could be the result of the dwarf lacking sufficient gas accretion and star formation activity to generate a strong metallicity gradient. If this is the case, then there may be a mass dependence to the presence of such gradients, which makes it particularly significant that And XXVIII is a relatively low-mass galaxy to host such a behavior. It is also notable that other galaxies more luminous than And XXVIII, such as Fornax and Sextans, do not have observed metallicity gradients (Kirby et al., 2011). Whether this is merely stochasticity, or the influence of external forces, or if it requires a more complex model of the enrichment process is an open question.

3.7 Discussion and Conclusions

The analysis of And XXVIII and XXIX shows that both galaxies are relatively typical dwarf spheroidals, with old, metal-poor stellar populations and no measurable ongoing or recent star formation. The significance of these galaxies in distinguishing models of dSph formation comes from their considerable distances from M31. If environment-independent processess such as supernova feedback or reionization are responsible for transforming dIrrs into dSphs, then finding dSphs at these distances is quite natural (since the distance to a host becomes irrelevant). However, such models are by themselves largely unable to reproduce the radial depedence of the dSph distribution around the Milky Way and M31. An environment-based transformation process, based on some combination of tidal or ram pressure forces, can potentially account for the radial distribution, but correctly reproducing the properties of dSphs large radii is the critical test of such models. It is in this light that Andromeda XXVIII and Andromeda XXIX have the most power to discriminate between models.

Models of tidal transformation have been studied extensively and can account for many of the observed structural properties of dSphs (Mayer et al., 2001; Łokas et al., 2010, 2012). However, a critical component of understanding whether these models can reproduce the entire population of Local Group dSphs is the dependence of the transformation process on orbital pericenter distances and the number of pericentric passages. At large radii the weaker tidal force may lose its ability completely transform satellites into dSphs, potentially leaving observable signatures in satellites on the outskirts of host galaxies.

Observationally we cannot directly know the orbital history of individual satellites without proper motions (of which there are very few), and must test the radial distribution of dSphs in a statistical way. In Chapter IV I used the Via Lactea simulations to show that a significant fraction of the dwarf galaxies located between 300 and 1000 kpc from their host galaxy have made at least one pericentric passage near a larger galaxy. However, the fraction of dwarfs that have undergone two or more pericentric passages decreases sharply near 300 kpc. This suggests that it is unlikely for And XXVIII to have undergone multiple pericentric passages.

This presents a clear question for theories of dSph formation based on tidal interactions: can a dwarf galaxy be completely transformed into a dSph with only a single pericenter passage? Simulations of tidal stirring originally seemed to indicate that the answer was no, and when dwarfs were placed on different orbits it was only the ones with several ($\sim 4-5$) pericenter passages that were transformed into dSphs (Kazantzidis et al., 2011a). However, more recent simulations that used cored dark matter profiles for the dwarfs suggest that multiple pericenter passages might not be required. Kazantzidis et al. (2013) show that dwarfs with very flat central dark matter profiles (inner power-law slopes of 0.2) can be transformed into pressure supported systems after only one or two pericenter passages. This result is encouraging, but it also comes with the consequence that cored dark matter profiles also tend to make the dwarfs susceptible to complete destruction by tidal forces. In the simulations of Kazantzidis et al. (2013), five out of the seven dwarfs that were successfully transformed into dSphs after only one or two pericenter passages were subsequently destroyed. Taken together, these results indicate that rapid formation of a dSph is indeed plausible, but there may only be a narrow range of structural and orbital parameters compatible with such a process. Recent proper motion measurements of the dSph Leo I support this picture even further, as it appears to have had only one pericentric passage (Sohn et al., 2013) yet is unambiguously a dSph.

The properties of And XXVIII add an additional constraint that any tidal transformation must not have been so strong as to completely mix the older and younger stellar populations. A simple test case of this problem has been explored by Łokas et al. (2012), in which particles were divided into two populations by their initial position inside or outside of the half light radius. The dwarfs were then placed on reasonable orbits around a host galaxy, and evolved for 10 Gyr. The resulting radial profiles of the two populations are distinct in nearly all cases, with some variation depending on the initial conditions of the orbit. These tests may be overly optimistic, since initial differentiation into two populations is performed by such a sharp radius cut, but the simulations illustrate the plausibility of a dwarf retaining spatially distinct populations after tidal stirring.

An additional piece of the puzzle is provided by the metallicities. And XXVIII and XXIX are both consistent with the luminosity-metallicity relation shown by other Local Group satellites (see Section 3.5). This implies that they could not have been subject to substantial tidal *stripping*, as this would drive them off this relation by lowering the luminosity without substantially altering their metallicities. This point is further reinforced by the similarity of the luminosity-metallicity relation of both dSph and dIrr galaxies in the Local Group (Kirby et al., 2013), making it unlikely that the measured luminosity-metallicity relation itself is significantly altered by tidal stripping. Whether or not more gentle tidal effects can induce morphological transformation without altering the luminosity-metallicity relation remains to be seen.

Taken together, the properties of And XXVIII and XXIX present a range of challenges for detailed models of dwarf galaxy evolution to explain. Particularly for And XXVIII, the wide separation and low mass of the system add significant challenges to reproducing the gas-free spheroidal morphology with a stellar population gradient, while there may be similar challenges for explaining the apparent absence (or at least low-detectability) of such gradients in And XXIX. Though plausible explanations have been shown to exist for many of these features individually and under ideal conditions, whether the combination of these conditions can be accurately reproduced in a simulation is unknown. Further modeling of these types of systems is required before we can understand the physical drivers of these observed features.

CHAPTER IV

Confronting Models of Dwarf Galaxy Quenching with Observations of the Local Group[1]

4.1 Abstract

A number of mechanisms have been proposed to connect star-forming dwarf irregular galaxies with the formation of non-star-forming dwarf spheroidal galaxies, but distinguishing between these mechanisms has been difficult. We use the Via Lactea dark matter only cosmological simulations to test two well-motivated simple hypotheses—transformation of irregulars into dwarf spheroidal galaxies by tidal stirring and ram pressure stripping following a close passage to the host galaxy, and transformation via mergers between dwarfs—and predict the radial distribution and inferred formation times of the resulting dwarf spheroidal galaxies. We compare this to the observed distribution in the Local Group and show that 1) the observed dSph distribution far from the Galaxy or M31 can be matched by the VL halos that have passed near the host galaxy at least once, though significant halo-to-halo scatter exists, 2) models that require two or more pericenter passages for dSph-formation cannot account for the dSphs beyond 500 kpc such as Cetus and Tucana, and 3) mergers predict a flat radial distribution of dSphs and cannot account for the high

---

[1] This chapter was originally published in the Astrophysical Journal by Colin T. Slater and Eric F. Bell 2013, 773, 13.

dSph fraction near the Galaxy, but are not ruled out at large distances. The models also suggest that for dSphs found today beyond 500 kpc, mergers tend to occur significantly earlier than dwarf–host encounters, thus leading to a potentially observable difference in stellar populations. We argue that tidal interactions are sufficient to reproduce the observed distribution of dSphs if and only if a single pericenter passage is sufficient to form a dSph.

4.2 Introduction

The origin of the approximate dichotomy between the star-forming dwarf irregular galaxies (dIrrs) and the non-star-forming, pressure supported dwarf spheroidal galaxies (dSphs) has long been an open question (Hodge & Michie, 1969; Faber & Lin, 1983; Kormendy, 1985; Gallagher & Wyse, 1994). Several mechanisms have been proposed to create dSphs, such as tidal stirring and stripping (Mayer et al., 2001; Klimentowski et al., 2009; Kazantzidis et al., 2011a; Kravtsov et al., 2004), resonant stripping (D'Onghia et al., 2009), or ram pressure stripping (Mayer et al., 2006). This broad grouping of models all involve the influence of a large host galaxy, which is motivated by the observed trend in the Local Group for most dSphs to be found within 200-300 kpc of either the Milky Way or M31 (van den Bergh, 1994; Grebel et al., 2003). Other theories for dSph formation do not require the influence of a larger galaxy and transform dIrrs into dSphs via either heating of the dwarfs' cold gas by the UV background (Gnedin, 2000), strong feedback (Dekel & Silk, 1986; Mac Low & Ferrara, 1999; Gnedin & Zhao, 2002; Sawala et al., 2010), or mergers between dwarfs at early times (Kazantzidis et al., 2011b).

Since many of these mechanisms can all be shown to plausibly produce dSphs given the right initial conditions, it can become difficult to distinguish between these theories as many leave only weak signatures on the individual galaxies. Because of this limitation, one might alternatively study the signatures these processes leave on the population of Local Group dwarfs as a whole. The orbital and assembly histories of the dwarfs in the Local Group vary significantly, and the link between these histories and the resulting morphologies of the dwarfs may be a telling indication of which processes are at work. This perspective aims for differentiating between mechanisms for dSph formation where they are most different—where and when they act—rather than where they are all generally similar in the injection of energy into the orbits of stars in the dwarf.

In this work we use cosmological simulations (Via Lactea I & II, Diemand et al., 2007, 2008, herein VL1 and VL2) to trace the histories of the dwarfs that survive to today, and use these histories to infer which dwarfs (in aggregate) may have been affected either by tidal stirring or by mergers between dwarfs. The large difference in when and where these mechanisms act on dwarfs creates significant differentiation in the resulting distribution of dSphs. These two cases are also particularly suitable for study with high resolution dark-matter-only simulations, since the behavior of the luminous components can be inferred from the behavior of the dark matter. That is, we can infer the effects of tidal forces or mergers experienced by a galaxy by tracking the dark matter halo and applying relatively simple criteria based only on the halo properties. These criteria are physically motivated based on controlled simulations of the individual processes (e.g., Kazantzidis et al., 2011b, 2013). Clearly these simulations will predict some detailed properties of the dwarfs that will not be captured by our binary dSph-or-not criteria, but our focus on the bulk properties of the dwarf population as a whole will minimize the impact of these differences on our conclusions. These simplifications enable us to understand the formation of dSph galaxies in a broader cosmological context rather than only in controlled experiments.

Much of this work focuses on the dwarfs currently outside the virial radius of the Galaxy (or M31). The distribution of distant satellites that were once found inside the virial radius of a host has been investigated before in simulations of cluster or group environments (Balogh et al., 2000; Moore et al., 2004; Gill et al., 2005; Wetzel et al., 2013) and Milky Way-like environments (Diemand et al., 2007; Teyssier et al., 2012). The existence of such galaxies is well established. Similarly, the rate and timing of mergers between dwarfs in a Milky Way-like environment has been studied with simulations (Klimentowski et al., 2010), but comparisons to observations have remained limited. Our work focuses on bringing both of these mechanisms for the formation of dSphs to a specific comparison with the observed distribution of Local Group dwarfs.

Towards that goal, we discuss the simulations and our criteria for both interactions and major mergers in Section 4.3, and present the results and a comparison to the observed dSph distribution in the Local Group in Section 4.4. The distribution of times at which galaxies either merge or experience close passages is described in Section 4.5, and we discuss the implications of these results in Section 4.6.

4.3 Analysis of Simulations

We use both the Via Lactea simulation (Diemand et al., 2007) and Via Lactea II[2] (Diemand et al., 2008) for our analysis of tidal interactions, and only the VL2 simulation for our analysis of mergers. Both are cosmological, dark matter only simulations centered on a Milky Way-sized halo with a virial mass of $1.93 \times 10^{12} M_\odot$ in VL2 ($1.77 \times 10^{12} M_\odot$ in VL1), corresponding to a virial radius (r_{200}) of 402 kpc (389 kpc in VL1). VL1 used 234×10^6 particles of mass 2×10^4 $M_\odot$, while VL2 had 1.1×10^9 particles each of mass 4.1×10^3 $M_\odot$. Both simulations are entirely sufficient to resolve all of the luminous observable satellites, and we will generally restrict our results to halos with a maximum circular velocity ($V_{\rm max}$) greater than 5 km/s at $z = 0$. At this limit halos have an average of 350 particles in VL1 and 800 particles in VL2. Dark matter halos were identified in the simulation using a phase-space friends-of-friends

---

[2] `http://www.physik.uzh.ch/~diemand/vl/`

(6DFOF) algorithm, as described in detail in Diemand et al. (2006). These halos were then linked across snapshots by identifying halos which share significant numbers of particles; in identifying the most massive progenitor at least 50% of the particles in the descendant are required to be present in the progenitor, and conversely 50% of the progenitor particles to be present in the descendent. This constraint is later relaxed when computing merger trees, but the process is similar. Note that 6DFOF only links the central, low energy particles together; that is, the fraction of common particles between the progenitor and the descendant is usually significantly larger among the 6DFOF particles than among all particles within the virial radius.

In addition to the Milky Way-analog halo (referred to as the "main" halo for convenience), in VL2 there is also a second large galaxy present in the simulations that happens to have properties similar to Andromeda. This was identified in Teyssier et al. (2012), who refer to it as "Halo 2" and showed that it has a total gravitationally-bound mass of $6.5 \times 10^{11}\ M_{\odot}$, and lies 830 kpc from the main halo. Both of these properties are conveniently similar to Andromeda, and as a result, when we discuss the interaction between dwarf galaxy-sized halos and a massive host, we consider either the main halo or Halo 2 to be sufficient for this purpose. Ignoring Halo 2 would significantly bias our results, since dwarf galaxy halos that become bound to it may experience substantial tidal interactions while their distance from the main halo is still large. Treating both large halos on an equal footing also reflects our treatment of the observed Local Group dwarfs, where we consider the dwarfs' distance to either the Milky Way or Andromeda, whichever is less. VL1 has no such analogous component, so we do not apply the same conditions.

4.3.1 Tidal Interactions

With the evolutionary tracks of halos in place, we can identify halos that are strong candidates to have undergone some form of interaction with a larger galaxy.

This process is similar to that of Teyssier et al. (2012) but not identical. Of the several thousand most massive halos identified at $z = 0$, we select only those with $V_{\rm max}$ values between 5 and 35 km/s. This cut conservatively ensures that the halos we track are well resolved, and broadly spans the $V_{\rm max}$ values of classical dwarf galaxies. The position of the halo's most massive progenitor is then tracked back through each snapshot, and both it and the position of the two host halos are linearly interpolated between snapshots. The pericenter distance and the number of pericenter passages between the halo and either host is then recorded. While interpolation between timesteps is not ideal, it does provide some assurance that we are not substantially overestimating the minimum radius of each pericenter passage by only taking the distance at individual snapshots. We have verified that this interpolation produces accurate results for VL2 (where the larger timesteps make it more important) by using the more densely sampled Via Lactea 1 simulation, downsampling the timesteps to the VL2 resolution and testing the interpolation. The results show the interpolation works particularly well for the distant halos we focus on here as most of them are on strongly radial, fly-by trajectories.

The distance between the halo and either of the hosts is then compared to the virial radius ($r_{\rm 200,mean}$, defined to enclose a density 200 times the cosmic mean density) of the main galaxy as a function of redshift, and the minimum of this ratio is found. This establishes the depth to which the halo has reached in a large galaxy. We assume the virial radius of Halo 2 is the same as that of the main halo, and we later show that our results are not particularly sensitive to the exact radius criterion. We also track the number of pericentric passages the halos have undergone inside of $R_{vir}/2$ of the host halo by finding minima in the halo-host distance. The resulting halo statistics are in good agreement with those obtained by Teyssier et al. (2012); out of all selected halos, a very large majority (96%) have at some point been inside of half the host virial radius, and approximately 11% of those that have been inside this radius are later found at $z = 0$ outside of virial radius.

We note that our model relies on the assumption that the halos in the simulations are populated with observable dwarf galaxies in an unbiased way. This assumption is potentially called into question by the “missing satellites problem”, which may suggest that the number of subhalos in simulations is substantially larger than the number of dwarf galaxies in the Local Group (Moore et al., 1999; Klypin et al., 1999). For example, in VL1 and VL2 we include 9992 and 2224 halos, respectively, in our analysis, but only 101 observed dwarfs (from the catalog of McConnachie, 2012). This discrepancy can be plausibly resolved within the cold dark matter framework by a combination of observational incompleteness and supression of star formation in small halos, thus decreasing their luminosity below detectability in current surveys (Somerville, 2002; Koposov et al., 2009), or by (additionally) destroying or diminishing the mass of halos through tidal stripping (Kravtsov et al., 2004; Brooks et al., 2013). Our use of ratios of number counts of halos limits our sensitivity to models that alter the mapping between halos and dwarfs based only on their mass, since the motion of the halos through the group environment remains unchanged. The selective destruction of halos by tidal stripping has the potential to decrease the fraction of dSphs at large radii, but as we argue below the dominant uncertainty at large radii is variation between halo realizations, and thus we do not impose a more complex tidal destruction criteria. We discuss tidal destruction further in the conclusions.

4.3.2 Merger Trees

The fraction of galaxies that have experienced major mergers is calculated from the same $z = 0$ sample and uses the same method of linking halos at each snapshot to their possible progenitors. However, in the merger trees the selection requirement for the number of dark matter particles shared between halos is relaxed, since we are interested in all progenitor halos and not only the most massive progenitor. Starting at $z = 0$, we traverse the merger tree following the most massive progenitor at each step, until locating a halo that has two progenitors in a $3:1$ dark matter mass ratio or greater. The timestep where the two halos are identified as a single 6DFOF halo is noted as the merger time.

Visual inspection of the merger trees suggests that this simple criteria is effective in identifying whether a halo has merged or not, even though the merger process may be more complex in detail. Halos can often undergo close passages, which can cause particles to be lost from the halos by tidal stripping and thus alter the mass ratio we measure at the final coalescence of the 6DFOF halos. Other halos undergo passages that temporarily appear as one 6DFOF group in a snapshot, even though they will later separate and re-coalesce in subsequent snapshots. Because we track the time of the most recent merger snapshot, in these cases our merger times will tend to reflect this final coalescence rather than initial passes. We are also limited by only tracing the dark matter; we cannot say when the baryonic components of these galaxies will merge. In general we expect that when the dark matter halos merge, the baryons must follow, but this should be delayed by the time required for dynamical friction to bring the baryonic components together. We present a simple calculation of the dynamical friction timescale in Section 4.6 and find that it is of order 200 Myr or less, which is much smaller than the offset in formation times between the merger model and the tidal processing model.

Our ability to resolve mergers at very high redshifts is also limited. Beyond $z > 2.5$ (11.3 Gyr ago), halos are poorly linked in time and mergers may not be properly resolved while they undergo an initial phase of rapid assembly. We consequently do not track mergers before $z = 2.5$. Since there is significant merger activity near these redshifts, we note that total fraction of dwarfs that have undergone mergers could be sensitive to the exact cut-off we select, and consequently we focus primarily on the distribution of merged dwarfs rather than their absolute fraction. As we will show, the shape of the radial distribution is unaffected by varying this high redshift cut-off.

4.4 Comparison to Observations

We compare these simple models to the observed set of Local Group dwarf galaxies, using the catalog assembled by McConnachie (2012), which includes all of the known galaxies within 3 Mpc of the Sun. The catalog labels galaxies with $M_V > -18$ as dwarfs by convention, and though this cutoff is somewhat arbitrary, we use the same criterion here. This excludes, for example, M32 and the Large Magellanic Cloud, but includes the Small Magellanic Cloud. The catalog provides both galactocentric and M31-centric distances, and also classifies galaxies as either dSphs, dIrrs, or an intermediate "dSph/dIrr" class. Most of these classifications are uncontroversial. The dSph/dIrr class contains most of the galaxies for which either observational uncertainty or peculiar combinations of properties makes it difficult to definitively call them either a dSph or a dIrr. Since it is beyond the scope of this work to reconsider the classification of each of these galaxies, we treat the classification of McConnachie (2012) as authoritative. We account for the uncertainity in the dSph/dIrr class by evaluating two scenarios: one where all of these galaxies are treated as dSphs, and one where they are all treated as dIrrs. The range of values produced by these two cases yields some estimate of the uncertainty from classification. We make only two updates to the classifications of McConnachie (2012) based on more recent works: the galaxy Andromeda XXVIII has been confirmed to be a dSph (Slater et al., in prep), as has the galaxy KKR 25 (Makarov et al., 2012). It is important to note that the set of known dwarfs is not complete, and there may be underlying observational biases in the catalog. In this work we do not attempt to correct for biases in the selection function. We make the assumption that dSphs and dIrrs are equally likely to be detected, and thus the relative fraction of these two types is independent of the selection function. Inside of roughly 800 kpc this condition in general is met,

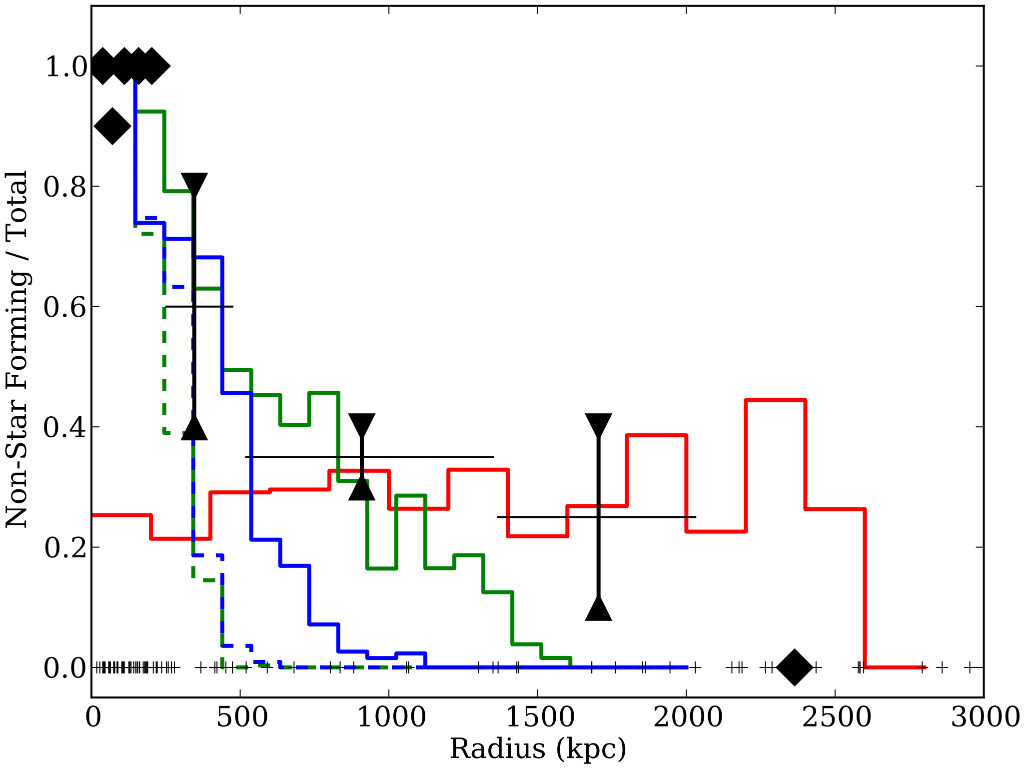

Figure 4.1: Fraction of dSph galaxies as function of galactic radius (minimum of either Galactocentric or M31-centric), grouped into bins of ten dwarfs and plotted with black symbols. Upper and lower black triangles differ by including or excluding intermediate type dwarfs as non-star forming. The span of radius covered by each bin is shown by the horizontal black lines, and the black points are plotted at the mean radius of that bin. The green lines show the fraction of halos that have passed inside $R_{vir}/3$ in VL2, either once (solid green) or through more than one pericentric passage (dashed green). The blue lines show the same values but for VL1. The red line shows the distribution of dwarfs that have undergone major mergers. The horizontal series of ticks along the bottom indicate the positions of the dwarfs in the sample. The Magellanic Clouds are included in the bin at 50 kpc.

since both dSphs and dIrrs can be detected by their red giant branch stars in the available large surveys (e.g., Irwin et al., 2007; Slater et al., 2011). Outside of this range dIrrs may be preferentially detected, since their young stars can be brighter than the tip of the red giant branch in dSphs. We remain mindful of this potential bias when interpreting the observations, but do not believe it affects our results. Our conclusions are necessarily more cautious at very large radii.

For each dwarf we compute the minimum of either its Galactocentric or its M31-centric distance, since we are not concerned with which galaxy the dwarfs may have interacted with. The dwarfs are then binned into groups of ten, and the fraction of dSphs in each bin is plotted as the black symbols in Figure 4.1 at the mean radius of its constituent dwarfs. This fixed-number rather than fixed-width binning scheme is used to compensate for the large dynamic range in the number of dwarf galaxies as a function of radius. For each bin, we evaluate the non-star forming fraction with the intermediate dSph/dIrr type galaxies included as dSphs (upper triangles) and as dIrrs (lower triangles), and the two points are connected by the vertical black lines. Bins with no transition galaxies appear as diamonds. The range of radius values spanned by each grouping of ten dwarfs is shown by the black horizontal lines on each point.

In Figure 4.1, the red line shows the radial distribution of Via Lactea II halos that have had a major merger since $z = 2.5$. This distribution is clearly flat, and does not exhibit the rise in non-star forming dwarfs inside of 1 Mpc as is seen in the Local Group. *This radial dependence alone suggests that mergers cannot be the only channel for dSph formation.*

Also in Figure 4.1, the fraction of satellite halos from the simulations that have passed inside of $R_{vir}/3$ is shown by the solid blue line for VL1 and the green line for VL2. (For VL2 this also uses the minimum distance between a halo at $z = 0$ and either the main host halo or Halo 2.) This is a simple proxy for the dwarfs that could have undergone transformation by a tidal interaction.

The radial profile in VL2 agrees quite well with the distribution of observed dSphs, with a gradual decline in non-star-forming fraction from 400 to 1500 kpc. This illustrates that tidal processes can plausibly reproduce the observed set of dSphs. However, the VL1 profile falls off much more rapidly, with very few tidally processed halos found beyond 800 kpc. The difference between the VL1 and VL2 results suggests that the predicted radial profile of dSphs in this model is clearly not a smooth, universal function. There is a large stochastic component that is evident even with only two realizations of a Local Group-like environment, which produces variations in the dSph profile beyond what would be expected from just Poisson noise. This variation comes from the accretion of subgroups of halos, which follow similar trajectories and introduce correlations in the fraction of processed halos. The accretion of discrete subgroups has been seen in other simulations, such as Li & Helmi (2008) and Klimentowski et al. (2010), and we include a more detailed illustration of this effect in Section 4.4.1. With only two realizations we are unable to quantify this effect beyond showing the two simulations as illustrating the possible magnitude of variations.

The confirmed dSph KKR 25 at 1.9 Mpc is the most significant outlier from the agreement between the observations and the simulations. Though this discrepancy could result from our two simulations failing to span the entire range of possible outcomes, it is also possible that our simple criteria for forming dSphs is imprecise and a more lenient criteria could account for KKR 25. With these caveats it is difficult to convincingly argue that tidal processing cannot account for KKR 25, but it is an interesting test case that could be suggestive of merger activity. As discussed above, the normalization on the fraction of merged dwarfs is somewhat sensitive to the details of the merger criteria, primarily the upper redshift cutoff and the mass ratio of merger required. While this sensitivity and the limitations of Poisson noise limit our ability to draw conclusions about whether the two furthest bins are compatible with any merger-based dSph formation, the figure does show the range of radii over which the two formation scenarios could be active.

The dashed blue and green lines in Figure 4.1 take the same tidal processing criteria as the solid lines, but adds an additional constraint that the halo must have experienced more than one pericentric passage inside of $R_{vir}/2$. This is slightly less restrictive in distance than the single pass criterion, since multiple weaker tidal interactions could replace a single strong interaction. As shown in the figure, the fraction of halos in either simulation with two or more passages drops steeply outside of 300 kpc, and is essentially zero beyond 500 kpc. This agrees with the results of a simple orbital timescale calculation at these radii, which shows that the single orbits require a significant fraction of a Hubble time. Performing this test in a cosmological simulation accounts for more complicated factors such as the growth the main halo and the initial positions and velocities of the halos that are today found at these radii. The result of the simulation clearly shows that dwarfs such as Cetus, Tucana, and KKR 25 could not have made multiple close passages by a large galaxy; if they were transformed into dSphs by tidal forces, it must have been done by a single passage.

4.4.1 Accretion History

In discussing Figure 4.1 it was argued that the significant difference in the histories of halos in VL1 and VL2 was due to coherent subgroups of halos. In VL2 several of these subgroups had passed near the host galaxy, while in VL1 very few did. This difference is illustrated in Figure 4.2, which shows the trajectories in comoving coordinates of halos that have $z = 0$ radii of 500-1500 kpc. The trajectories are all relative to the host galaxy, which is fixed at the origin (denoted by the red star). The trajectories of halos that have not passed inside $R_{vir}/3$ are shown in black with blue dots at their $z = 0$ position, while those that have are shown with green lines and red dots. In the VL2 panels, the trajectory of Halo 2 is shown in red with a large red dot.

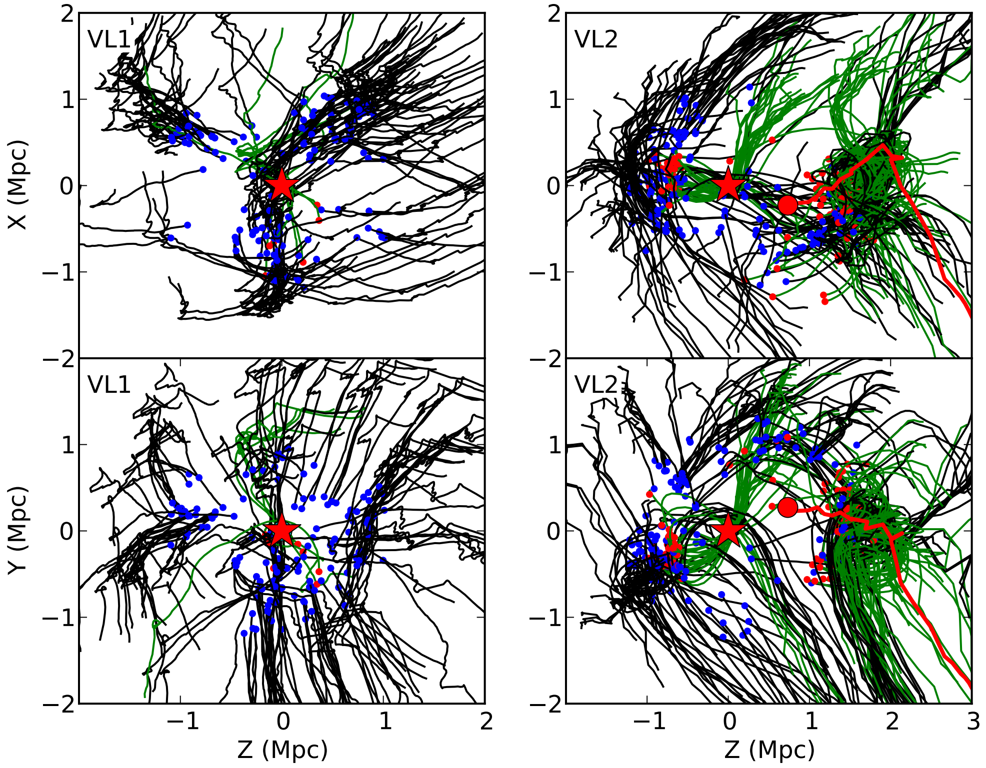

Figure 4.2: Trajectory of present-day distant halos in VL1 (left) and VL2 (right), in comoving coordinates relative to the motion of the main halo which is held fixed at the origin. The $z = 0$ location of the halos are marked with dots. Halos that have passed inside $R_{vir}/3$ are marked with green lines and a red dot, while all others are marked with black lines and a blue dot. Halo 2 in VL2 is marked by the large red dot and the red track. The clumpy nature of the accretion is clearly visible. VL1 has several subgroups which have not passed by the main halo yet, while several of the subgroups in VL2 clearly have and are receding from the main halo.

In both simulations it is clear that many halos are organized into small groups with correlated trajectories. The left side of the VL1 plots show one of these groupings clearly. The same effect is shown in VL2, most clearly seen in the paths, but with the distinct difference that several of these groups have passed through the main halo (or Halo 2), and have thus potentially been tidally processed. This correlated nature of the infalling halos is what causes the significant variation in the radial profile of processed halos, above and beyond what would be expected from pure Poisson noise on the individual halos. Infall of small subgroups of dwarfs has been seen in many other simulations (Li & Helmi, 2008; Klimentowski et al., 2010; Lovell et al., 2011; Helmi et al., 2011) and has been argued to be the cause of the apparent position or velocity correlations amongst satellites around the Milky Way (Lynden-Bell, 1976; Libeskind et al., 2005; Fattahi et al., 2013), M31 (Ibata et al., 2013; Conn et al., 2013), and more distant neighbors of the Local Group (Tully et al., 2006).

4.4.2 Parameter Sensitivity

Though our analysis includes some fixed parameters that could potentially alter the results, the robustness of the general conclusions can be shown by recalculating the results under slightly different assumptions. Figure 4.3 shows the result of changing these assumptions. The solid green line is the same as used in Figure 4.1, while the dashed green line shows the same calculation but under the relaxed assumption that a galaxy could be tidally affected inside $R_{vir}/2$, rather than $R_{vir}/3$. This increases the non-star forming fraction at all radii (as it must), but shows a similarly-shaped radial dependence. The solid black line in Figure 4.3 also shows the same calculation as before, but tightening the $V_{\max}$ constraint to only include halos with $V_{max} > 10$ km/s rather than 5 km/s. This includes many fewer halos, so the resulting plot is more noisy and we have had to double the bin size accordingly, but again the radial dependence is similar.

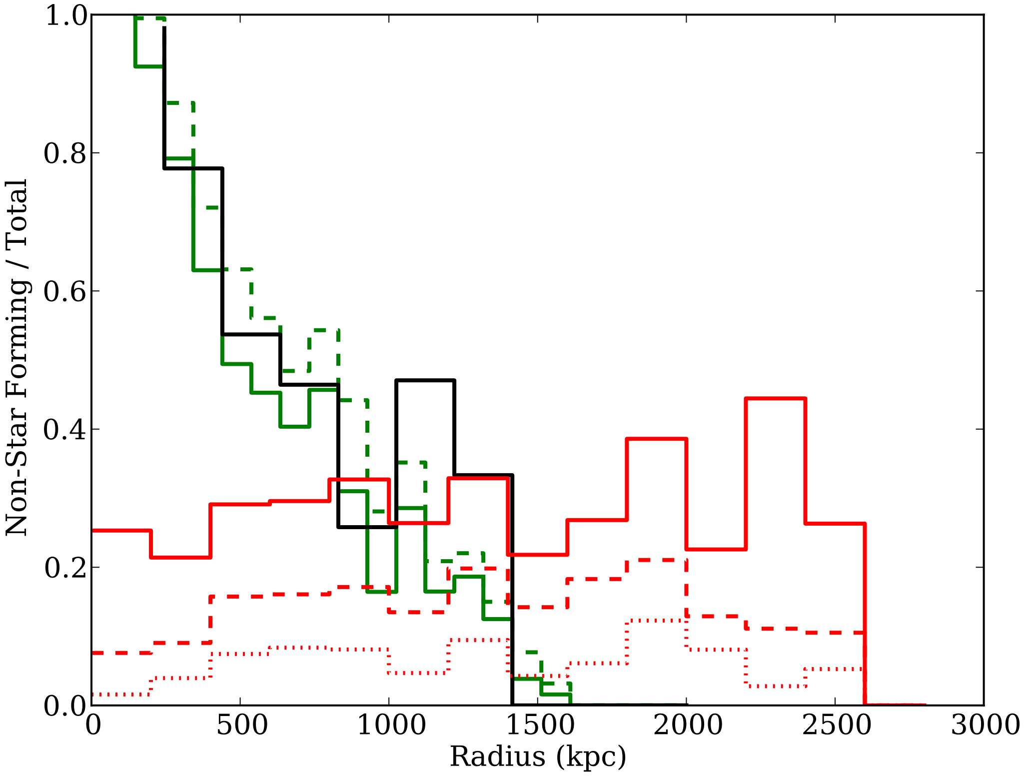

Figure 4.3: Illustration of the sensitivity of our results to to various parameter choice, using the VL2 data. The solid green line is the same as in Figure 4.1, while the dashed green line shows those that have passed inside $R_{vir}/2$ instead of $R_{vir}/3$. The black line illustrates changing the $V_{\max}$ criterion to $V_{\max} > 10$ km/s rather than 5 km/s. The solid, dashed, and dotted red lines show halos that have undergone mergers in the last 11.3, 10, and 8 Gyr, respectively. All of these variations may change the normalization of the model results, but do not affect the general form.

The most significant parameters in the merger calculation are the redshift cut-off and the required merger mass ratio. Both of these alter the absolute number of dwarfs that have undergone mergers without altering the $z = 0$ radial distribution. This is shown by the red lines in Figure 4.3, where the solid line shows dwarfs with mergers more recent than 11 Gyr, the dashed shows those more recent than 10 Gyr, and the dotted corresponds to 8 Gyr ago. The number of dwarfs with mergers drops by over half in the most restrictive of these cases, but no other effects are seen. Our analysis remains cognizant of this effect and thus it should not compromise our conclusions.

4.5 Transformation Timescales

By tracing the merger and the tidal transformation scenarios with cosmological simulations, we are able to infer the timescales on which either of these processes would have been active. The time at which star formation stopped in the dwarf is imprinted in the stellar populations and could be used to differentiate between the two scenarios for dSph formation. Figure 4.4 shows the cumulative distribution of times at which the distant halos of our $z = 0$ sample (located between 500 and 1500 kpc from either host galaxy) either underwent its most recent merger (red line) or first met the tidal criteria (passing inside $R_{vir}/3$, shown as the solid blue line for VL1 and sold green for VL2). The vertical dashed line indicates the first timestep at which we are able to resolve mergers or close passages. For comparison we also show the distribution of times at which surviving halos at any present day radius first crossed $R_{vir}/3$ (dashed blue VL1, dashed green VL2).

The distribution of merger times is clearly weighted towards early times. From the plot, roughly 50% of the observed dwarf-sized dark matter halos that experienced mergers did so more than 11 Gyr ago. This is partly due to the epoch of assembly for small halos being biased towards early times, but there is also the factor of the small halos' infall onto the larger host increasing the relative velocities of halos to

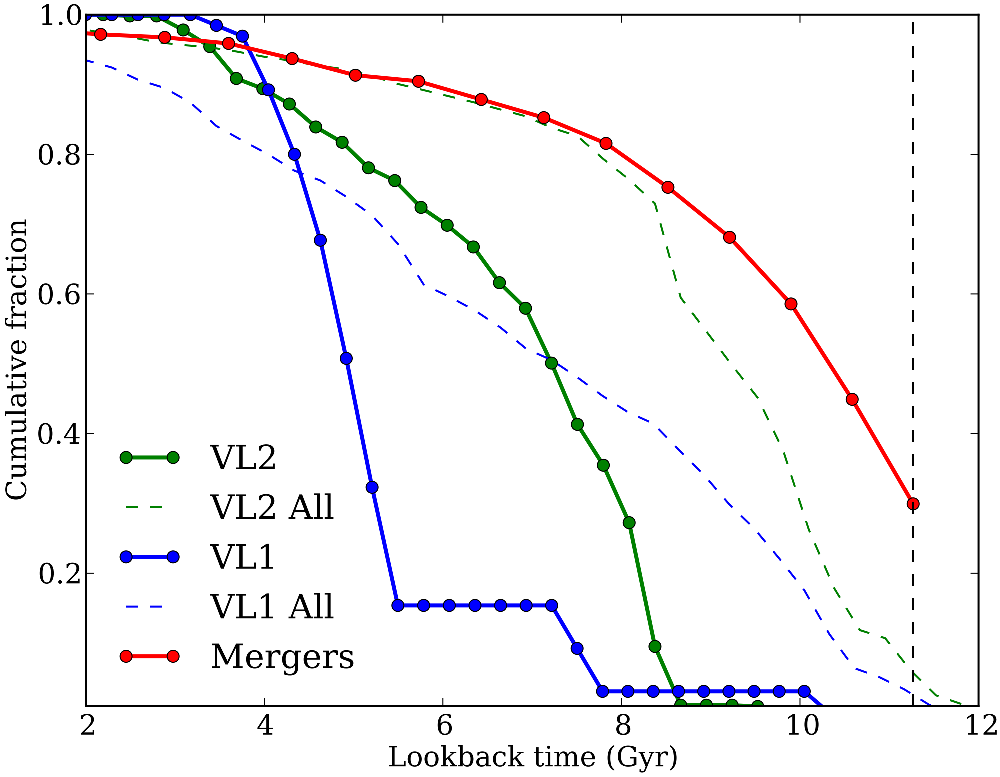

Figure 4.4: Cumulative distribution of the timescales at which the selected $z = 0$ halos first met various dSph formation criteria. The blue (VL1) and green (VL2) solid lines show when halos the halos today found between 500 and 1500 kpc from their host first crossed $R_{vir}/3$. The dashed lines show the same calculation for each simulation, but without the present-day radius restriction. The red line shows the time at which dark matter halos (those at $z = 0$ between 500 and 1500 kpc) first underwent a major merger. The vertical dashed line indicates the time at which we are first able to resolve mergers or close passages.

each other and thus inhibiting dynamical friction and further merging.

Though we can directly measure the time at which dark matter halos merged in the simulation, we must also account for the fact that the baryonic components of these galaxies may require additional time for dynamical friction to bring the baryons to coalescence. This is not directly observable, but we can estimate the time lag between the merger of the dark matter and the baryons with the dynamical friction formula from Binney & Tremaine (2008),

$$t_{\mathrm{fric}} = \frac{2.34}{\ln \Lambda} \left(\frac{\sigma_h}{\sigma_s} \right)^2 \frac{r}{\sigma_s}, \tag{4.1}$$

where σ_h and σ_s are the velocity dispersions of the "host" and "satellite" halos, r is a characteristic radius over which dynamical friction must act to bring the baryonic components together, and $\ln \Lambda$ is the Coulomb logarithm. Our selection of only major mergers constrains σ_h/σ_s to be roughly the square root of the mass ratio, and the Coulomb logarithm can be calculated as $\Lambda = 2^{3/2}\sigma_h/\sigma_m$ (Binney & Tremaine, 2008). The dynamical friction time thus reduces to a small factor of crossing time. An order of magnitude estimate with $r \sim 1$ kpc and $\sigma \sim 10$ km/s yields $t_{\mathrm{fric}} = 200$ Myr. Assuming a delay of 1 Gyr between the dark matter merger and the baryonic merger would be a relatively conservative estimate.

Given that we see significant merger and accretion activity occurring at such early times, it is logical to ask why the infall of distant dwarfs ($z = 0$ radii of 500-1500 kpc) onto the host galaxy is so delayed. For example, the rapid rise of the VL2 cumulative infall fraction in Figure 4.4 seems to start suddenly between 8–9 Gyr ago. Two points can help explain this. First, as discussed above, the accretion of halos onto the host galaxy is stochastic and several "clumps" of subhalos are sometimes accreted together. This effect contributes to the stochasticity of the infall rate, particularly in the VL1 simulation where there are fewer halos found at large radii at $z = 0$. The other effect that causes the delayed infall times is related to the distance cut we have applied. The solid green and blue lines in Figure 4.4 only shows halos that today are found between 500 and 1500 kpc; for comparison, the dashed lines shows the same infall calculation but with that present-day radius constraint removed. In the VL2 case, by the time the infall of the present-day distant dwarfs is starting more than 70% of all surviving halos have already been accreted onto the host galaxy. These halos accreted at early times join a galaxy which is much smaller at the time of accretion, and thus fall in close to the galaxy, while satellites that fall in at later times encounter a much larger galaxy which has grown around the close-in satellites. The VL1 case is more stochastic and the accretion is weighted towards even later times, but the delay is still present. Though this is merely a rough sketch to illustrate the process, the simulation is clear in predicting late infall times for distant dwarfs. When contrasted with the timescale for the merger scenario, the simulations clearly point to a difference in formation times for the two channels.

4.6 Discussion and Conclusions

We have shown that the radial distribution of galaxies of dwarf galaxies of different morphological types can be used to constrain their formation mechanisms, when combined with simple models based on cosmological simulations. The simulations show that these models produce substantially different sets of properties for the Local Group dwarfs. Mergers of dwarfs are clearly insufficient to explain all of the dSphs, and tidal processes that require multiple pericenter passages cannot account for the number of dwarfs found further than 500 kpc from their host galaxy. These two points are robust.

The fact that the simple close passage model is able to reproduce the observed radial profile of dSphs, even if it does not do so in all cosmological realizations, suggests that this model could be sufficient to create the observed dSphs. However, it hinges critically on the single-passage requirement. Many simulations have shown that multiple passages are necessary with some dwarf models (Mayer et al., 2001; Kazantzidis et al., 2011a), though the more recent simulations of Kazantzidis et al. (2013) suggest that a single-passage transformation is plausible if the progenitor dwarfs have shallow mass profiles in the center (cores). Such profiles contradict early predictions of Cold Dark Matter models (Dubinski & Carlberg, 1991; Navarro et al., 1996, 1997), but observational studies have shown that cores are prevalent in dwarf galaxies (Walker & Peñarrubia, 2011; Oh et al., 2011) and simulations (Read & Gilmore, 2005; Governato et al., 2010, 2012; Zolotov et al., 2012) have shown reasonable methods to create cores from baryonic processes. Cored profiles, however, carry the risk that the halos are more susceptible to tidal stripping and even complete destruction (Peñarrubia et al., 2010). The fine balance between tidal transformation/stirring and tidal destruction may further constrain distant dSphs to a narrow range of structural and orbital parameters.

The alternative formation pathway we have studied, that of mergers between dwarfs, has less evidence to support it but is difficult to rule out. We show that it is unable to be the dominant pathway by which dSphs form, simply because it does not recreate the large dSph fraction at small radii to a host galaxy. However, assuming our understanding of dark matter is correct, mergers must occur. Whether these mergers leave signatures that are observable today is a challenging question that requires further study. At very high redshifts dwarfs may be able to reform gas disks and continue forming stars, which would lead us to identify them as dIrrs. At what redshift, if any, mergers cause these galaxies to no longer sustain any star formation is a complex question best answered with hydrodynamical simulations.

We have shown that, for distant dwarfs, mergers must occur at very early times, while their infall onto a host potential occurs much later. The time at which star formation ended in the dwarf should therefore be a signature in the stellar populations that cannot be erased. Do the distant dSphs of the Local Group exhibit star formation histories that could differentiate between the early shut-off in the merger scenario and the later shut-off by tidal interactions?

Studies of the star formation histories of Tucana and Cetus show that both dwarfs reached the peak star formation rate more than 12 Gyr ago and subsequently the star formation rates declined (Monelli et al., 2010a,b), but from this history it is difficult to ascribe a specific time at which some process shut off star formation. In either case it took nearly 3 Gyr for the star formation rate to decline from its peak value to negligible levels; such a slow and gradual process does not lend itself to an easy comparison to our binary off-or-on model. This is particularly true in the case of mergers, where additional star formation may be triggered by the merger itself. More sophisticated modeling of the detailed star formation history, including the hydrodynamical processes that eventually render a dSph devoid of gas, could be able to extract conclusions from the stellar populations seen in Cetus and Tucana.

A logical extension of our work would be to ask if there exist comparable trends outside the Local Group. The work of Geha et al. (2012) used a sample of somewhat more massive dwarfs to show that below a mass threshold of $10^9\ M_\odot$, non-star-forming galaxies do not exist in any substantial number beyond 1500 kpc of a massive galaxy. This matches well with the predictions of the tidal processing scenario, which also shows very few processed halos beyond 1500 kpc. The Geha et al. (2012) sample substantiates the hypothesis that at low masses tidal processing is sufficient to recreate the distribution of dSphs, without requiring mergers. At slightly higher masses of $10^{9.5} - 10^{9.75} M_\odot$, a small fraction of quenched halos are observed at all radii (their Figure 4), much in agreement with the expectations for mergers. If mergers are responsible at large radii, this suggests that it is only above a certain mass threshold that mergers (which must happen at all masses) are capable of quenching galaxies in the field. Such a model has been shown by Hopkins et al. (2009) to reproduce the mass dependence of the fraction of bulge-dominated galaxies in the field, and could extend to their star formation properties as well. This picture of combining tidal processes with mergers above a threshold provides a natural link between the behavior of satellites and of central galaxies.

One difference between the Geha et al. (2012) results and the Local Group is in the fraction of quenched galaxies at small radii. In the Local Group substantially all galaxies inside 200 kpc are quenched, but the quenched fraction only reaches at most 30% in the Geha et al. (2012) sample. This could suggest a mass dependence to tidal processing, where perhaps the more massive dwarfs of the Geha et al. (2012) sample require longer timescales to shut off star formation, and thus many of their galaxies at radii are slowly on the way to quenching. Our instantaneous tidal processing model does not capture this behavior, but a more sophisticated mass-dependent model may better explain this effect.

CHAPTER V

The Mass Dependence of Dwarf Satellite Galaxy Quenching[1]

5.1 Abstract

We combine observations of the Local Group with data from the NASA-Sloan Atlas to show the variation in the quenched fraction of satellite galaxies from low mass dwarf spheroidals and dwarf irregulars to more massive dwarfs similar to the Magellanic clouds. While almost all of the low mass ($M_\star \lesssim 10^7\ M_\odot$) dwarfs are quenched, at higher masses the quenched fraction decreases to approximately 40-50%. This change in the quenched fraction is large, and suggests a sudden change in the effectiveness of quenching that correlates with satellite mass. We combine this observation with models of satellite infall and ram pressure stripping to show that the low mass satellites must quench within 1-2 Gyr of pericenter passage to maintain a high quenched fraction, but that many more massive dwarfs must continue to form stars today even though they likely fell in to their host > 5 Gyr ago. We also characterize how the susceptibility of dwarfs to ram pressure must vary as a function of mass if it is to account for the change in quenched fractions. Though neither model predicts the quenching effectiveness *a priori*, this modeling illustrates

---

[1] This chapter was originally published in the Astrophysical Journal by Colin T. Slater and Eric F. Bell 2014, 792, 141.

the physical requirements that the observed quenched fractions place on possible quenching mechanisms.

5.2 Introduction

The shut-off of star formation in galaxies presents one of the most central features in galaxy evolution but the physical mechanisms at work, along with the conditions required for quenching, remain poorly constrained. Many mechanisms have been shown to be capable of shutting off star formation, as the underlying requirement of denying cold gas to the galaxy can be met in numerous ways. Broadly speaking, these mechanisms can heat and remove the gas as in ram pressure stripping (Lin & Faber, 1983; Mayer et al., 2006) or supernova-driven outflows (Dekel & Silk, 1986; Ferrara & Tolstoy, 2000; Sawala et al., 2010), or prevent cooling and accretion of gas onto the galaxy to replenish the gas supply (Efstathiou, 1992; Gnedin, 2000; Dijkstra et al., 2004). In general it can be easily illustrated that each of these routes for quenching star formation can plausibly accomplish the task, but it has been difficult to distinguish which of these mechanisms dominate the quenching process, and under which circumstances.

A fruitful method to help understand the various quenching mechanisms has been to distinguish between a quenching process that occurs in galaxies which are satellites of a larger host galaxy and that which occurs in central galaxies which are the most massive galaxy in their halo (Weinmann et al., 2006; van den Bosch et al., 2008; Tinker & Wetzel, 2010). This is motivated both by the long-standing observation that galaxies in dense environments are preferentially quenched compared to those in the field (Dressler, 1980; Postman & Geller, 1984; Balogh et al., 2004), and by the physical differences between mechanisms which could quench satellite and central galaxies (e.g., an isolated galaxy is unlikely to experience ram pressure stripping, or satellites are unlikely to merge with each other). This distinction in mechanisms was readily incorporated into semi-analytic models (Cole et al., 1994) and tuned to accurately reproduce the distribution of satellite galaxy colors (Font et al., 2008; Weinmann et al., 2010). Further observations have sought to measure the dependence of quenching on both satellite and host halo mass (Wetzel et al., 2013). For dwarf galaxies with stellar masses between 10^7 and 10^9 $M_\odot$ the differentiation between satellites and field galaxies is most acute, as quenched field galaxies are exceedingly rare ($< 0.06\%$) in this range (Geha et al., 2012).

The severity of this cut-off in field galaxy quenching provides a strong motivation to understand how satellite galaxies at similar masses respond to possible quenching mechanisms. Our primary objective in this work is to illustrate how the quenched fraction of satellites varies from LMC-mass galaxies (as in Geha et al., 2012) down to the lowest mass dwarfs we observe in the Local Group. One of the principal challenges for this is to achieve a homogeneous selection of galaxies despite the necessarily heterogeneous parent samples required. Extending our sample to galaxies below roughly $10^8 M_\odot$ in stellar mass requires including satellites of the Local Group, which cannot be seen elsewhere in wide-area surveys like SDSS. Conversely, galaxies above this mass are infrequent in the Local Group and a larger survey is required to obtain meaningful statistics. As a result of these challenges, covering such large ranges in galaxy mass requires combining heterogeneous samples of the Local Group dwarfs with larger scale samples like SDSS. This is the strategy we adopt in this work, which will enable us to illustrate how the quenching behavior of galaxies changes over five orders of magnitude in mass. From these measurements, we use N-body simulations to translate the observed quenched fractions into physical constraints on possible mechanisms, with the intention of providing guidance to future detailed simulations of the quenching mechanisms themselves.

In this work we will detail the observed datasets, including the various corrections for selection effects, in Section 5.3, and we describe the resulting quenching fraction behavior in Section 5.4. This result will then be interpreted in Section 5.5 with a comparison to the distribution of satellite pericenter passage times in Section 5.5.1 and separately modeled as ram pressure stripping process in Section 5.5.2. We will discuss the implication of these results and conclude in Section 5.6.

5.3 Observations

Our goal in this work is to study satellite quenching as homogeneously as possible over a wide range of mass scales. This necessarily imposes constraints on our methods. In particular, in the absence of three-space velocities it is nearly impossible to select only satellite galaxies which are gravitationally bound to their hosts. We must instead rely on selecting any galaxies within some representative volume around a host as satellites, in this case all galaxies within 500 kpc of a host, keeping in mind that some fraction of these galaxies may be unbound or on first infall onto their host. All of our comparisons to simulations will be performed with the same selection process.

Covering a wide range of satellite masses requires us to combine observations from multiple sources. At the lowest masses we are limited to galaxies in the Local Group, which is itself a heterogeneous mixture of individually discovered dwarfs. To put some consistency in this data we use the compilation of McConnachie (2012), in which all known galaxies inside of 3 Mpc of the Sun are included. Each galaxy is classified with a "Morphological" Hubble type denoting it as either a star forming or a non-star forming type, though in general this classification is based on studies of resolved stellar populations rather than morphology alone. The presence of young stars and cold gas is usually sufficient to identify a Local Group galaxy's star forming status, but in some cases there is either not sufficient data or a conflicting set of properties exist, making this determination difficult. These galaxies are marked as such (e.g., with a Hubble type "dIrr/dSph") in the McConnachie (2012) catalog, and in our figures we include this ambiguity of classification in the uncertainty on the quenched fraction. The other main quantity of interest for this work is the stellar mass of each galaxy, which is computed from the integrated absolute magnitude assuming a mass-to-light ratio of 1. This is inherently imprecise, but avoids the much more complex uncertainties present in dynamical measurements of the total mass of dwarf galaxies. The uncertainties in mass are relatively small compared to the wide mass bins we adopt, and thus a change in the overall mass to light ratio or even a systematic difference between star forming and quenched dwarfs only changes our reported quenched fractions by a factor smaller than the reported uncertainity from simply Poisson noise and classification difficulties.

Though the set of known Local Group satellites is certainly incomplete in an absolute sense, our focus on the relative fraction of star forming versus quenched galaxies minimizes the impact of this incompleteness. Over the volume and range of masses we consider here both dSphs and dIrrs are readily detected in the SDSS, as the red giant branch present in both can be detected out to at least 750 kpc (e.g., Slater et al., 2011; Bell et al., 2011). The bright stars present in dIrrs certainly make detection easier, but for any such dIrr that would fall in our sample a dSph of comparable mass and distance is also likely to be detectable. That is, over the area covered by the SDSS the detection efficiency is high for both dSphs and dIrrs, and thus it is unlikely that our measured quenched fractions are strongly biased by differences in detectability. Furthermore, as our main result rests on the very high quenched fraction of low mass satellites, any bias in favor of detecting the brighter dIrrs would only reinforce this conclusion.

At the mid-range of masses, our sample comes from the NASA-Sloan Atlas of galaxies (NSA, Blanton et al., 2011). This sample reprocesses the images from the SDSS in a manner that better treats the extended surface brightness photometry required for large galaxies (on the sky) than the standard SDSS pipeline. The NSA also cross-matches sources with other large surveys and provides stellar masses estimated with the kcorrect software package (Blanton & Roweis, 2007).

From this sample of galaxies, we wish to subselect only galaxies that are satellites of a more massive host. For this we closely follow the method used in Geha et al. (2012), which we summarize here. A sample of candidate "hosts" with $M_{K_s} < -23$ (or approximately $2.5 \times 10^{10} M_{\odot}$ in stellar mass) was compiled from SDSS and 2MASS and combined with several different sources of redshift data. This sample is designed to be complete out to $z = 0.055$, which is the redshift limit of the NSA. Each galaxy in the NSA was then matched with potential host galaxies by selecting the closest host galaxy on the sky with a difference in redshift less than 1000 km s^{-1}. The projected distance at the redshift of the host is then recorded as the physical separation.

In the work of Geha et al. (2012) this selection process was used to produce a very clean sample of isolated field dwarfs. In this work our purpose differs in that we require a clean sample of satellites with minimal numbers of projected "interlopers". This is a much more challenging selection process, since the significant peculiar velocities of satellites relative to their hosts requires a wide redshift cut, but such a cut also permits substantial numbers of isolated galaxies along the line of sight to be included as satellites. This is a fundamental limitation that cannot be easily remedied by changing the selection criteria, and instead we attempt to model and correct for the effect.

We can compute the number of interlopers that fall into our redshift cuts by constructing mock observations of an N-body simulation. We use the Millennium simulation for this purpose (Springel et al., 2005), which simulated a 100 h^{-1} Mpc^3 box. This is large enough that the observed volume of the NSA can fit within the simulation, simplifying the creation of the mock observations. From the simulation halo catalogs we create a catalog of "host" halos and a catalog of "dwarfs", differing only in their halo mass requirements. We apply the same redshift and projected separation cuts as for the observed data, then measure the fraction of these selected galaxies that actually lie within 500 kpc of their host. Since in the NSA our mass cuts are based on stellar masses, which are not directly available in the N-body simulation, we convert the stellar mass bins into halo mass bins using the relation from Moster et al. (2010), and also use this to set the limiting mass of a host halo.

The measured contamination fraction (interlopers over total number of selected galaxies) varies smoothly from 65% at the lowest stellar mass bin in the NSA to 51% at the highest mass bin. This relatively weak mass dependence limits the effects of uncertainties in the stellar mass determination, and testing with an artifically shallow relation (as could be caused by tidal stripping of satellites) does not substantially affect our results. The contamination fraction f_{contam} can directly be used to estimate the corrected quenched fraction f'_Q,

$$f'_Q = f_Q + (f_Q - f_{FQ})\left(\frac{f_{\mathrm{contam}}}{1 - f_{\mathrm{contam}}}\right), \tag{5.1}$$

where the inclusion of f_{FQ} for the fraction of quenched field galaxies accounts for the fact that some of the interlopers could themselves be quenched. Since this factor f_{FQ} is small, the effect of interlopers is to artificially lower the observed quenched fractions, while the high contamination fraction causes interlopers to constitute roughly half of the observed sample. The resulting correction is thus substantial, raising quenched fractions in the NSA from $\sim$ 20% to nearly 50% and underlining the importance of correcting these measurements. We note that interlopers primarily affect selection of satellite galaxies; the selection of field galaxies like in Geha et al. (2012) is much cleaner simply because the broad redshift cut only admits galaxies to the field sample if they are unambiguously isolated. There is unfortunately no such unambiguous criteria for satellites.

In addition to the contamination correction, it is also necessary to account for the relative volumes over which quenched and star-forming galaxies can be detected in the

SDSS. To correct for this we weight each galaxy in the quenched fraction calculation by the inverse of the volume over which that galaxy could be detected, which is frequently referred to as a $V_{\rm max}$ correction[2]. This selection bias would otherwise drive the quenched fractions down, since the brighter star-forming galaxies would be over-represented. Using the $V_{\rm max}$ correction raises the final quenched fraction by 15-20%. We apply this correction only to the NSA sample, as it is impractical for the Local Group sample where an entirely heterogeneous set of surveys are responsible for the detection of dwarfs.

For the NSA sample we distinguish star-forming and quenched galaxies by a combination of the Hα equivalent width (EW) and the D_n4000 measure of the break in the spectrum at 4000Å. We adopt the criteria of Geha et al. (2012), which required quenched galaxies to have an Hα EW less than 2Å and required $D_n4000 > 0.6 + 0.1\log_{10}(M_\star/M_\odot)$. The quenched fraction is not very sensitive to the specific value of the Hα cut; allowing galaxies with equivalent widths of 4Å to be counted as quenched only changes the resulting quenched fractions by 2-4%.

5.4 Observational Results

The resulting quenched fractions are shown as a function of satellite mass in Figure 5.1. There is some ambiguity inherent in the classifications of LG dwarfs into a binary "star-forming or quenched" system, so the error bars on the LG quenched fraction extend from the lowest possible quenched fraction (assuming all ambiguous galaxies are star forming) to the highest possible fraction (assuming all ambiguous galaxies are quenched). While this is clearly not a statistical uncertainty, it does provide an illustration of the possible range of quenched fractions.

At the lowest-mass end, the data are consistent with nearly all satellites having

---

[2] This $V_{\rm max}$ is not to be confused with the maximum circular velocity of a galaxy, which we will also use in the modeling section. Sorry.

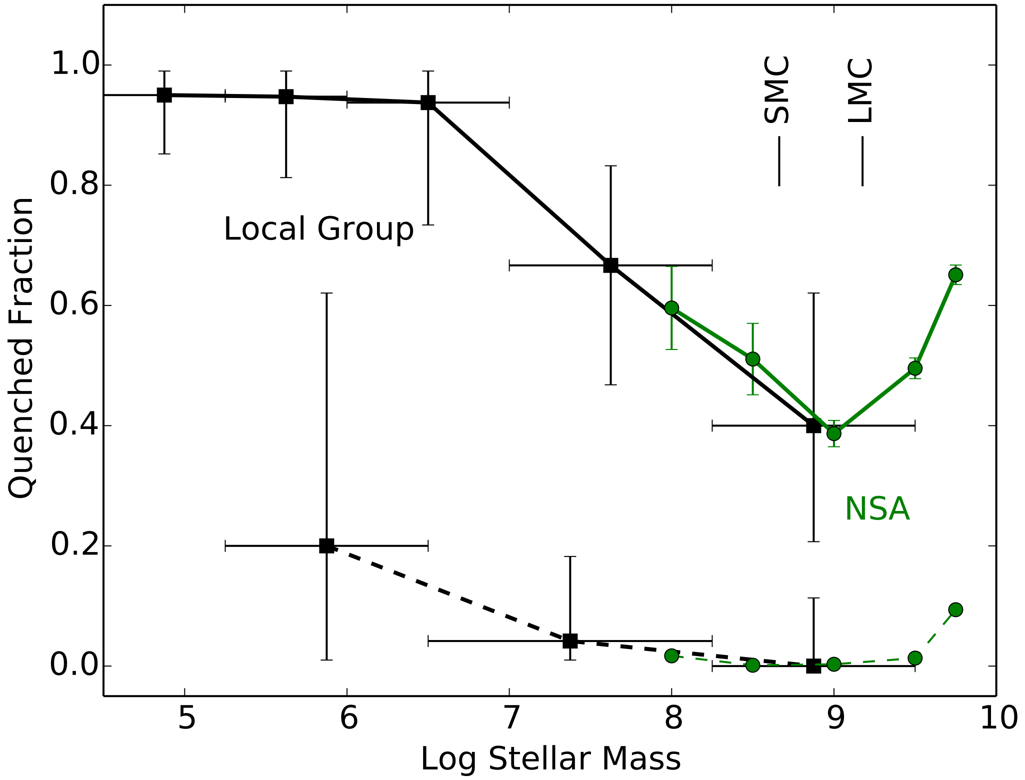

Figure 5.1: Fraction of quenched satellites as a function of galaxy stellar mass (solid line), along with fraction of quenched field galaxies (dashed line). The data comprise three samples: dwarfs in the Local Group (black squares), more massive satellites from the NSA catalog after correction for contamination (green circles). There is a clear transition near $10^7 - 10^8\ M_\odot$ from nearly ubiquitous quenching of satellites at low mass to much lower quenched fractions at higher masses.

no ongoing star formation. The lowest-mass satellite with evidence for recent star formation is Leo T, with a stellar mass of $1.4 \times 10^5\ M_\odot$ (under the M/L=1 assumption of McConnachie, 2012), but determining the recent star formation history of such low mass galaxies is challenging (Weisz et al., 2012). Other examples of low-mass star forming dwarfs include LGS3 ($9.6 \times 10^5\ M_\odot$) and Phoenix ($7.7 \times 10^5\ M_\odot$), but these are substantially outnumbered by quenched dSphs at these masses. This is in spite of the fact that both types of galaxies down to masses of $10^5\ M_\odot$ (e.g., Draco) are well-detected to beyond the limits of the volume considered here, and that star forming dwarfs are generally easier to detect. Not until reaching masses of $10^{6.5} - 10^8\ M_\odot$ do substantial numbers of dIrrs begin to reduce the quenched fraction, with galaxies such as IC 10 ($8.6 \times 10^7\ M_\odot$), WLM ($4.3 \times 10^7\ M_\odot$) and IC 1613 ($10^8\ M_\odot$), for example. It's worth noting that some of these galaxies may be on initial infall into the LG, and it could be argued that they are thus not representative of true satellites. While this could of course modify the absolute quenched fraction depending on the selection criteria, we argue that this does not affect the mass dependence we seek to illustrate. If there were no mass dependence in the quenched fraction, then where are the lower-mass star forming galaxies that are on first infall? Higher mass dwarfs are not preferentially infalling compared to lower mass dwarfs, as confirmed with the Via Lactea simulations, and we see little room for selection effects to cause the mass dependence we observe. The resulting conclusion is that some changing aspect of the quenching process itself must be responsible for this effect.

This drop-off in quenched fraction is corroborated by the NSA sample, which shows similar quenched fractions in the vicinity of 40-60%. This is an entirely independent measurement that shares very little in terms of potential observational biases with the LG data. We have not fine-tuned the quenching criteria in either sample to create this correspondence, as the criteria for both samples were originally defined by other works. The risk of detection biases related to the host-satellite distance are lessened in the NSA data, but they are replaced by projection and redshift-related effects. The principal uncertainty in the NSA measurement is the contamination correction, which changes the quenched fraction by roughly 20-30% in each bin. Even with such a substantial correction, the contamination fraction would have to be in the range of 80% or greater to bring the NSA quenched fractions as high as the seen in the LG.

Low quenched fractions at LMC-range masses are also seen in the work of Wheeler et al. (2014), which reached a similar conclusion with an alternate methodology. While we have corrected our observed sample for contamination by redshift-interlopers, Wheeler et al. (2014) has created mock observations of their models which include such contamination and left the observations unchanged. Either process should be equally valid, and the similarity in resulting values provides an additional confirmation of our conclusions, but the difference between methods should be noted in making any direct comparisons. In particular our correction for contamination is necessary to homogenize the NSA quenched fractions with observations of the Local Group, which do not suffer from this problem. We also note that the host galaxies of the NSA satellites are not selected to have a common mass. This may have implications if the relative mass of satellite and host is an important determinant of quenching, but in general we expect that the inclusion of LMC-mass galaxies around much larger hosts than the Milky Way would serve to raise the quenched fraction rather than lower it, thus minimizing the difference between the mass ranges rather than artifically increasing the difference. The conclusion of a substantially lower quenched fraction from $10^{7.5}$ to $10^{9.5}$ $M_\odot$ appears robust.

In addition to the fraction of quenched satellites, we also show the fraction of quenched field galaxies from both the NSA and the Local Group. As shown by Geha et al. (2012), quenched field galaxies are extremely uncommon at stellar masses below 10^9 $M_\odot$. The causes of this behavior are beyond the scope of this work, but we show this to demonstrate that the quenched fraction of satellites at the masses we are interested in is set primarily by interactions, and not set by quenching of galaxies in the field. This is certainly true in the NSA sample, where there is less room for observational biases to act differentially on field and satellite populations.

We note that the sample of field galaxies at stellar masses of 10^7 $M_\odot$ may be incomplete, since such intrinsically faint galaxies at distances of 1 Mpc and greater are observationally challenging. This also affects field dSphs more than field dIrrs due to their differences in intrinsic luminosity at fixed stellar mass. For these reasons we do not want to make any firm statements about the lack of field dSphs. In the LG sample we know of only a single field galaxy, KKR 25 (Makarov et al., 2012), that appears quenched, but it would be difficult to extrapolate from this one galaxy whether a larger population of field dSphs exists or if this galaxy is somehow peculiar. In our modeling we will assume that no dwarfs are quenched in the field, but we acknowledge that this is not yet certain and could be open to revision.

5.5 Quenching Models

Given the changes in the quenched fraction that we see, we would like to understand how this population-based observation can constrain physical models for the quenching process. To restate it simply, if we seek to create a scenario in which 50% of the high mass dwarfs are quenched, we need to find a criterion for quenching which is met by only 50% of the dwarfs at that mass. In this work we posit two such possible criteria: one which is based on the time since a galaxy's first pericenter passage around its host, and another based on the maximum ram pressure experienced by each dwarf. We can then set the parameters of these criteria such that they reproduce the observed mass dependence of quenched fraction.

This goal of these models is to illustrate the magnitude of the change in the quenching criteria with mass required to match the observations, and to put physical constraints on possible quenching mechanisms based on our observations of the populations. We note that these simplified models are each taken in isolation, requiring the change in quenching fraction to be the result of a single parameter, when in reality there may be several factors that all combine to produce the observed population. While detailed hydrodynamical simulations are required for any *ab initio* modeling of the quenching process, these simple models will hopefully demonstrate the magnitude of the problem.

5.5.1 Quenching Delay Time

We first seek to model the changing quenched fraction by positing that the time since the satellite's first pericenter passage around the host is the critical parameter. This "delay time" model may be interpreted differently depending on the physical mecahnism involved; for example, for large galaxies falling into clusters the delay time could correspond to a scenario where gas accretion onto the satellite is stopped upon infall, but some additional time is required for the star formation to consume the pre-existing gas. This is primarily of interest when the delay time, as measured in population studies, is roughly the same duration as the gas consumption timescale for a galaxy. Such a delay time has been used to model the quenching of massive galaxies by Wetzel et al. (2013), but we note that our model differs in that we assume instantaneous quenching after a delay, whereas Wetzel et al. (2013) have both a delay and a timescale for star formation to decay. Since we lack both specific star-formation rates for the dwarfs and sufficient numbers of dwarfs to disentangle these effects, the assumption of instantaneous quenching will suffice.

The cumulative distribution of satellite infall times is shown in Figure 5.2, with the original Via Lactea run in blue and Via Lactea II shown in green to illustrate the scatter between halo realizations. From this figure we can see the delay time that would be required for a given fraction of satellites to remain star-forming in this

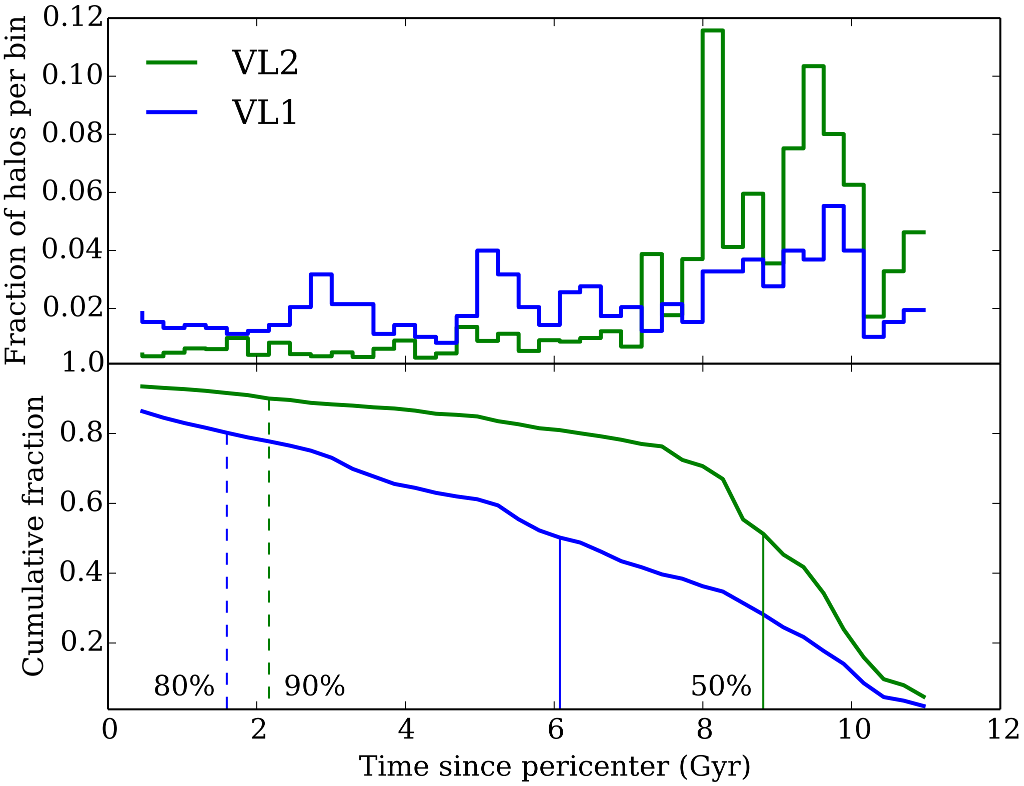

Figure 5.2: Differential (top panel) and cumulative distribution (bottom panel) of time between a satellite's first pericenter passage and $z = 0$, shown for both Via Lactea simulations. The solid vertical lines indicate where the cumulative distribution exceeds 50%, while the dashed vertical lines indiciate 80% and 90%. This provides a direct estimate of the quenching delay time that would be required to produce a desired quenched fraction. To reproduce the quenched fraction of the highest mass LG dwarfs thus requires a delay of 6-9 Gyr between pericenter passage and quenching, under this model. To reproduce a quenched fraction of 80% or more for low mass galaxies, noting that 10-15% of selected halos have not yet experienced a pericenter passage, short quenching times of order 2 Gyr are required.

model. The solid vertical lines are drawn where the cumulative fraction of satellites that have undergone pericenter is 0.5, which is roughly the quenched fraction observed for satellites at $10^8 - 10^{10}\ M_\odot$. The dashed vertical lines are drawn at cumulative fractions of 80% and 90%, which is characteristic of the low mass quenched fractions observed in the Local Group.

These cumulative pericenter fractions suggest that a rapid quenching process with a median delay time of ~ 2 Gyr is sufficient to reproduce the high fraction of quenched satellites seen in the LG, though considerable scatter exists between simulations. This rapid quenching is required to maintain the high quenched fraction, as recently-infalling satellites would tend to depress the quenched fraction if they were not quenched quickly. Rapid quenching upon pericenter also dovetails well with the observed radial distribution of dSphs. In Chapter IV we showed that reproducing the radial distribution of quenched LG dwarfs via a close interaction with the host requires a single such pericenter passage to be sufficient for quenching; any scenario in which more than one pericenter is required is strongly excluded by the existence of quenched dwarfs at ~ 700 kpc. Rapid removal of gas on a single pericenter fits both the high quenched fraction and the radial dependence quite well in the LG.

This short quenching time stands in contrast to the very long gas consumption timescales of these dwarfs. In general, dIrrs in the field frequently have as much cold gas as they have stars, if not more (Grcevich & Putman, 2009), and at their mean star formation rates many are unlikely to consume their gas in less than a Hubble time (Hunter & Gallagher, 1985; Bothwell et al., 2009; Huang et al., 2012). The short timescale for quenching that we measure reaffirms that the cut-off of gas accretion cannot be responsible for quenching low mass satellites; such a mechanism would leave far too many star forming dwarfs in the LG to match the observations. A rapid *removal* of cold gas appears to be necessary to quench a sufficient number of low mass satellites in a short period of time.

In comparison to the rapid quenching times for low mass dwarfs, Figure 5.2 suggests that to reproduce the roughly 50% quenched fraction at the masses characteristic of the NSA, a median delay time of 6-9 Gyr is required. This is in line with the conclusions of Wheeler et al. (2014) that satellite quenching at these masses is inefficient. Though this observation is clear, the cause of such inefficiency is difficult to determine since it can be the result of a quenching process which is either slow or which operates only on select dwarfs. It is possible that the time since pericenter is truly a clock which quenches galaxies that have been satellites for 6-7 Gyr or greater, and that all unquenched satellites are more recent additions to the LG. This scenario could arise if infall stopped the accretion of gas and the delay before a galaxy became quenched was set by the gas consumption time. However, this is not the only possible interpretation. For example, Wheeler et al. (2014) suggests that using the degree of mass loss as a proxy for the strength of interactions with the host is a more reasonable parameterization for what stops a dwarf's star formation. While it is possible that time since pericenter is not the factor that *determines* if a galaxy is quenched, it is unavoidable that some LMC-mass galaxies have been forming stars as satellites for as much as 6-7 Gyr after their first pericenter passage. If there were not, and only recent accretions could continue to form stars, the quenched fraction would necessarily be much higher at these masses. Thus while the evidence is inconclusive as to whether time is the dominant factor in quenching, whatever does cause quenching at these masses must permit some satellites to continue to form stars for many gigayears.

5.5.2 Ram Pressure

A possible mechanism for the removal of gas from satellites is ram pressure stripping by hot gas surrounding galaxies and clusters. Initially suggested to explain the relative infrequence of spiral galaxies in clusters (Gunn & Gott, 1972), the presense of hot halos around galaxies has been suggested as a way of accounting for the deficit of

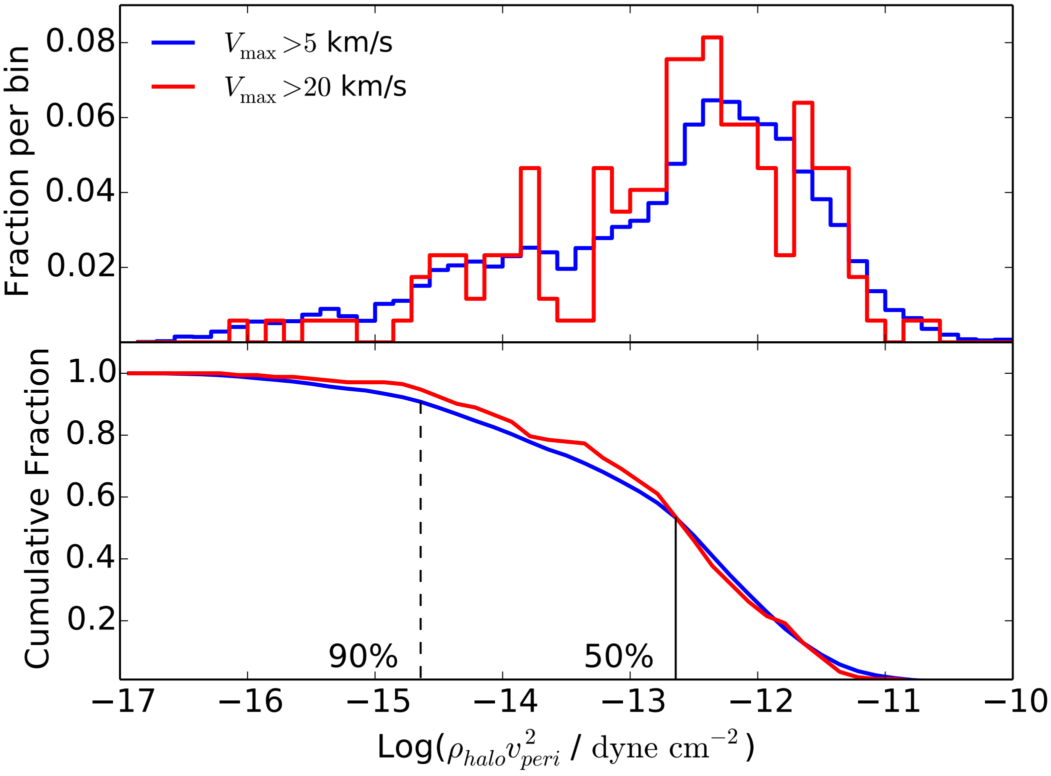

Figure 5.3: Histogram of the maximum ram pressure experienced by halos in the Via Lactea simulation (top), along with the cumulative distribution of ram pressures (bottom). The data are split into all halos with $V_{\rm max} > 5$ km/s in blue, and only halos with $V_{\rm max} > 20$ km/s in red, to show that the ram pressure distribution is largely independent of satellite mass. From the cumulative plot we can read the ram pressure required for quenching either 90% or 50% of satellites, and note that the two values differ by roughly a factor of 100.

baryons present in the stars and cold gas of galaxies when compared to the cosmological baryon fraction (Fukugita et al., 1998; Read & Trentham, 2005; Cen & Ostriker, 1999). Though the observed halos may not be massive enough to contain all of the missing baryons (Benson et al., 2000; Anderson & Bregman, 2010), they may still be able to affect the satellites passing through the hot gas (Lin & Faber, 1983; Mayer et al., 2006; McConnachie et al., 2007).

As noted above, the short timescales required for quenching at low masses appears to fit naturally with a model where the bulk of the satellite's cold gas is removed quickly by ram pressure stripping. The ram pressure force experienced by a galaxy is ρv^2, where ρ is the density of the gas the satellite moves through and v is its velocity. These two factors are greatest when a galaxy passes pericenter around its host, thus causing an "impulsive" effect on the satellite. The response of a satellite to such a force will clearly depend on its mass distribution, which determines how strongly it can hold on to its cold gas. However, the mass distribution of gas, stars, and dark matter in dIrrs is uncertain, and the magnitude of the restoring force which resists stripping is difficult to compute *a priori* for dwarfs of differing masses. Our modeling seeks to circumvent this problem by measuring ram pressure experienced by the population of satellites, and then use this to constrain how individual galaxies must respond. Other studies in the LG (e.g., Grcevich & Putman, 2009; Gatto et al., 2013) have sought to use the distribution of stripped and non-stripped dwarfs to constrain the density profile of the Milky Way's hot halo. We wish to turn this around; using a model of the halo from X-ray absorption studies (Miller & Bregman, 2013), what would the quenching criterion have to be to reproduce the observed quenched fractions?

To compute this, we want to estimate the range of pressures experienced by satellites as they fall into their host. At each of these pericenters we can compute the hot gas density, which together with the orbital velocity gives us the ram pressure force ρv^2. To obtain the kinematic information on satellite halos we use both the Via Lactea and the Via Lactea II simulations (Diemand et al., 2007, 2008), which sought to reproduce a Milky Way-like environment in a dark-matter-only simulation and together provide a rough estimate of the scatter between halo realizations. Using these N-body simulations lets us avoid the uncertainties of hydrodynamic simulations of ram pressure stripping, in which small satellites are difficult to resolve given the enormous dynamical range required. We track the orbit of each surviving subhalo in the simulations through each of its pericenter passages around either the Milky Way-mass halo or "Halo 2", a rough analog of the Andromeda that appears in VL2 (see Chapter IV and Teyssier et al., 2012 for further details on Halo 2). In finding the pericenter distances of subhalos we interpolate between snapshots in the simulation, which prevents pericenter distances from being overestimated due to the limited number of snapshots. As we showed in Chapter IV, we have used the more frequent snapshots in the VL1 simulation to verify that interpolation does not add significant errors.

In this model we assume that the single closest pericenter passage is entirely responsible for stripping. This is motivated by the strong velocity dependence of ram pressure, in which pericenter passages should dominate over the rest of the galaxy's orbit, but also imposed by uncertainties in the cumulative effect of ram pressure over an extended period of time or multiple pericenter passages.

From the closest pericenter we compute the density of the host galaxy's hot halo, using the Miller & Bregman (2013) model of the Milky Way as an example density profile. Their work uses a β-model for the functional form of the profile, constrained by measurements of X-ray absorption against various extragalactic and galactic sources, with a total hot gas mass of $3.8 \times 10^{10}\ M_\odot$ inside of 200 kpc. We note that this is a measurement of the present-day halo, and the halo may have been weaker or non-existent in the past. In assigning gas pressures seen by halos in the past we should be using the halo profile present at that time, but the evolution of hot gas halos is even more uncertain than the structure of halos that exist today. We thus make as simple of an assumption as is plausible, that the halo has had the same structure and mass since $z = 1$, before which it did not exist. This cut-off redshift is not critical to the results, and could even be omitted entirely without significant changes, as the majority of satellites have short enough orbital periods that they have a pericenter passage after the halo has turned on. If the density of the hot halo were to change substantially at very late times then it may have a more significant effect on our results, but any such halo growth would be entirely an assumption.

The resulting distribution of peak ρv^2 values seen by the subhalos in Via Lactea is show in Figure 5.3. The top panel shows a histogram of these values, while the bottom panel shows the cumulative distribution. In both panels the blue line samples all halos in the simulation with a maximum circular velocity at $z = 0$ of $V_{\max} \geq 5$ km/s, while the red line only includes halos with $V_{\max} \geq 20$ km/s. While this division is arbitrary, we include it to show that there is no significant correlation between satellite masses and the ram pressures they experience, so we will treat the results we derive from orbits as essentially independent of mass.

This bottom panel can be read as the fraction of galaxies that have experienced ram pressure of *at least* a given strength; in case we see that 90% of all halos have seen ram pressure in excess of $10^{-14.8}$ dyne cm^{-2}, while only 50% have experienced pressures greater than $10^{-12.8}$ dyne cm^{-2}. This is the key result of this model. If we ascribe the entirety of the quenched fraction change between $M_\star = 10^6$ and $10^{7.5}$ $M_\odot$ to changes in a galaxy's response to a given force of ram pressure, then it is this factor of 100 change in pressure that galaxy models must account for.

Such a model would need to treat the changing gas densities, stellar disk densities, and dark matter halo all to obtain a better estimate of the quenching criterion. This can be seen schematically by rewriting the force balance from Gunn & Gott (1972) in terms of surface densities (Mo et al., 2010),

$$\rho v^2 \sim 2\pi G \Sigma_\star \Sigma_{\rm gas}, \tag{5.2}$$

where now the relative distribution of stars and gas may lead to both a complicated dependence on total mass and could also suggest varying degrees of partial stripping in some cases. Unfortunately these mass distributions are not well constrained observationally, and the dark matter distribution may also play a role if its contribution to the restoring force is more significant than the stellar density (Abadi et al., 1999). This is difficult to assess from an observational standpoint, as the behavior of gas which is hypothetically stripped from the disk but remains bound to the dwarf is unclear. Even so, better models of dIrrs may not produce more accurate results if the underlying assumption of a stripping criterion based on force balance is itself inaccurate. This has been suggested by simulations that better treat the hydrodynamic instabilities in interactions, resulting in a stripping that proceeds more via ablation than by impulsive momentum transfer (Weinberg, 2014). Similarly, the addition of tidal effects during pericenter passage (Mayer et al., 2006) or internal heating by star formation (Nichols & Bland-Hawthorn, 2011) could play a significant role in determining a satellite's repsonse to ram pressure and particularly the dependence on satellite mass. The sum of these uncertainties both in models of dIrrs and in the physics of stripping limit our ability to provide a more detailed explanation for the evolution in stripping efficiency, but the magnitude of the effect is clearly demonstrated in the range of ram pressure forces experienced.

5.6 Discussion and Conclusions

We have shown that the fraction of quenched satellite galaxies undergoes significant variation across masses ranging from low mass dwarfs around the Milky Way and

Andromeda to more massive satellites in the LG and beyond. This a measurement spanning five orders of magnitude in mass, which highlights the commonality of satellite quenching as a phenomenon but conversely the large span of masses should also temper our surprise that a complex process like quenching exhibits varied behavior at different masses. The structure of galaxies across this range of masses changes substantially, and hence their strongly differing response to environmental factors may be a reflection of that fact.

We argue that our conclusion of a rapid quenching process for low mass satellites is unavoidable given the ubiquity of quenched satellites at these masses. The speed of quenching immediately places a constraint on plausible mechanisms, and the rapid removal of gas by ram pressure stripping appears to be a logical possibility. Quenching processes that proceed on the gas consumption timescale are difficult to reconcile with the observations. At the masses of the NSA sample, where the quenched fraction is closer to 50% than 90%, the long delay times leave the question of physical mechanisms open. Here the issue of a time delay may interact with repeated pericenter passages to remove gas only gradually in these massive dwarfs. Such a scenario is both beyond the capabilities of our model and poorly understood physically.

Our model of ram pressure stripping has sought to illustrate how dwarfs of differing masses must respond to ram pressure, if it is the dominant source of quenching. This method turns the observed quenched fractions into a value for the cut-off ram pressure between stripping and leaving a galaxy to continue forming stars, which provides a characterization of the forces at work. As with the delay time, it is possible that additional factors add complications to our picture of a simple ram pressure cut-off. For instance, the inclination of the disk of a dIrr as it falls into the galaxy may tip the balance if it would otherwise be on the cusp of being stripped. We argue that our characterization of the factor of 100 change in ram pressure seen by 50% and 90% of satellites provides an estimate of the average behavior, which may not apply to each satellite individually.

While our modeling has attempted to assess the general characteristics of satellite quenching, our models are clearly not the *ab initio* models of quenching that could explain the mechanisms behind the observed behavior. We emphasize the importance of attempts to construct such models in order to narrow what is presently a wide-open range of physical processes that are suggested to affect quenching. Accurate modeling of the input dIrr galaxies to be stripped is also critical in this effort, since our understanding of the stripping process requires detailed knowledge of the systems to be stripped. We have shown at a basic level what evolution in this effectiveness one might expect with mass, but this does not attempt to account for the changes in dwarf structure with mass. What was set up in Gunn & Gott (1972) as a simple force balance between ram pressure and the restoring force likely has substantial uncertainties on both sides.

We also must emphasize an important caveat of our study, which is that all of our data below $M_\star = 10^{7.5}\ M_\odot$ comes from satellites of the Milky Way and Andromeda. While we argue that these data are robust, the limited number of systems makes it impossible to know if the high quenched fractions are truly universal across Milky Way-like systems, or whether they are a peculiar result tied to the specific accretion history of the Local Group. This is a particularly important question in the light of results suggesting that the quenched fraction of satellites is dependent on whether or not the central galaxy is forming stars, an observation referred to as "galactic conformity" (Weinmann & Lilly, 2005; Phillips et al., 2014). We note that our Local Group results show a high fraction of quenched satellites around what are clearly star-forming hosts (the Milky Way and Andromeda). This perhaps illustrates the lower limit at which galactic conformity is effective; the lowest mass dwarfs appear to quench regardless of their host.

Despite this potential complication at LMC-masses, in the absence of any further information our best estimate of the quenching behavior comes from assuming that our galaxy is “average” and does truly represent a universal behavior, but we would surely have greater confidence if observations of other systems could confirm this universality rather than leave it as an assumption. This is but one of many subjects that stand to gain from the development of larger samples of dwarfs beyond the Local Group.

CHAPTER VI

The Complex Structure of Stars in the Outer Galactic Disk as revealed by Pan-STARRS1[1]

6.1 Abstract

We present a panoptic view of the stellar structure in the Galactic disk's outer reaches commonly known as the Monoceros Ring, based on data from Pan-STARRS1. These observations clearly show the large extent of the stellar overdensities on both sides of the Galactic disk, extending between $b = -25°$ and $b = +35°$ and covering over 130° in Galactic longitude. The structure exhibits a complex morphology with both stream-like features and a sharp edge to the structure in both the north and the south. We compare this map to mock observations of two published simulations aimed at explaining such structures in the outer stellar disk, one postulating an origin as a tidal stream and the other demonstrating a scenario where the disk is strongly distorted by the accretion of a satellite. These morphological comparisons of simulations can link formation scenarios to observed structures, such as demonstrating that the distorted-disk model can produce thin density features resembling tidal streams.

---

[1] This chapter was originally published in the Astrophysical Journal by Colin T. Slater, Eric F. Bell, Edward F. Schlafly, Eric Morganson, Nicolas F. Martin, Hans-Walter Rix, Jorge Pearrubia, Edouard J. Bernard, Annette M. N. Ferguson, David Martinez-Delgado, Rosemary F. G. Wyse, William S. Burgett, Kenneth C. Chambers, Peter W. Draper, Klaus W. Hodapp, Nicholas Kaiser, Eugene A. Magnier, Nigel Metcalfe, Paul A. Price, John L. Tonry, Richard J. Wainscoat, and Christopher Waters 2014, 791, 9.

Although neither model produces perfect agreement with the observations—the tidal stream predicts material at larger distances which is not detected while in the distorted disk model the midplane is warped to an excessive degree—future tuning of the models to accommodate these latest data may yield better agreement.

6.2 Introduction

The stellar overdensity usually termed the Monoceros Ring (MRi) has been studied for over a decade, but remains a poorly understood phenomenon in the outer Galactic disk. First identified by Newberg et al. (2002) and later shown prominently by Yanny et al. (2003) and Belokurov et al. (2006), in the Sloan Digital Sky Survey (SDSS) the structure appears as an overdensity of stars at ~ 10 kpc from the Sun, spanning Galactic latitudes from $b \sim +35^\circ$ to the edge of the SDSS footprint of $b \sim +20^\circ$ and in Galactic longitude extending between $l = 230^\circ$ and $l = 160^\circ$.

As the initial detections were widely-separated but approximately centered on the constellation Monoceros, and it appeared to lie at a constant Galactocentric distance, it was termed the Monoceros Ring [2]. Subsequent studies based on modest numbers of photometric pointings have elucidated the distance dependence of the structure and provided pencil beam mappings of the structure (e.g., Ibata et al., 2003; Conn et al., 2005; Vivas & Zinn, 2006; Conn et al., 2007, 2008, 2012; Li et al., 2012). These pointings have also shown that the feature appears both north and south of the Galactic plane at similar Galactic longitudes (Conn et al., 2005; de Jong et al., 2010), further expanding the known size of the structure. A summary of many of the detections of the MRi is shown in Figure 6.1, along with the MSTO stellar density map from the SDSS showing the MRi detections within its footprint. Spectroscopic observations have shown that much of the MRi is consistent with a

---

[2] Though, the structure clearly extends beyond the borders of the constellation Monoceros, we retain this terminology for convenience herein.

nearly circular orbit at a velocity of $\sim$ 220 km s^{-1} (Crane et al., 2003; Conn et al., 2005; Martin et al., 2006) and have potentially identified related star clusters at similar velocities (Frinchaboy et al., 2004). The association between the MRi and other density structures in the Galactic disk and halo has been the source of considerable controversy, with the Canis Major overdensity (Martin et al., 2004) and the Triangulum-Andromeda overdensity (Rocha-Pinto et al., 2004) both lying near detections of the MRi, and with debate as to whether the density structure seen in SDSS is of a common origin or multiple distinct structures (Grillmair, 2006; Grillmair et al., 2008).

While the basic observations of the MRi are generally agreed on, there is very little consensus on details beyond these, and particularly in the origin of the structure there is wide disagreement. One possibility is that the MRi is the tidal debris from a disrupting dwarf satellite galaxy (Martin et al., 2004; Peñarrubia et al., 2005; Sollima et al., 2011). In this scenario the stream's orbital plane is similar to that of the Galactic disk by virtue of a low-inclination progenitor orbit. An alternative scenario is that the stars in the MRi originally formed in the Galactic disk, but were stirred up by some dynamical perturbation to heights of 1-5 kpc above and below the disk. Qualitatively, such scenarios can be simply stated, but their parameterization and characterization can be complex.

Some models have sought to characterize the observations of overdensity by modeling a flare and a warp in the Galactic stellar disk (Momany et al., 2006; Hammersley & López-Corredoira, 2011), while numerical models have sought to recreate a MRi-like feature in N-body simulations by perturbing a disk with satellite galaxies (Younger et al., 2008; Kazantzidis et al., 2008). Perturbations to the disk by satellites have been studied both in observations (Widrow et al., 2012) and in N-body simulations of spiral arms (Purcell et al., 2011) and vertical density waves (Gómez et al., 2013), all reinforcing the picture that the disk can exhibit complex structure in response to close satellite passages. Observationally, in M31 disk-like stellar populations have been found at large distances from the bright stellar disk (Richardson et al., 2008), and appear to also have disk-like kinematics (Ibata et al., 2005). Distortions and warps in the outer stellar disks and HI gas of galaxies appear common (Sanchez-Saavedra et al., 1990; García-Ruiz et al., 2002), and some have been shown to cause the formation of young stars at large heights from the plane as defined by the central region of the galaxy (Radburn-Smith et al., 2014).

Most of the models of the Monoceros Ring can produce qualitative matches to the available data, which has left little leverage to distinguish between these scenarios. In particular, the lack of a contiguous map of the MRi has forced models to rely on matching the distances and depth of the structure as seen by the available sparse pointings. This limited dataset has made it difficult to see a correspondence (or disagreement) between the N-body simulations and the actual MRi structure, since the complex density structure predicted by these simulations can be masked when only a limited number of discontiguous pointings are available for comparison.

In this work we present a panoramic view of the Monoceros Ring using Pan-STARRS1 (PS1; Kaiser et al., 2010), extending both north and south of the Galactic disk and covering 160° in Galactic longitude. This is the most comprehensive map of the MRi to date, enabled by extensive sky coverage of PS1 and its survey strategy that — unlike SDSS — fully includes the Galactic plane. As we will show, this panoptic view provides a dimension of spatial information that had previously only been hinted at and incomplete, particularly in the southern Galactic hemisphere.

To illustrate the utility of these new maps, we also present a first comparison to physically motivated N-body simulations. Though qualitative in nature, we will show that such comparisons can immediately be used to refine our understanding of the physical ingredients necessary for reproducing the structure. In the following work we describe the PS1 survey and the data processing in Section 6.3, followed by a

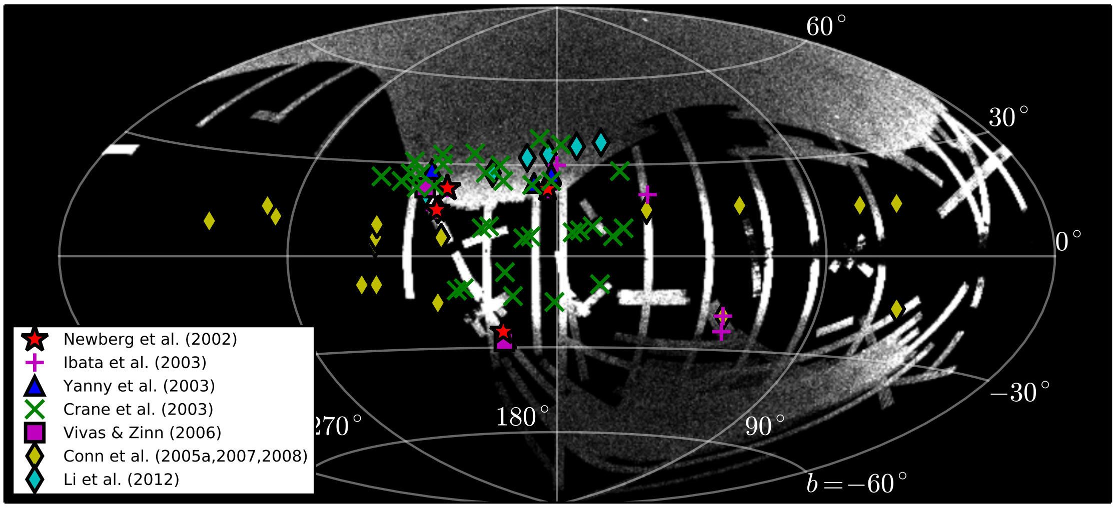

Figure 6.1: A comparison of previous detections of the MRi from various authors (each listed in the figure legend), overlaid on the map of the MRi as seen by the SDSS (showing the density of stars with $0.2 < (g-r)_0 < 0.4$ and $18.6 < g_0 < 19.8$). While the individual pointings clearly show that the MRi occupies a significant amount of area in the Galactic anticenter, both north and south of the Galactic plane, it is difficult to understand the morphology of the structure without contiguous imaging coverage.

discussion of the resulting MRi maps in Section 6.4. We show the comparisons to the two N-body models in Section 6.5, and we discuss the results and conclusions in Section 6.6.

6.3 The Pan-STARRS1 Data

PS1 is a 1.8m telescope on the summit of Haleakela, Hawaii, which operates as a dedicated survey instrument (Chambers et al., in preparation). The telescope images in five bands ($g_{\rm P1}r_{\rm P1}i_{\rm P1}z_{\rm P1}y_{\rm P1}$) with average exposure times on the order of 30-45s (Metcalfe et al., 2013). The individual exposures are photometered by an automated pipeline (Magnier, 2006) and calibrated to each other self-consistently using partially overlapping exposures (Schlafly et al., 2012), yielding a calibration precision better than 10 mmag as measured against SDSS. In this work we use data from the 3π survey, which covers the entire sky north of declination $-30°$ and is designed to obtain approximately four exposures per pointing, per filter, per year. Although the survey does produce stacked images and the resulting photometry, in this work we use data that is the merger of the photometric catalogs of all individual exposures. Stacked data from PanSTARRS-1 will reach more than a magnitude deeper, but the processing pipeline for the single epoch data is currently more mature and reliable. MSTO stars in Monoceros are easily detected in the PS1 single epoch images, and so we accordingly use that data in this work. We use the most recent consistent reprocessing of the 3π observations, termed Processing Version 1 (PV1), which contains observations obtained primarily between May 2010 and March 2013. As measured against the SDSS stripe 82 coadd catalog, our 50% completeness levels range from roughly $g_{P1} = 21.4$ to 22.0, and $r_{P1} = 21.2$ to 21.8 (Slater et al., 2013). Since these are limits are substantially fainter than our target MSTO stars in the MRi, this limited photometric depth will not impair our results.

Because the stars we focus on in this work are much brighter than the completeness limit, our photometric uncertainties are largely the result of large scale systematic effects and calibration uncertainties rather than photon noise on the photometry itself. In general this results in a typical uncertainity of $0.01-0.02$ magnitudes (see Schlafly et al., 2012, for further details). The most significant remaining uncertainity is the correction for Galactic extinction. The relatively narrow color selection we use makes the number counts of MSTO stars sensitive to small color shifts, which can be caused by errors in the extinction maps used for dereddening. For extinction correction we use the maps of Schlegel et al. (1998), corrected with the factors prescribed by Schlafly & Finkbeiner (2011). While the Schlegel et al. (1998) maps are in general excellent, there are regions of our maps where changes in the measured stellar density correlate strongly with dust extinction features. This is primarily an issue within

$20 - 30^\circ$ of the north celestial pole, and we therefore do not want to overinterpret the results there. Beyond this particular region the extinction correction appears to be well-behaved and there are fewer correlations between MSTO map features and extinction features. The regions where we have marked Monoceros-like features do not show significant dust features.

Here our principal objective with the PS1 observations is to create a series of stellar density maps showing the spatial extent and morphology of the MRi in a low-latitude version of the "Field of Streams" (Belokurov et al., 2006). To do this, we impose cuts on color and magnitude of stars in a way designed to select main sequence turn-off (MSTO) stars of an old ($\sim$ 9 Gyr) population with $-1 \lesssim$ [Fe/H] $\lesssim 0$ and at the range of heliocentric distances of interest. A color range of $0.2 < (g - r)_0 < 0.3$ optimizes the contrast between the MRi and any foreground (nearby Galactic disk) or background (stellar halo) contamination. We have estimated the distance to the stars selected by this color cut with the BaSTI set of isochrones (Pietrinferni et al., 2004). We use a 9 Gyr old, [Fe/H]=-1.0 isochrone populuated with a Kroupa (2001) initial mass function and with realistic observational uncertainties added. The choice of stellar population parameters are in line with the metallicity measured for the MRI by both Conn et al. (2012) and Meisner et al. (2012), though substantial scatter in the metallicity of the MRi has been reported (e.g., Yanny et al., 2003; Crane et al., 2003). The median magnitude of the synthesized stars selected by this color cut is $M_{g,P1} = 4.4$, which we shall adopt for our quoted distances, though the spread is considerable and 70% of synthesized stars are found within ±0.5 magnitudes of the median value. The uncertainity in the stellar populations of the MRi, particularly the age, adds an additional $\sim$ 0.2 magnitude systematic uncertainity, but this is substantially less than the intrinsic magnitude spread of the MSTO in a single stellar population. The uncertainity between different sources of isochrones is at a similar level, and studies of globular clusters also produce similar results (Newby et al., 2011).

6.4 Observed MRi Morphology

Figure 6.2 shows the MSTO stellar density map, projected in Galactic coordinates, centered on the Galactic anticenter. The components of the three-color image were chosen to show stars with $17.8 < g_0 < 18.4$ (centered on roughly 4.8-6.3 kpc, but also broadened by the intrinsic MSTO magnitude spread) in blue, stars with $18.8 < g_0 < 19.6$ in green (7.6-11.0 kpc), and more distant stars with $20.2 < g_0 < 20.6$ in red (14.4-17.4 kpc). The most prominent features of the MRi are the broad horizontal arcs on both the northern and southern sides of the disk, primarily in blue and green, showing several sharp density features at large heights above the disk. On the northern side multiple arcs are visible, which we have labeled in Figure 6.3 for convenience in describing them. The MRi features seen in SDSS are what we have labeled Features B and C, with some small part of Feature A also visible towards the edge of the SDSS coverage. Where the Pan-STARRS and the SDSS coverage overlap there is good agreement on the morphology of the features, while the additional new area available in the PS1 coverage shows all of these features in a contiguous map, revealing that they extend substantially beyond the SDSS footprint.

The southern extent of the MRi has not been seen before in a wide-area map. The broad southern sharp-edged arc is strikingly similar to the observed arc on the northern side of the disk, particularly Feature C, and leaves little doubt that these features are related. In our maps the MRi clearly encompasses a vast area of the Galactic anticenter region, spanning from $b = -25°$ to $b = +35°$ and covering nearly 130° in longitude on both sides. It is interesting to note that the material that makes up Features C and D appears to blend smoothly in with the disk closer to the Galactic plane, with no second sharp edge at lower latitudes to denote an "end" of the MRi material. This is particularly apparent in the south, as some extinction features may be affecting the north slightly more.

Though the bulk of the MRi appears similar on both sides of the Galactic plane,

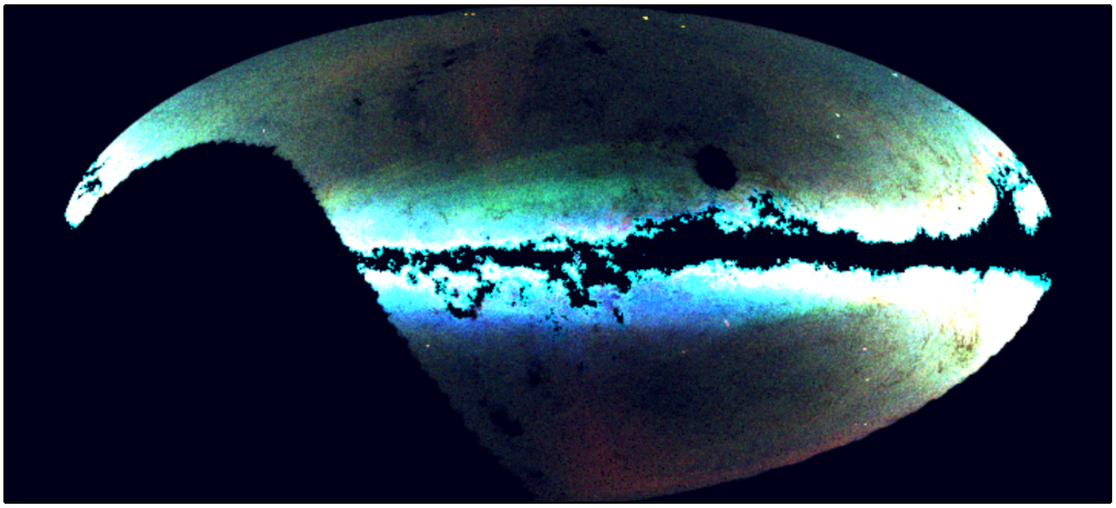

Figure 6.2: Pan-STARRS1 map of star counts in Galactic coordinates for stars with $0.2 < (g-r)_0 < 0.3$. Nearby stars with $17.8 < g_0 < 18.4$ (4.8-6.3 kpc) are shown in blue, stars with $18.8 < g_0 < 19.6$ (7.6 - 11.0 kpc) are shown in green, and more distant stars with $20.2 < g_0 < 20.6$ (14.4 - 17.4 kpc) are shown in red. The Galactic anticenter is in the middle, and the Galactic center is on the right edge. The Monoceros Ring can clearly be seen in broadly horizontal green structure on the nothern side of the plane and in the similar structure on the southern side of the plane in blue, both of which extend over 130° in Galactic longitude. The difference in color as presented suggests that the southern component is slightly closer to the Sun than the northern component. The Galactic plane and some localized regions near the plane are missing due to high extinction, while the apparent hole near the north celestial pole was imaged but not included in this processing of the data. There are some regions of the north Galactic cap and near the celestial pole that suffer from poor PS1 coverage. The Sagittarius stream appears nearly vertical in red on both sides of the disk.

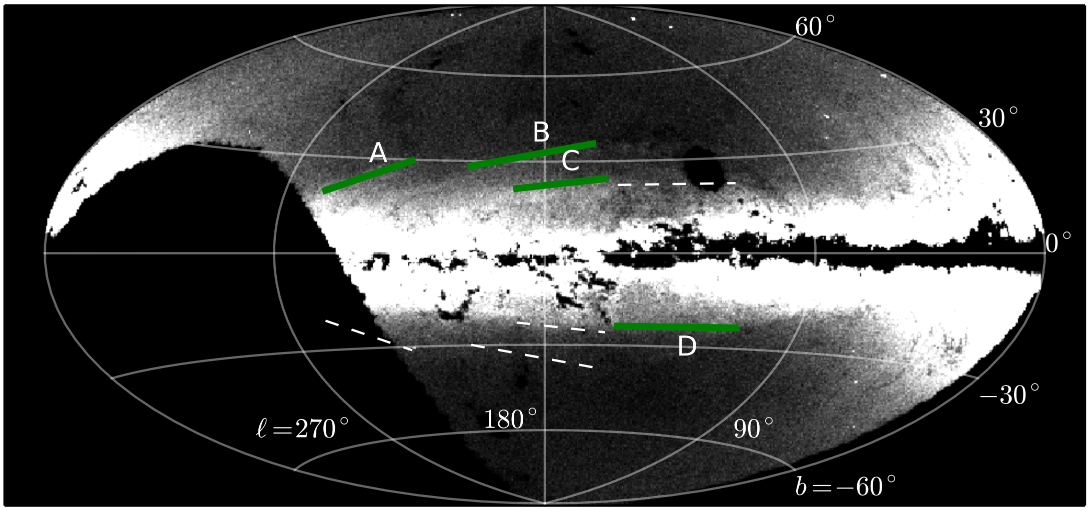

Figure 6.3: Same as Figure 6.2, showing the middle (green in Figure 6.2) distance slice and with several density features labeled. These markings are not intended to be comprehensive, and many of the features extend beyond the extent of the labels. The white dashed lines show the location of the labeled features reflected across the Galactic plane. The grid shows $l = 90°$ (right side), $l = 180°$, and $l = 270°$ (left side), along with lines at $b = \pm 30°$ and $\pm 60°$.

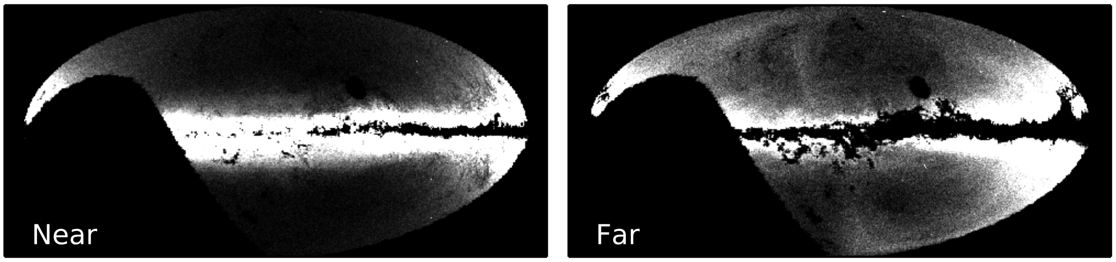

Figure 6.4: Two distance slices, one nearer than the main body of the MRi (left, shown in blue in Figure 6.2, $17.8 < g_0 < 18.4$) and one further (right, shown in red in Figure 6.2, $20.2 < g_0 < 20.6$). In the nearer slice there is very little evidence of the MRi in the north, though southern structure remains visible. In the far slice the MRi has become much less prominent and there is little new MRi-related structure that becomes apparent.

there are small but noticeable asymmetries between the northern and southern features. To aid in seeing this, the marked features have also been reflected across the Galactic equator and denoted with dashed white lines. The A and B features clearly extend further off the Galactic plane than any feature in the south, though C and D seem to be very similar in extent both in latitude and longitude. There does not appear to be the same multiplicity of arcs on the southern side as compared to the north.

These arcs, which we refer to as Features A and B, have been previously pointed out by Grillmair (2006) and revisited in Grillmair (2011), which referred to these features the anticenter stream and the eastern banded structure, respectively. Though these stellar density features certainly exist, their decomposition into "distinct" features does not appear obvious or unique.

In Figure 6.4 we show the nearer (blue in Figure 6.2) and farther (red in Figure 6.2) distance slices separately from Figure 6.2, so that they can be examined independently. These maps show that the structure is relatively well-confined in heliocentric distance, with the southern part becoming visible in the near slice and only hints of the structure remaining in the far slice. We will illustrate the utility of these distance slices for constraining models in Section 6.5, but from the data alone we can show that the structure is not very extended in heliocentric radius. There is, however, an offset in distance between the northern and southern components of the MRi, with the southern component somewhat closer to the Sun than the northern side.

6.5 Model Comparisons

In order to guide the understanding of the observed MRi, we have created "mock observations" of two N-body simulations. One of these models the MRi as perturbed disk stars that have been stirred up by satellite galaxies (Kazantzidis et al., 2009), while the other models the MRi as simply the debris from a disrupted satellite (Peñarrubia et al., 2005). These two simulations serve to illustrate the range of morphologies that these categories of models generate, along with demonstrating the utility of the PS1 maps for differentiating between these models. We note that at this stage neither simulation has been tuned to reproduce the PS1 observations, so discrepancies must be expected, but our goal is to highlight these discrepancies so that future models may be better tuned to match the observations.

To produce maps of the simulations with similar observational characteristics to the PS1 data, we use the same isochrones as in Section 6.3 to determine the extent to which each simulation particle contributes to the various magnitude slices, with the considerable magnitude spread of the MSTO causing simulation particles to potentially contribute to multiple slices. As per our population modeling in Section 6.3, we account for this spread by approximating the MSTO absolute magnitude distribution as a Gaussian centered on $M_{g,P1} = 4.4$ and a width of 0.5 magnitudes. This center and width approximate the synthesized distribution of MSTO stars, though in detail the shape likely deviates somewhat from a Gaussian. After determing each particle's contribution to a given magnitude slice, the particles are projected onto the "sky" as would be seen by an observer and summed to produce the star counts map. It is important to note that the simulations are run at resolutions much coarser than single stars, and hence individual simulation particles are visible in some regions of the maps which contributes to a "grainy" appearance. We do not correct for this.

6.5.1 Satellite Accretion Model

As an example of models that recreate the MRi as the tidal debris of a dwarf galaxy, we show the simulations of Peñarrubia et al. (2005). This simulation attempted to reproduce all of the positions, distances and velocities of the MRi that were known at the time of publication. To do so, the authors varied the properties of the accreted dwarf along with its orbit and the shape of the Galactic potential to find a solution that best reproduced the known observations. The resulting best fit has the hypothesized dwarf on a very low-eccentricity orbit ($e \sim 0.1$) and at a low inclination relative to the Galactic plane, which allows it to make multiple wraps over a relatively narrow range of Galactocentric radii and relatively close to the disk in height. The simulation is also designed so that the main body of the disrupting satellite appears in the region of the Canis Major overdensity (Martin et al., 2004), as an attempt to link the two structures. As more recent evidence suggests that the Canis Major overdensity may not be related to a disrupted dwarf (Mateu et al., 2009), in our comparison we will focus on the general behavior of the tidal stream component rather than the specific location of the progenitor. Also note that this simulation focused on the properties of tidal debris, there are no N-body particles from the Galactic disk, which is instead modeled with a static potential. The particles used to reproduce the stream are the dark matter particles from the satellite, as there was no distinction made between a central concentration of luminous particles and a larger dark matter halo. As a result, the model predictions of the surface brightness of the stream along its orbit may be inaccurate, and further work would be needed to make more precise predictions. Our focus is thus on the general morphological comparison between the model and observations.

A visualization of the simulation can be seen in Figure 6.5 as green points (satellite debris particles) plotted on top of the observed PS1 data. Three magnitude slices are plotted, corresponding to the cut targeting the main body of the MRi in Figure 6.2 (labeled “mid”) and the two cuts on the near side and far side of the MRi from Figure 6.4. From this we can see that the overall shape of the MRi is reproduced quite well in the “mid” distance slice of the simulation. The north and south both exhibit very broad structures with a sharp edge on the side away from the Galactic plane, along with a convincing degree of symmetry across the two hemispheres that is reminiscent of the symmetry of Features C and D.

Though the “mid” distance slice exhibits considerable resemblance (though with some spatial offset), there is substantial discrepancy between the simulation and the observed structure in the “far” slice. Some of the material in the far slice does trace northern and southern edges of the MRi as observed, but generally the material appears in new regions of the sky that were not as well-populated in the “mid” slice. This is noticible in the south, where a broad stream paralelling the observed MRi in the “mid” slice is replaced by a different wrap of the stream at a different angle in the far slice, cutting across the plane rather than paralleling it. In the north the simulated MRi material is prominent in differing regions; while both match some portion of the MRi, the mid and far slices do not match each other. These features are in contrast to the strong similarity between the observed mid and far slices, in which the far slice does not show any new features of MRi appearing that were not prominent in the mid slice. Some of the structures that appear most prominently at closer distances still appear in the far slice, due to the intrinsic spread in magnitude of the MSTO, but no new components of the MRi appear in the far slice. A portion of the features in the simulation do fall outside the PS1 footprint on the sky, particularly structures on the far left side of the figure, which corresponds to the southern celestial hemisphere, but there appears to be substantial structure even within the area covered by PS1. The recent deep mapping near Andromeda (Martin et al., 2014) may show some material resembling the stream model shown here (which they refer to as the “PAndAS MW stream”, near $l = 120^\circ$, $b = -20^\circ$), but the detected material is further than both our “far” slice and the predicted stream, so the correspondence is tentative. The overdensity in the simulation between $l = 180^\circ$ and $l = 270^\circ$ and just south of the Galactic plane is the main body of the disrupting dwarf. We do not find an overdensity of this significance in the PS1 data, but this is mostly off the edge of the PS1 coverage and is also likely to be a specific prediction of this particular simulation rather than a general prediction of tidal stream models.

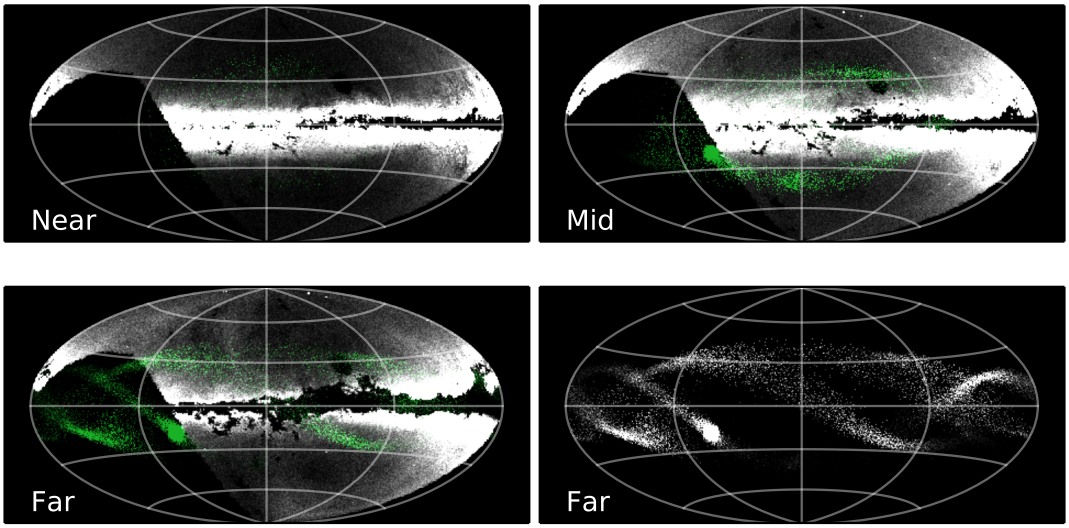

Figure 6.5: Visualization of the Peñarrubia et al. (2005) model for the formation of the MRi by accreted satellite material (green points), plotted on top of the PS1 observations. We show three magnitude slices (approximately corresponding to distance slices used in the observations), with the top-right "mid" slice matching Figure 6.2 and the "near" (top left) and "far" (bottom left) slices matching Figure 6.4. The "far" simulation slice is repeated by itself on the bottom right for clarity. The PS1 images are the same as Figures 6.2 and 6.4. The "mid" slice shows broad agreement with the observed structure, though somewhat offset, while the "far" slice shows a considerably different set of overdensities that do not appear to match the observations.

The general discrepancy between the simulation and the observed MSTO maps in the amount of structure at large distances may be intrinsic to satellite accretion models, which in general require dwarfs to be on at least mildly eccentric orbits and thus causing the widely spread debris. The challenge for future accretion models that attempt to reproduce the MRi is thus to plausibly explain the circular orbit, or to present some other way in which the debris at larger distances is hidden from view.

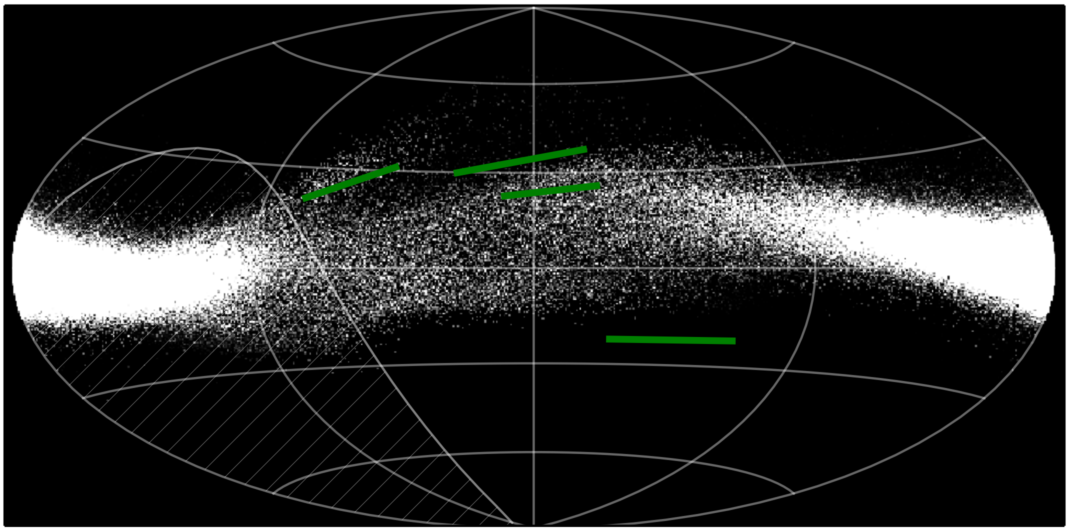

Figure 6.6: Visualization of the Kazantzidis et al. (2009) model, approximating the distance cut and uncertainties from the PS1 data in Figure 6.2. The feature annotations from Figure 6.3 have been included to give a sense of scale of the out of plane features. The hatched region indicates the area south of declination −30°, which is not observed by PS1. For clarity and as the model already includes a galactic disk, we have not overplotted it on the existing data. While the simulation is not designed to replicate individual features, there is a striking similarity between the model and the observed MRi in the presence of thin wisp-like features, but also a clearly excessive level of warping of the disk midplane beyond that seen in the Milky Way.

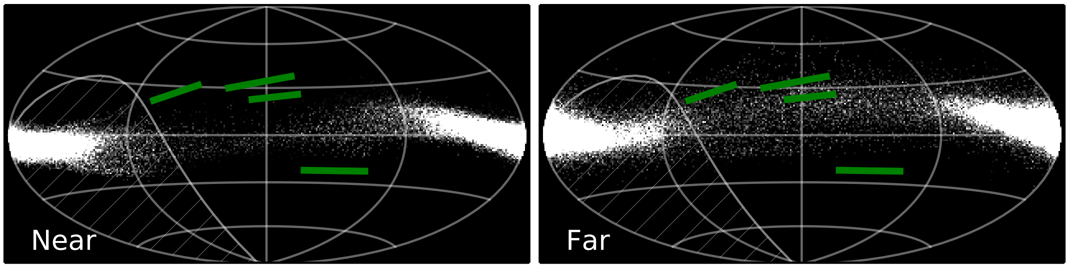

Figure 6.7: Visualization of Kazantzidis et al. (2009), showing a closer and a further distance cut (same as in Figure 6.4).

6.5.2 Disrupted Disk Model

The simulation of Kazantzidis et al. (2009) present a case where the disk of the galaxy has been strongly disrupted by the impact of satellite galaxies. The simulation we show is one of a suite of controlled experiments where a Milky Way-sized disk was subjected to bombardment by a cosmologically-motivated set of six dark halos. These halos range from 20%-60% of the mass of the disk itself, with the majority of the effect on the disk being driven by the most massive accretion event. The disk in the simulation has a mass of $3.53 \times 10^{10}\ M_{\odot}$, and the satellite halos hence had masses ranging from $7.4 \times 10^{9}\ M_{\odot}$ to $2 \times 10^{10}\ M_{\odot}$. The pericenters of the satellite orbits ranged from 1.5 kpc to 18 kpc. In contrast to the Peñarrubia et al. (2005) model, in this visualization there are no particles from the dwarfs shown; the particles we show were all originally in the simulated disk.

While the transformation from simulation particles into "mock" MSTO slices is the same for this simulation as for our presentation of the Peñarrubia et al. (2005) simulation, there are a few additional complications. Because the Kazantzidis et al. (2009) simulation was not tuned to reproduce any observations of the MRi, there is no preferred position for the observer. That is, we can visualize the simulation as if we were at any point on the Solar circle, each time obtaining a unique view of the disrupted disk. We chose an observer position that gives the best qualitative resemblance between the simulations and the observations in order to show as many positive features of this type of model as possible. There is also some question as to how best to define the Galactic plane in such a simulation. A gas disk would be the natural choice, but since this is an N-body only simulation, that option is not available. Following the initial analysis of the simulation in Kazantzidis et al. (2009), we have chosen to align the galactic plane of our visualization perpendicular to the total angular momentum axis summed over all of the particles in the simulation.

The resulting mock observations are shown in Figure 6.6, where a substantial warping of the disk is clearly evident. To the right of the anticenter there is very little material remaining along the Galactic equator, as nearly all of it has been displaced. This level of disk distortion is evident regardless of where the observer is placed along the solar circle. This level of disk warping is substantially beyond what is observed in the Galaxy, where the offset between the Galactic plane and peak density of the stellar disk is at most $1-2^\circ$ (Momany et al., 2006) rather than the $\sim 10^\circ$ in the simulation.

Despite this drawback, we find the simulation to be very useful in showing the possible disk response morphologies generated by a substantial perturbation. There are very clear "streamers" visible which appear to fly off from the disk (in Figure 6.6 coincidentally overlapping where Feature A is), along with features of higher density and sharp edges up off the disk (near Features B and C). As discussed above, we have intentionally selected the position of the observer in this simulation to best highlight the agreement between the simulation and the observations, so we should not over-interpret this agreement as a conclusive statement about the origin of the MRi. The presence of such strikingly similar features should lend credibility to the hypothesis that the complex and highly structured MRi features in the Galaxy have a common origin, but only if the degree of disk disruption can be brought into line with observations.

Figure 6.7 shows the nearer and further distance slices of the Kazantzidis et al. (2009) model. The warp clearly extends across all of these distance slices, with somewhat lower projected heights in the more distant slice. However, these alternate slices show similar substructure as in the "mid" slice, with no morphologically distinct components becoming visible as is predicted by the Peñarrubia et al. (2005) model. On this basis the tidal stream model is more easily seen to be in conflict with the observations, but the disrupted disk may similarly be too extended in radius. A quantiative comparison of the radial extent of the simulated disruption with the observed MRi would be necessary to confirm this. The radial profile of the disrupted disk material may also depend strongly on the disk's initial profile, adding another degree of freedom to such models.

Based on these comparisons, the crucial question for future simulations to test is whether such MRi-like features can be created without causing such an unrealistically large distortion of the disk. This could be a matter of the particular accretion history of the simulated disk, and less massive satellites or particular infall trajectories could be more favorable. Including cold gas in simulated accretion events could affect the outcome, possibly absorbing energy of the infall or forming new stars within a distorted gas disk (as in, e.g., NGC 4565, Radburn-Smith et al., 2014). The behavior of the gas may also provide additional points of comparison between observations and simulations, as the warping of the HI disk is well-studied (Kalberla & Kerp, 2009).

Additionally, a more comprehensive search of the available parameter space in the simulations could produce more realistic results. For example, the Kazantzidis et al. (2009) simulations were run until the disk had "settled", in that its bulk properties ceased to change significantly with time. While reasonable for understanding the properties of disks under bombardment in general, it is possible that we see the MRi today at a unique time in its dynamical evolution, and a search of multiple timesteps in a simulation may show transient effects (or possibly more evolved and settled states) that more closely resemble the MRi.

6.6 Discussion and Conclusions

Exploiting the photometric accuracy and 3π sky coverage of the PS1 photometry, we have presented the first distance-sensitive MSTO map of the Milky Way's stellar distribution at low ($|b| < 30°$) Galactic latitudes. This map shows rich substructure, much of which has been referred to as the MRi structure in the past. This map (Figure 6.2) presents the most complete and only contiguous map of the MRi structure to date, showing its extent on both sides of the Galactic plane and covering over 130° in longitude. The characteristic sharp edge in density at large heights above the disk is readily distinguished on the northern and southern sides of the disk. The other arc-like features in the north have positions and morphologies that are suggestive of a connection to the MRi. The PS1 maps also suggest that the MRi is relatively confined in radius, and we find no evidence of new structures related to the MRi either closer to or further from the Sun.

It is not obvious how to decompose the structure we see in the MRi into a set of distinct components. If the structure is the remnant of a tidal disruption, its position along the Galactic disk certainly makes it challenging to recognize it as such. As we have discussed, the superposition of a stream atop the exponential density distribution of the disk could mask the signature of a stream. However, it is difficult to see how an orbit (or orbits) could yield a distribution of material over a narrow range in distance, since an accreted satellite must have fallen in from large distances. This observed behavior in distance is a strong constraint which future attempts to model an accretion event must agree with.

Likewise, it is difficult to intuitively understand what features are generated when a stellar disk is disrupted by satellites. It is likely that the state of the disk after such events is highly dependent on the mass and orbital parameters of the satellite (or satellites), and additionally is likely to be highly time-dependent. These difficulties in visualizing and modeling such events should not cause us to exclude them.

The challenges of understanding and recreating either formation scenario necessitate the use of models to both guide our understanding of the features we see and to provide predictions that can be used for differentiating between theories of the formation of such substructure. In both our comparisons to the accretion model of Peñarrubia et al. (2005) and perturbed disk model of Kazantzidis et al. (2009) we find qualitative agreement in reproducing some of the features of the MRi, but both also show areas of conflict with the observations. Our objective with the PS1 maps is to show where these models need improvement, and to show how even qualitative morphological constraints can be used to further refine the models of different formation scenarios.

Though we have explored two models which are particularly well-suited for comparison to the PS1 maps this is certainly not an exhaustive list of possible models for the MRi. There are also analytical models for the MRi that we have not considered in depth, such models that parameterize the structure as part of a Galactic flare (Momany et al., 2006; Hammersley & López-Corredoira, 2011). Proper consideration of these models requires a comprehensive fitting of the spatial and distance dependence of the observed distribution of disk stars as a whole, which is beyond the scope of this work. However, there are general morphological features of the flare models that we can compare to the observations. The sharp edge in latitude that has been characteristic of the MRi since its initial discovery, and which we have shown also exists prominently in the southern hemisphere, is a particularly strong constraint on Galactic flare models. Such a feature strongly suggests the existence of some dynamically cold component with a low velocity dispersion, which is at odds with flare models that require large vertical velocity dispersions to raise stars to greater heights above the disk.

Our presentation of these models is designed to link physical processes with the morphological features they create on the sky, demonstrating where these simulations perform best and drawing attention to where they most need refinement in order to plausibly explain the observed substructure. In the case of a tidal stream, we have shown that the challenge for future models is to limit the debris to a compact range of Galactocentric radii while still filling that range with a substantial amount of substructure. For perturbed disk models the goal must be to create substantial structures out of the plane without causing the disk to warp to such an unsupportable degree. The ability or inability of future models to accommodate these conditions as dictated by the data should help to narrow in on the origin of the MRi. This map provides an obvious starting point for follow-up observations, as 3D velocities and metallicities of the stars in the various “features” should help to untangle their nature. Most of the stars should be bright enough to get good proper motion estimates from *Gaia*, but radial velocities and metallicities may require spectroscopy beyond the current set of spectroscopic surveys (RAVE, SEGUE, APOGEE, LAMOST or *Gaia*). Nonetheless, it is clear that the Galactic disk offers a rich example of how galaxy disks are being disturbed, and how they respond to such disturbances.

CHAPTER VII

Conclusions

7.1 Results from this work

In this work I have attempted to extend the sample of known dwarf galaxies, improving our knowledge of satellites on the outskirts of their hosts. I have used this sample to constrain the possible mechanisms for setting the dichotomy between quenched and star-forming galaxies, both at fixed mass with varying distance from the host, and as a function of mass of the satellite. Finally, I have shown that dwarfs may be responsible for some of the structure we see in the Milky Way disk, by gravitationally distorting and disrupting the ordered rotation into a distribution with significant out of plane motion.

The dwarfs we have observed, Andromeda XXVIII and XXIX, are unusual for their location but otherwise almost entirely as would be expected for satellite galaxies at similar masses. Their shapes and radial profiles are not unusual, they show no substantial deviations from the profile of a typical dSph. Their mean metallicities are as expected from the mass-metallicity relation derived from other Local Group dwarfs. Their metallicity spreads are indicative of star formation that lasted long enough for some self-enrichment to occur (rather than being monoabundance single stellar populations), and the complex horizontal branch morphology of Andromeda XXVIII is also suggestive of this. The confirmation that And XXVIII lacks any detectable HI gas is yet another check box that the galaxy is a “typical” dSph.

All of these aspects would be unexceptional for dwarfs at small distances from their hosts, but at the 250-350 kpc separation that Andromeda XXVIII and XXIX lie from M31, the galaxies become potentially interesting probes of the dwarf irregular to dwarf spheroidal transformation process. One might have expected satellites at large distances to exhibit intermediate properties—perhaps only partial gas stripping, or a more disk-like morphology—but this is not what we see. The formation of dSphs appears to be an “all or nothing” situation (with a few dwarfs potentially in the middle of this transition, e.g. Leo T).

The sharpness of this transition set up the question posed by Chapter IV: can we define a strict criterion based on a galaxy’s orbit to define if it is quenched or not, which then reproduces the radial distribution of quenched dwarfs in the Local Group? There is no reason *a priori* why a fixed radius for quenching needs to reproduce the observed radial distribution, but to the extent the limited number of Local Group galaxies allows us to tell, requiring that any galaxy that passes inside half of the virial radius of the host at least once can adequately reproduce the quenched satellites we see, including Andromeda XXVIII and XXIX. The physical mechanism may remain quite complex, but the phenomenology is straightforward. Furthermore, quenching scenarios where galaxies must make multiple orbits of their host are entirely unable to reproduce the quenched satellites beyond ~ 300 kpc. There is very little room to avoid this constraint since it is largely a result of the long orbital timescales at such radii relative to the age of the universe. Only quenching through an entirely distinct channel, not dependent on the host, could accommodate these galaxies otherwise.

Such an unequivocal criterion for satellite quenching faces two exceptions: the Large and Small Magellanic Clouds. These galaxies are large enough to straddle the border of many definitions of dwarf galaxies, and their behavior could very well be dissimilar to lower mass dwarfs and more common to higher mass galaxies. Fortunately galaxies of this mass are detectable in the SDSS, giving a much more statistically useful sample than is available in the Milky Way alone, and it is this combination of SDSS data plus low mass Local Group dwarfs that we use in Chapter V to show that LMC/SMC mass galaxies are indeed more likely to remain star forming as satellites than lower mass galaxies. This difference is stark, from approximately 50% quenching of massive dwarf satellites inside of 500 kpc to approximately 90% at lower masses. *Ab initio* models of this change in quenching efficiency are not readily available, so instead we try to parameterize the change in alternative terms. If one uses a delay time between infall and quenching as the determining factor, then LMC/SMC mass galaxies must remain star forming inside a host halo for 6-8 Gyr, compared to the maximum of 1-2 Gyr required to keep high quenched fractions of low mass satellites. This aligns with what might be expected from a transition between rapid ram pressure based quenching of small satellites to a strangulation (deprivation of new gas accretion plus exhaustion of existing gas) scenario for larger dwarfs. Confirming these scenarios is beyond the reach of these limited measurements and simple models though.

The last question posed in this work relates to the effect of dwarfs on their host, rather than the host's effects on dwarfs. Though most dwarfs are not massive enough to cause anything like quenching, it may be possible for them to distort the Galactic disk enough to leave identifiable signatures of their (at least temporary) presence. Such might be the case with the Monoceros Ring—a stellar overdensity of ambiguous origin near the Galactic disk. Chapter VI presents the largest filled map of the structure to date, showing its presence on both sides of the disk and its extent over 130° in longitude. The structure extends 5 kpc above and 4 kpc below the disk, making it either oddly aligned with the Galactic disk if it is an accreted halo structure, or exceedingly tall for a feature of the disk itself. Our comparison of both accreted stream and disrupted disk models for the overdensity demonstrate the difficulty that both models have in reproducing all of the observed features. The accreted stream leaves significant material at large distances which we do not see in observations, while the disrupted disk is perhaps too disrupted, to the point that little material is left in the midplane. However, neither of these simulations were tuned to reproduce the Pan-STARRS1 observations, and so disagreement at this stage does not mean that better agreement cannot be achieved with some adjustment.

7.2 Open Questions

After having summarized the questions that this work has attempted to answer, it is worth reflecting on the most important unanswered questions that relate to these problems.

Can dwarf galaxies quench in isolation? Much of this work has proceeded under the assumption that the answer to this question is no, but that answer is not definitively known. The detectability of quenched galaxies is always worse than for star forming galaxies, causing selection effects which can be difficult to disentangle in heterogeneously-discovered samples of galaxies. The discovery of galaxies in blind HI surveys, such as Leo P (Giovanelli et al., 2013) and Pisces A and B (Tollerud et al., 2015; Sand et al., 2015), also contributes to this bias towards star forming galaxies. Quenched galaxies have only been more serendipitously discovered. One of the only such examples is KKR 25 (Makarov et al., 2012), but the presence of an intermediate age (1-4 Gyr old) population is inconsistent with quenching in isolation in the early universe. It is unclear what could have acted to end star formation in this galaxy.

In detail this question must be answered as a function of mass. The difficulty will be in discovering the very faintest dwarfs like Bootes II, Willman 1, or Segue II at large enough distances that they are unlikely to have interacted with the Milky Way. At present we cannot disentangle from the present dense environment of these dwarfs what their “pristine” state would have been, and so there are numerous possible stripping scenarios that could have resulted in the dwarfs we see. Pushing the detection limits farther for these galaxies will likely require LSST.

Are galaxies quenched by reionization? This is related to the question of quenching in isolation by any means, but answering if reionization can be responsible is much more challenging. Via modeling with synthetic stellar populations it is possible to extract the star formation history from dwarf galaxies (e.g., Weisz et al., 2011), but in the oldest populations the time resolution is relatively poor. One would like 100 Myr time resolution to make clear links between reionization and specific events in the star formation history, though this is generally out of reach. It is not clear if any substantial improvements to the methods of star formation history fitting are available to yield better answers on this question in the future. It may instead be necessary to develop an improved set of expectations from simulations of how reionization quenches galaxies, and exactly what dwarfs are most susceptible. If reionization leaves a signature in the population of dwarfs, or in the chemical abundance patterns, then perhaps its effects will be distinguishable.

Are some low mass dark matter halos "dark"? A key assumption of Chapters IV and V was that the dark matter halos from simulations and the observed dwarf galaxies were related in an unbiased way. That is, although the halos predicted by simulations were much more numerous than observed galaxies, we assumed that our observations traced simply a fraction of these halos that was not dependent on the individual halo properties. This discrepancy is a manifestation of the missing satellites problem, and our assumed "solution" is admittedly a simplistic one.

Understanding what accounts for this discrepancy between observed and predicted satellite counts is one of the most formidable challenges in the field of dwarf galaxies today. Several different approaches to this problem are available. Some recent works have focused on making models where satellite halos are tidally disrupted more easily due to the influence of baryons than would be predicted from dark matter only simulations (Brooks & Zolotov, 2014). Other simulation work has attempted to predict the star formation histories of low mass halos, with the possibility that for stochastic reasons some of these halos host exceedly fewer stars, making them undetectable by today's standards. These simulation efforts are operating where observational evidence is scarce. If, for example, the simulations predict that many halos are "dark", how can this be observationally confirmed?

It is unclear what observational evidence would be most decisive in attempting to solve the missing satellites problem. Further extending the census of low mass galaxies beyond the Local Group could give leverage in comparing the numbers and properties of galaxies that are most sensitive to tidal distruction by a larger host to those that have no host to affect them. Such a census may also improve our ability to associate observed galaxy luminosities with inferred halo properties, reducing another source of uncertainity in comparisons of simulations to observations. And as our census expands at large distances, it is also likely to be pushed to fainter galaxies nearby. What galaxies we find there may produce unexpected information about the evolution of both brighter and fainter dwarfs.

Are there galaxies below current surface brightness detection limits? Again our assumption in this work is that observed dwarfs are an unbiased sampling of halos, but the known dwarf galaxies are almost certainly affected by substantial selection effects (beyond simple area coverage of surveys). Surface brightness is the principal criterion for detecting dwarfs; the number counts of resolved stars must exceed the background source density by a statistically significant amount for the galaxy to be detected. Compact dwarfs are thus more likely to be detected at fixed luminosity. What this leaves is a sample of known dwarfs that live at roughly constant surface brightness, below which we have little knowledge. This is another problem that LSST is needed to solve. A combination of both depth and large area coverage is required for dwarf detection, and this will be what LSST excels at. There is every reason to suspect that the results from even the first year of LSST data will be substantially change what we know about faint, low-mass stellar systems.

BIBLIOGRAPHY

Abadi, M. G., Moore, B., & Bower, R. G. 1999, *MNRAS*, 308, 947

Ahn, C. P., Alexandroff, R., Allende Prieto, C., et al. 2012, *ApJS*, 203, 21

Aihara, H., et al. 2011, *ApJS*, 193, 29

An, D., Johnson, J. A., Clem, J. L., et al. 2008, *ApJS*, 179, 326

Anderson, M. E., & Bregman, J. N. 2010, *ApJ*, 714, 320

Balogh, M. L., Navarro, J. F., & Morris, S. L. 2000, *ApJ*, 540, 113

Balogh, M. L., Baldry, I. K., Nichol, R., et al. 2004, *ApJ*, 615, L101

Battaglia, G., Tolstoy, E., Helmi, A., et al. 2006, *A&A*, 459, 423

Bell, E. F., Slater, C. T., & Martin, N. F. 2011, *ApJ*, 742, L15

Bellazzini, M., Ferraro, F. R., & Pancino, E. 2001, *ApJ*, 556, 635

Belokurov, V., Zucker, D. B., Evans, N. W., et al. 2006, *ApJ*, 642, L137

Belokurov, V., Zucker, D. B., Evans, N. W., et al. 2007, *ApJ*, 654, 897

Benson, A. J., Bower, R. G., Frenk, C. S., & White, S. D. M. 2000, *MNRAS*, 314, 557

Binney, J., & Tremaine, S. 2008, Galactic Dynamics: Second Edition, Princeton University Press, Princeton, NJ

Birnboim, Y., & Dekel, A. 2003, *MNRAS*, 345, 349

Blake, C., Brough, S., Colless, M., et al. 2012, *MNRAS*, 425, 405

Blanton, M. R., & Roweis, S. 2007, *AJ*, 133, 734

Blanton, M. R., Kazin, E., Muna, D., Weaver, B. A., & Price-Whelan, A. 2011, *AJ*, 142, 31

Blitz, L., & Robishaw, T. 2000, *ApJ*, 541, 675

Bothwell, M. S., Kennicutt, R. C., & Lee, J. C. 2009, *MNRAS*, 400, 154

Bramich, D. M., Vidrih, S., Wyrzykowski, L., et al. 2008, *MNRAS*, 386, 887

Brasseur, C. M., Martin, N. F., Macciò, A. V., Rix, H.-W., & Kang, X. 2011, *ApJ*, 743, 179

Brooks, A. M., Kuhlen, M., Zolotov, A., & Hooper, D. 2013, *ApJ*, 765, 22

Brooks, A. M., & Zolotov, A. 2014, *ApJ*, 786, 87

Bullock, J. S., Kravtsov, A. V., & Weinberg, D. H. 2000, *ApJ*, 539, 517

Carrera, R., Pancino, E., Gallart, C., & del Pino, A. 2013, *MNRAS*, 434, 1681

Cattaneo, A., Dekel, A., Devriendt, J., Guiderdoni, B., & Blaizot, J. 2006, *MNRAS*, 370, 1651

Cen, R., & Ostriker, J. P. 1999, *ApJ*, 514, 1

Chen, Y. Q., Zhao, G., & Zhao, J. K. 2009, *ApJ*, 702, 1336

Chiboucas, K., Jacobs, B. A., Tully, R. B., & Karachentsev, I. D. 2013, arXiv:1309.4130

Chung, A., van Gorkom, J. H., Kenney, J. D. P., & Vollmer, B. 2007, *ApJ*, 659, L115

Cole, S. 1991, *ApJ*, 367, 45

Cole, S., Aragon-Salamanca, A., Frenk, C. S., Navarro, J. F., & Zepf, S. E. 1994, *MNRAS*, 271, 781

Collins, M. L. M., et al. 2010, *MNRAS*, 407, 2411

Collins, M. L. M., Chapman, S. C., Rich, R. M., et al. 2013, *ApJ*, 768, 172

Conn, B. C., Lewis, G. F., Irwin, M. J., et al. 2005, *MNRAS*, 362, 475

Conn, B. C., Martin, N. F., Lewis, G. F., et al. 2005, *MNRAS*, 364, L13

Conn, B. C., Lane, R. R., Lewis, G. F., et al. 2007, *MNRAS*, 376, 939

Conn, B. C., Lane, R. R., Lewis, G. F., et al. 2008, *MNRAS*, 390, 1388

Conn, B. C., Noël, N. E. D., Rix, H.-W., et al. 2012, *ApJ*, 754, 101

Conn, A. R., Lewis, G. F., Ibata, R. A., et al. 2013, *ApJ*, 766, 120

Cortese, L., Marcillac, D., Richard, J., et al. 2007, *MNRAS*, 376, 157

Crane, J. D., Majewski, S. R., Rocha-Pinto, H. J., et al. 2003, *ApJ*, 594, L119

Croton, D. J., Springel, V., White, S. D. M., et al. 2006, *MNRAS*, 365, 11

Danielson, A. L. R., Lehmer, B. D., Alexander, D. M., et al. 2012, *MNRAS*, 422, 494

de Jong, J. T. A., Harris, J., Coleman, M. G., et al. 2008, *ApJ*, 680, 1112

de Jong, J. T. A., Yanny, B., Rix, H.-W., et al. 2010, *ApJ*, 714, 663

Dekel, A., & Silk, J. 1986, *ApJ*, 303, 39

Diemand, J., Kuhlen, M., & Madau, P. 2006, *ApJ*, 649, 1

Diemand, J., Kuhlen, M., & Madau, P. 2007, *ApJ*, 667, 859

Diemand, J., Kuhlen, M., Madau, P., et al. 2008, *Nature*, 454, 735

Dijkstra, M., Haiman, Z., Rees, M. J., & Weinberg, D. H. 2004, *ApJ*, 601, 666

D'Onghia, E., Besla, G., Cox, T. J., & Hernquist, L. 2009, *Nature*, 460, 605

Dotter, A., Chaboyer, B., Jevremović, D., Kostov, V., Baron, E., & Ferguson, J. W. 2008, *ApJS*, 178, 89

Dressler, A. 1980, *ApJ*, 236, 351

Dubinski, J., & Carlberg, R. G. 1991, *ApJ*, 378, 496

Efstathiou, G. 1992, *MNRAS*, 256, 43P

Einasto, J., Saar, E., Kaasik, A., & Chernin, A. D. 1974, *Nature*, 252, 111

Faber, S. M., & Lin, D. N. C. 1983, *ApJ*, 266, L17

Fattahi, A., Navarro, J. F., Starkenburg, E., Barber, C. R., & McConnachie, A. W. 2013, *MNRAS*, 431, L73

Ferguson, A. M. N., Irwin, M. J., Ibata, R. A., Lewis, G. F., & Tanvir, N. R. 2002, *AJ*, 124, 1452

Ferrara, A., & Tolstoy, E. 2000, *MNRAS*, 313, 291

Font, A. S., Bower, R. G., McCarthy, I. G., et al. 2008, *MNRAS*, 389, 1619

Frinchaboy, P. M., Majewski, S. R., Crane, J. D., et al. 2004, *ApJ*, 602, L21

Fukugita, M., Hogan, C. J., & Peebles, P. J. E. 1998, *ApJ*, 503, 518

Gallagher, J. S., III, & Wyse, R. F. G. 1994, *PASP*, 106, 1225

García-Ruiz, I., Sancisi, R., & Kuijken, K. 2002, *A&A*, 394, 769

Gatto, A., Fraternali, F., Read, J. I., et al. 2013, *MNRAS*, 433, 2749

Geha, M., Blanton, M. R., Yan, R., & Tinker, J. L. 2012, *ApJ*, 757, 85

Gill, S. P. D., Knebe, A., & Gibson, B. K. 2005, *MNRAS*, 356, 1327

Giovanelli, R., Haynes, M. P., Adams, E. A. K., et al. 2013, *AJ*, 146, 15

Gnedin, N. Y. 2000, *ApJ*, 542, 535

Gnedin, O. Y., & Zhao, H. 2002, *MNRAS*, 333, 299

Gómez, F. A., Minchev, I., O'Shea, B. W., et al. 2013, *MNRAS*, 429, 159

Governato, F., Brook, C., Mayer, L., et al. 2010, *Nature*, 463, 203

Governato, F., Zolotov, A., Pontzen, A., et al. 2012, *MNRAS*, 422, 1231

Grcevich, J., & Putman, M. E. 2009, *ApJ*, 696, 385

Grebel, E. K., Gallagher, J. S., III, & Harbeck, D. 2003, *AJ*, 125, 1926

Grillmair, C. J. 2006, *ApJ*, 651, L29

Grillmair, C. J., Carlin, J. L., & Majewski, S. R. 2008, *ApJ*, 689, L117

Grillmair, C. J. 2011, *ApJ*, 738, 98

Gunn, J. E., & Gott, J. R., III 1972, *ApJ*, 176, 1

Hammersley, P. L., & López-Corredoira, M. 2011, *A&A*, 527, A6

Helmi, A., Cooper, A. P., White, S. D. M., et al. 2011, *ApJ*, 733, L7

Hinshaw, G., Larson, D., Komatsu, E., et al. 2013, *ApJS*, 208, 19

Ho, N., Geha, M., Tollerud, E. J., et al. 2015, *ApJ*, 798, 77

Hodge, P. W. 1964, *AJ*, 69, 438

Hodge, P. W., & Michie, R. W. 1969, *AJ*, 74, 587

Hollenbach, D. J., Werner, M. W., & Salpeter, E. E. 1971, *ApJ*, 163, 165

Hopkins, P. F., Somerville, R. S., Cox, T. J., et al. 2009, *MNRAS*, 397, 802

Huang, S., Haynes, M. P., Giovanelli, R., et al. 2012, *AJ*, 143, 133

Hunter, D. A., & Gallagher, J. S., III 1985, *ApJS*, 58, 533

Ibata, R. A., Irwin, M. J., Lewis, G. F., Ferguson, A. M. N., & Tanvir, N. 2003, *MNRAS*, 340, L21

Ibata, R., Chapman, S., Ferguson, A. M. N., et al. 2005, *ApJ*, 634, 287

Ibata, R., Chapman, S., Irwin, M., Lewis, G., & Martin, N. 2006, *MNRAS*, 373, L70

Ibata, R., Martin, N. F., Irwin, M., Chapman, S., Ferguson, A. M. N., Lewis, G. F., & McConnachie, A. W. 2007, *ApJ*, 671, 1591

Ibata, R. A., Lewis, G. F., Conn, A. R., et al. 2013, *Nature*, 493, 62

Irwin, M. J., Belokurov, V., Evans, N. W., et al. 2007, *ApJ*, 656, L13

Irwin, M. J., Ferguson, A. M. N., Huxor, A. P., Tanvir, N. R., Ibata, R. A., & Lewis, G. F. 2008, *ApJ*, 676, L17

Jordi, K., Grebel, E. K., & Ammon, K. 2006, *A&A*, 460, 339

Kaiser, N., Burgett, W., Chambers, K., et al. 2010, *Proc. SPIE*, 7733,

Kalberla, P. M. W., Burton, W. B., Hartmann, D., Arnal, E. M., Bajaja, E., Morras, R., Pöppel, W. G. L. 2005, *A&A*, 440, 775

Kalberla, P. M. W., & Kerp, J. 2009, *ARA&A*, 47, 27

Kawata, D., Arimoto, N., Cen, R., & Gibson, B. K. 2006, *ApJ*, 641, 785

Kazantzidis, S., Bullock, J. S., Zentner, A. R., Kravtsov, A. V., & Moustakas, L. A. 2008, *ApJ*, 688, 254

Kazantzidis, S., Zentner, A. R., Kravtsov, A. V., Bullock, J. S., & Debattista, V. P. 2009, *ApJ*, 700, 1896

Kazantzidis, S., Łokas, E. L., Callegari, S., Mayer, L., & Moustakas, L. A. 2011, *ApJ*, 726, 98

Kazantzidis, S., Łokas, E. L., Mayer, L., Knebe, A., & Klimentowski, J. 2011, *ApJ*, 740, L24

Kazantzidis, S., Łokas, E. L., & Mayer, L. 2013, *ApJ*, 764, L29

Kirby, E. N., Lanfranchi, G. A., Simon, J. D., Cohen, J. G., & Guhathakurta, P. 2011, *ApJ*, 727, 78

Kirby, E. N., Cohen, J. G., Guhathakurta, P., et al. 2013, arXiv:1310.0814

Klimentowski, J., Łokas, E. L., Kazantzidis, S., Mayer, L., & Mamon, G. A. 2009, *MNRAS*, 397, 2015

Klimentowski, J., Łokas, E. L., Knebe, A., et al. 2010, *MNRAS*, 402, 1899

Klypin, A., Zhao, H., & Somerville, R. S. 2002, *ApJ*, 573, 597

Klypin, A., Kravtsov, A. V., Valenzuela, O., & Prada, F. 1999, *ApJ*, 522, 82

Koch, A., Grebel, E. K., Kleyna, J. T., et al. 2007, *AJ*, 133, 270

Koch, A., Wilkinson, M. I., Kleyna, J. T., et al. 2007, *ApJ*, 657, 241

Koposov, S. E., Yoo, J., Rix, H.-W., et al. 2009, *ApJ*, 696, 2179

Kormendy, J. 1985, *ApJ*, 295, 73

Kravtsov, A. V., Gnedin, O. Y., & Klypin, A. A. 2004, *ApJ*, 609, 482

Kroupa, P. 2001, *MNRAS*, 322, 231

Li, Y.-S., & Helmi, A. 2008, *MNRAS*, 385, 1365

Li, J., Newberg, H. J., Carlin, J. L., et al. 2012, *ApJ*, 757, 151

Libeskind, N. I., Frenk, C. S., Cole, S., et al. 2005, *MNRAS*, 363, 146

Lin, D. N. C., & Faber, S. M. 1983, *ApJ*, 266, L21

Łokas, E. L., Kazantzidis, S., Klimentowski, J., Mayer, L., & Callegari, S. 2010, *ApJ*, 708, 1032

Łokas, E. L., Kazantzidis, S., & Mayer, L. 2011, *ApJ*, 739, 46

Łokas, E. L., Kowalczyk, K., & Kazantzidis, S. 2012, arXiv:1212.0682

Lovell, M. R., Eke, V. R., Frenk, C. S., & Jenkins, A. 2011, *MNRAS*, 413, 3013

Lynden-Bell, D. 1976, *MNRAS*, 174, 695

Mac Low, M.-M., & Ferrara, A. 1999, *ApJ*, 513, 142

Magnier, E. 2006, The Advanced Maui Optical and Space Surveillance Technologies Conference,

Majewski, S. R., Frinchaboy, P. M., Kunkel, W. E., et al. 2005, *AJ*, 130, 2677

Makarov, D., Makarova, L., Rizzi, L., Tully, R. B., Dolphin, A. E., Sakai, S., & Shaya, E. J. 2006, *AJ*, 132, 2729

Makarov, D., Makarova, L., Sharina, M., et al. 2012, *MNRAS*, 425, 709

Martin, C. L. 1999, *ApJ*, 513, 156

Martin, N. F., Ibata, R. A., Bellazzini, M., et al. 2004, *MNRAS*, 348, 12

Martin, N. F., Irwin, M. J., Ibata, R. A., et al. 2006, *MNRAS*, 367, L69

Martin, N. F., Ibata, R. A., Irwin, M. J., Chapman, S., Lewis, G. F., Ferguson, A. M. N., Tanvir, N., & McConnachie, A. W. 2006, *MNRAS*, 371, 1983

Martin, N. F., de Jong, J. T. A., & Rix, H.-W. 2008, *ApJ*, 684, 1075

Martin, N. F., et al. 2009, *ApJ*, 705, 758

Martin, N. F., Ibata, R. A., Rich, R. M., et al. 2014, arXiv:1403.4945

Mateo, M. L. 1998, *ARA&A*, 36, 435

Mateu, C., Vivas, A. K., Zinn, R., Miller, L. R., & Abad, C. 2009, *AJ*, 137, 4412

Mayer, L., Governato, F., Colpi, M., et al. 2001, *ApJ*, 559, 754

Mayer, L., Mastropietro, C., Wadsley, J., Stadel, J., & Moore, B. 2006, *MNRAS*, 369, 1021

McConnachie, A. W., Irwin, M. J., Ferguson, A. M. N., Ibata, R. A., Lewis, G. F., & Tanvir, N. 2005, *MNRAS*, 356, 979

McConnachie, A. W., & Irwin, M. J. 2006, *MNRAS*, 365, 1263

McConnachie, A. W., Peñarrubia, J., & Navarro, J. F. 2007, *MNRAS*, 380, L75

McConnachie, A. W., Venn, K. A., Irwin, M. J., Young, L. M., & Geehan, J. J. 2007, *ApJ*, 671, L33

McConnachie, A. W., et al. 2009, *Nature*, 461, 66

McConnachie, A. W. 2012, *AJ*, 144, 4

McKee, C. F., & Ostriker, E. C. 2007, *ARA&A*, 45, 565

Meisner, A. M., Frebel, A., Jurić, M., & Finkbeiner, D. P. 2012, *ApJ*, 753, 116

Metcalfe, N., Farrow, D. J., Cole, S., et al. 2013, *MNRAS*, 435, 1825

Miller, M. J., & Bregman, J. N. 2013, *ApJ*, 770, 118

Mo, H., van den Bosch, F. C., & White, S. 2010, Galaxy Formation and Evolution, by Houjun Mo , Frank van den Bosch , Simon White, Cambridge, UK: Cambridge University Press, 2010,

Momany, Y., Zaggia, S., Gilmore, G., et al. 2006, *A&A*, 451, 515

Monelli, M., Hidalgo, S. L., Stetson, P. B., et al. 2010, *ApJ*, 720, 1225

Monelli, M., Gallart, C., Hidalgo, S. L., et al. 2010, *ApJ*, 722, 1864

Moore, B., Diemand, J., & Stadel, J. 2004, IAU Colloq. 195: Outskirts of Galaxy Clusters: Intense Life in the Suburbs, 513

Moore, B. 1994, *Nature*, 370, 629

Moore, B., Ghigna, S., Governato, F., et al. 1999, *ApJ*, 524, L19

Moster, B. P., Somerville, R. S., Maulbetsch, C., et al. 2010, *ApJ*, 710, 903

Muñoz, R. R., Padmanabhan, N., & Geha, M. 2012, *ApJ*, 745, 127

Navarro, J. F., Frenk, C. S., & White, S. D. M. 1996, *ApJ*, 462, 563

Navarro, J. F., Frenk, C. S., & White, S. D. M. 1997, *ApJ*, 490, 493

Navarro, J. F., & White, S. D. M. 1993, *MNRAS*, 265, 271

Newberg, H. J., Yanny, B., Rockosi, C., et al. 2002, *ApJ*, 569, 245

Newby, M., Newberg, H. J., Simones, J., Cole, N., & Monaco, M. 2011, *ApJ*, 743, 187

Nichols, M., & Bland-Hawthorn, J. 2011, *ApJ*, 732, 17

Oh, S.-H., de Blok, W. J. G., Brinks, E., Walter, F., & Kennicutt, R. C., Jr. 2011, *AJ*, 141, 193

Palma, C., Majewski, S. R., Siegel, M. H., et al. 2003, *AJ*, 125, 1352

Peeples, M. S., Werk, J. K., Tumlinson, J., et al. 2014, *ApJ*, 786, 54

Peñarrubia, J., Martínez-Delgado, D., Rix, H. W., et al. 2005, *ApJ*, 626, 128

Peñarrubia, J., Benson, A. J., Walker, M. G., et al. 2010, *MNRAS*, 406, 1290

Phillips, J. I., Wheeler, C., Boylan-Kolchin, M., et al. 2014, *MNRAS*, 437, 1930

Pietrinferni, A., Cassisi, S., Salaris, M., & Castelli, F. 2004, *ApJ*, 612, 168

Planck Collaboration, Adam, R., Ade, P. A. R., et al. 2015, arXiv:1502.01582

Postman, M., & Geller, M. J. 1984, *ApJ*, 281, 95

Purcell, C. W., Bullock, J. S., Tollerud, E. J., Rocha, M., & Chakrabarti, S. 2011, *Nature*, 477, 301

Radburn-Smith, D. J., de Jong, R. S., Streich, D., et al. 2014, *ApJ*, 780, 105

Read, J. I., & Gilmore, G. 2005, *MNRAS*, 356, 107

Read, J. I., & Trentham, N. 2005, Royal Society of London Philosophical Transactions Series A, 363, 2693

Reines, A. E., Greene, J. E., & Geha, M. 2013, *ApJ*, 775, 116

Revaz, Y., & Jablonka, P. 2012, *A&A*, 538, AA82

Richardson, J. C., Ferguson, A. M. N., Johnson, R. A., et al. 2008, *AJ*, 135, 1998

Rocha-Pinto, H. J., Majewski, S. R., Skrutskie, M. F., Crane, J. D., & Patterson, R. J. 2004, *ApJ*, 615, 732

Ryan-Weber, E. V., Begum, A., Oosterloo, T., et al. 2008, *MNRAS*, 384, 535

Sanchez-Saavedra, M. L., Battaner, E., & Florido, E. 1990, *MNRAS*, 246, 458

Sand, D. J., Crnojević, D., Bennet, P., et al. 2015, arXiv:1503.00720

Sarajedini, A., Lee, Y.-W., & Lee, D.-H. 1995, *ApJ*, 450, 712

Sawala, T., Scannapieco, C., Maio, U., & White, S. 2010, *MNRAS*, 402, 1599

Schlafly, E. F., & Finkbeiner, D. P. 2011, *ApJ*, 737, 103

Schlafly, E. F., Finkbeiner, D. P., Jurić, M., et al. 2012, *ApJ*, 756, 158

Schlegel, D. J., Finkbeiner, D. P., & Davis, M. 1998, *ApJ*, 500, 525

Ségall, M., Ibata, R. A., Irwin, M. J., Martin, N. F., & Chapman, S. 2007, *MNRAS*, 375, 831

Slater, C. T., Bell, E. F., & Martin, N. F. 2011, *ApJ*, 742, L14

Slater, C. T., Bell, E. F., Schlafly, E. F., et al. 2013, *ApJ*, 762, 6

Smoot, G. F., Bennett, C. L., Kogut, A., et al. 1992, *ApJ*, 396, L1

Sohn, S. T., Besla, G., van der Marel, R. P., et al. 2013, *ApJ*, 768, 139

Sollima, A., Valls-Gabaud, D., Martinez-Delgado, D., et al. 2011, *ApJ*, 730, L6

Somerville, R. S. 2002, *ApJ*, 572, L23

Somerville, R. S., Hopkins, P. F., Cox, T. J., Robertson, B. E., & Hernquist, L. 2008, *MNRAS*, 391, 481

Springel, V., & Hernquist, L. 2003, *MNRAS*, 339, 289

Springel, V., White, S. D. M., Jenkins, A., et al. 2005, *Nature*, 435, 629

Stetson, P. B. 1987, *PASP*, 99, 191

Stetson, P. B., Hesser, J. E., Smith, G. H., Vandenberg, D. A., & Bolte, M. 1989, *AJ*, 97, 1360

Stinson, G., Seth, A., Katz, N., et al. 2006, *MNRAS*, 373, 1074

Sullivan, M., Guy, J., Conley, A., et al. 2011, *ApJ*, 737, 102

Teyssier, M., Johnston, K. V., & Kuhlen, M. 2012, *MNRAS*, 426, 1808

Thuan, T. X., & Martin, G. E. 1979, *ApJ*, 232, L11

Tinker, J. L., & Wetzel, A. R. 2010, *ApJ*, 719, 88

Tollerud, E. J., Geha, M. C., Vargas, L. C., & Bullock, J. S. 2013, *ApJ*, 768, 50

Tollerud, E. J., Geha, M. C., Grcevich, J., Putman, M. E., & Stern, D. 2015, *ApJ*, 798, L21

Tolstoy, E., Irwin, M. J., Helmi, A., et al. 2004, *ApJ*, 617, L119

Tully, R. B., Rizzi, L., Dolphin, A. E., et al. 2006, *AJ*, 132, 729

van den Bergh, S. 1994, *ApJ*, 428, 617

van den Bosch, F. C., Aquino, D., Yang, X., et al. 2008, *MNRAS*, 387, 79

Vivas, A. K., & Zinn, R. 2006, *AJ*, 132, 714

Vogelsberger, M., Genel, S., Springel, V., et al. 2014, *Nature*, 509, 177

Walker, M. G., & Peñarrubia, J. 2011, *ApJ*, 742, 20

Weinberg, M. D. 2014, *MNRAS*, 438, 3007

Weinmann, S. M., & Lilly, S. J. 2005, *ApJ*, 624, 526

Weinmann, S. M., van den Bosch, F. C., Yang, X., & Mo, H. J. 2006, *MNRAS*, 366, 2

Weinmann, S. M., Kauffmann, G., von der Linden, A., & De Lucia, G. 2010, *MNRAS*, 406, 2249

Weisz, D. R., Dalcanton, J. J., Williams, B. F., et al. 2011, *ApJ*, 739, 5

Weisz, D. R., Zucker, D. B., Dolphin, A. E., et al. 2012, *ApJ*, 748, 88

Werk, J. K., Prochaska, J. X., Tumlinson, J., et al. 2014, *ApJ*, 792, 8

Wetzel, A. R., Tinker, J. L., Conroy, C., & van den Bosch, F. C. 2013, *MNRAS*, 432, 336

Wheeler, C., Phillips, J. I., Cooper, M. C., Boylan-Kolchin, M., & Bullock, J. S. 2014, arXiv:1402.1498

White, S. D. M., & Rees, M. J. 1978, *MNRAS*, 183, 341

White, S. D. M., & Frenk, C. S. 1991, *ApJ*, 379, 52

Widrow, L. M., Gardner, S., Yanny, B., Dodelson, S., & Chen, H.-Y. 2012, *ApJ*, 750, L41

Willman, B., Blanton, M. R., West, A. A., et al. 2005, *AJ*, 129, 2692

Yagi, M., Yoshida, M., Komiyama, Y., et al. 2010, *AJ*, 140, 1814

Yanny, B., Newberg, H. J., Grebel, E. K., et al. 2003, *ApJ*, 588, 824

Younger, J. D., Besla, G., Cox, T. J., et al. 2008, *ApJ*, 676, L21

Zolotov, A., Brooks, A. M., Willman, b., et al. 2012, *ApJ*, 761, 71

Zucker, D. B., et al. 2004, *ApJ*, 612, L121

Zucker, D. B., et al. 2007, *ApJ*, 659, L21